Revised.

THE MEASUREMENT OF PARTICLE SIZE USING LIGHT SCATTERING

BY

ROBERT MICHAEL WATERSTON

A thesis submitted for the degree of Doctor of Philosophy in the

Faculty of Engineering

Department of Aeronautics and Astronautics

DECEMBER 1978

ABSTRACT

Faculty of Engineering and Applied Science

Department of Aeronautics and Astronautics

Doctor of Philosophy

The Measurement of Particle Size using Light Scattering

by R. M. Waterston.

Two methods of particle sizing have been investigated. The first uses least squares analysis to obtain particle size distribution information in sprays from the angular variation of scattered light intensity. The thesis presents theoretical proof of the potential of the technique and includes experimental verification of its accuracy. The second method involves a novel method of illuminating the suspension under investigation using crossed laser beams. The technique is applicable to submicron particles, affords a near point measurement and has an inbuilt discrimination against background noise.

ACKNOWLEDGEMENTS

Most sincere thanks are due to my supervisor Dr. M.J. Goodyer, who has been an unfailing source of help and encouragement during this project.

I would like to thank Professor G.M. Lilley and Dr. R.E.W. Jansson and the other members of the department for their help and support.

I am most grateful to Mr. H.P. Chou for his theoretical support without which the cross beam work would have been severely limited.

I would like to thank also the Aeronautics Department workshop and in particular Mr. Alan Tuck who were responsible for building the equipment for the project.

Thanks are due to Rolls Royce (1971) Ltd. for supporting the project.

Finally, I would like to thank Sally for her continuous personal and professional help throughout the project period.

CONTENTS

CONTENTS (Continued)

LIST OF SYMBOLS

a	PARTICLE RADIUS
a_n	SCATTERING FUNCTION
a_{ij}	GRAM-SCHMIDT ORTHONORMAL COEFFICIENT
A	VECTOR POTENTIAL RELATED TO $\underline{H}$ and $\underline{E}$
b_n	SCATTERING FUNCTION
C	SPEED OF LIGHT
C_{abs}	ABSORPTION CROSS SECTION
C_{sca}	SCATTERING CROSS SECTION
C_{ext}	EXTINCTION CROSS SECTION
Cv	VOLUME FRACTION
D	PARTICLE DIAMETER
D_{32}	SAUTER MEAN DIAMETER
E	EXTINCTION COEFFICIENT
E_θ, E_ϕ	AMPLITUDE FUNCTIONS
$\underline{E}$	ELECTRIC VECTOR
f(a)	PARTICLE NUMBER DENSITY
$\underline{H}$	MAGNETIC VECTOR
i_1, i_2	SCATTERING INTENSITY FUNCTIONS
I_{exp}	EXPERIMENTAL SCATTERED LIGHT INTENSITY
I_{ij}	SCATTERED LIGHT INTENSITY OF PARTICLE SIZE α_i AT ANGLE θ_j
I_ϕ	SCATTERED LIGHT INTENSITY (PERPENDICULAR POLARISATION)
I_θ	" " " (PARALLEL POLARISATION)
$I\alpha$	LIGHT INTENSITY SCATTERED BY PARTICLE OF SIZE α
J_n	BESSEL FUNCTION OF nth ORDER
k	$2\pi/\lambda$
ℓ	OPTICAL PATH LENGTH

LIST OF SYMBOLS (Continued)

L_p	DISTANCE FUNCTION
m	REFRACTIVE INDEX
$n(\alpha)$	PARTICLE NUMBER DENSITY
n_i	NUMBER DENSITY OF PARTICLES OF SIZE α_i
$p(\alpha)$	PARTICLE NUMBER DENSITY
Q_{sca}	SCATTERING EFFICIENCY
Q_{eff}	EFFECTIVE Q_{sca}
r,ϕ,θ	SPHERICAL CO-ORDINATES
T	TRANSMISSION
V	LASER ANEMOMETER VISIBILITY
W	STATISTICAL WEIGHT
Y_n	NEUMAN FUNCTION OF nth ORDER
α	NON DIMENSIONAL PARTICLE SIZE
α_m	MODAL NON DIMENSIONAL DIAMETER
$\bar{\alpha}$	MEAN NON DIMENSIONAL DIAMETER
β	SCATTER ANGLE
δ	LEAST SQUARES RESIDUAL
Σ_{sca}	SCATTERING COEFFICIENT
σ	STANDARD DEVIATION
σ_o	LOG NORMAL STANDARD DEVIATION
ϕ_i	ORTHOGONAL FUNCTION
λ	WAVELENGTH OF LIGHT
λ^*	LASER ANEMOMETER FRINGE SPACING
ψ	SCALAR POTENTIAL FUNCTION
$\rho(\theta)$	POLARISATION RATIO
$\rho(p,q)$	SCATTERING RATIO
τ	TURBIDITY
ω	SCATTER CONE

LIST OF FIGURES

LIST OF FIGURES (Continued)

SUMMARY

This thesis describes the development of two novel methods of using scattered light data in the sizing of particles.

The first section describes a new technique for processing scattered light data to obtain a particle size distribution. A series of particle size classes is preselected and the Least Squares Approximation Theory is used to determine the contribution made by these classes to the total light scattered by the whole distribution. The processing method represents a considerable improvement over previously tried techniques. It is easy to apply and does not require the assumption of a specific functional form for the distribution. Theoretical and experimental proof of the accuracy of the method are presented.

The second section describes the development of a new method of illuminating particles. In contrast to normal methods this affords a near point measurement and considerable discrimination against background noise. This is achieved by crossing two coherent laser beams in the test space. The intersection region resolves itself into a set of fringes each of which can be considered as a small beam of finite length. A particle situated within one of these fringes projects its forward and back scattered light into the free space between the two incoming beams. The ratio of these two components is a monotonic function of particle size in the range 0.02-0.5μm. Particles traversing the fring system will give rise to modulated light scatter the amplitude of which can be related to particle size. The modulation frequency can be used to isolate the signal from background noise and is a measure of the particle velocity.

PART 1. THE MEASUREMENT OF SPRAYS USING LIGHT SCATTERING

1.1 Introduction to Part 1

This thesis describes the development of two techniques for determining experimentally the sizes of particles in suspensions. Both methods are optical, and each is treated separately in the thesis.

There are many scientific and industrial fields in which there is a requirement for the accurate measurement of particle sizes in a suspension. These include the study of atmospherics, nucleation and particle growth and pigment manufacture. However, this work sprang from an investigation, begun in 1968, into the cooling of turbine blades of gas-turbine engines with water/air mists. The proposed method of cooling involved injecting atomised water into the turbine cooling air at compressor delivery conditions. A relatively small mass of added water would raise significantly the cooling capacity of the air because of its high latent heat of evaporisation. Various heat transfer experiments were carried out[38,39,40] the success of which led to a contract with Rolls Royce (1971) Ltd. to explore the method further. Several areas were identified where data was required. One of the most important concerned the behaviour of the water droplets following their injection into the hot, high pressure compressor delivery bleed cooling air. An experimental rig was built to simulate these conditions[27] which consisted of a 90 kw high pressure air heater, and a 1½ metre long 3.8 cm diameter test duct. It was planned to measure the evaporation of water droplets as they were swept, in the heated air stream, down the test duct. The duct was equipped with instrument ports and windows along its length. The sprays used to generate the

droplets produced water particles between 20 and 60μm.

A theoretical investigation indicated that within the test section length (1½ metres), the droplets would vaporise to a mean of approximately 5μm, but with rapid evaporation over the first few centimetres. The sizing technique used had to be capable of good spatial resolution and able to accommodate a wide range of particle sizes (5-100μm).

In the past, droplet sizes had been measured using a variety of methods, most of which required that a probe of some description be inserted into the flow. These techniques have been brought into question recently primarily because of the disturbing effect of the probe on the flow. Large particles tend to bounce off or shatter, the small specimens will tend to avoid capture altogether. Photographic techniques have overcome some of these problems but are limited in their range of applications. Small particles (<20μm) require large magnification which demands very intense light sources and, if the particles are moving, generate extremely high image velocities at the film plane. In many cases the recorded image is elongated or is a streak rather than a sphere. An additional disadvantage of photographic techniques concerns the measurement of the particle sizes from the photograph. This is an extremely exacting and time consuming procedure which would severely limit the number of tests it would be possible to make in a given time. It is against this background that light scattering methods have been developed and are finding increasing use.

In many cases of interest the particles or droplets are present in hostile or relatively inaccessible environments. Modern light scattering methods have the potential of measuring particle distributions from an area remote from the flow. The

only intrusion into the test space is made by a laser beam or equivalent light source which has an immeasurable effect on the suspension within. It will also be seen that they have the possibility of being built into an automatic 'on line' sizing system capable of providing results with the minimum of delay. Finally, light scattering methods are capable of measuring particles of a wide range of sizes. The extreme flexibility of light scattering methods has prompted the development of the systems described in this thesis. Both methods were designed specifically for making measurements in the evaporation experiment mentioned earlier. The subject of this section of the thesis is the development of a method of analysis designed to reconstruct a particle size distribution from scattered light data. It makes no assumptions about the shape of the distribution and is suitable for 'on line' operation. The work is a natural progression from the research of a colleague, Dr. J.D.C. Vardon[20], who made the first exploratory theoretical investigation of the methods potential. Following is a description of the theoretical and experimental work which was carried out in bringing the technique to the point of practical application.

1.2 The Scatter of Light by a Laser Illuminated Particle Suspension

The general theory of scatter of a plane polarised wave by a spherical particle was derived by Mie[1] in 1908. A detailed description of the solution procedure can be found in references 2 and 3. The strength of a particle sizing technique based on the scatter of light lies in the accuracy of the descriptive mathematics. The accuracy of Mie theory has often been proved experimentally in recent years[4]. This has enabled the experimenter to determine the size of particles by direct

comparison of experimental results with a reliable theory.

The general solution of Mie's theory predicts the intensity of scattered radiation at any point in space around the particle. Figure (1) defines the frame of reference around which the theory is derived. The solution is in two parts representing respectively components perpendicular and parallel to the scatter plane.

$$I_\phi = \frac{\lambda^2}{4\pi^2 r^2} i_1 \sin^2\phi \qquad \text{(perpendicular polarization)}$$

$$I_\theta = \frac{\lambda^2}{4\pi^2 r^2} i_2 \cos^2\phi \qquad \text{(parallel polarization)}$$

r is the distance from the particle centre

ϕ is defined in Figure (1)

i_1 and i_2, the intensity functions, are each dependent on a non-dimensional size parameter α, and on the refractive index of the particle relative to the medium, m. The size parameter is

$$\alpha = \frac{\pi D}{\lambda} \qquad \text{where } D = \text{particle diameter}, \quad \lambda = \text{light wavelength}$$

Two special cases of direct relevance to scattering experiments exist. These are:

(1) $\phi = 90°$

$$I_\phi = I_1 = (\lambda^2/4\pi r^2) i_1; \quad I_\theta = 0$$

This defines a scatter plane perpendicular to the electric vector.

(2) $\phi = 0°$

$$I_\theta = I_2 = (\lambda^2/4\pi r^2) i_2; \quad I_\phi = 0$$

In this case the electric vector is parallel to scatter plane.

If scattered light is measured in either of these planes only one component of scatter requires computation because

the $\sin^2\phi$ and $\cos^2\phi$ factors are either unity or zero. The light scattered at angle $\theta = 0°$ lies along the laser beam; that at $\theta = 180°$ is also coincident with the main beam but projects back towards the light source.

Measurements taken simultaneously in the vertical and parallel planes can provide unique information about the particle suspension under investigation. For particularly small (<1000 Å) particles the angular variations of scatter in the two planes are radically different. Work relevant to these small particles is described in Part II. With increase in size the difference between the planes of scatter becomes less apparent. The major differences occur in the region of 120° where I_2 generally reaches a minimum substantially lower than that of I_1. The intensity function i_1 is often more structured than i_2, as can be seen from the examples on Figure (2) and Figure (3). The intensity functions are unique indications of the particle size. If the angular variation of scattered light from a monodisperse was measured experimentally, the size of the particles could be deduced in principle by matching the data to a series of theoretical intensity distributions computed for a suitable range of α.

In most practical situations the light will be scattered from a suspension which consists of a wide range of particle sizes. In this case the scattering signature consists of the sum of the individual intensity functions for each α, scaled by its respective number density.

At any scatter angle θ_j the intensity is:

$$I_j = \sum_{i=1}^{m} \eta_i I_{\alpha_i}$$

where I_j is the observed intensity at θ_j

η_i is the number of particles of size α_i

I_{α_i} is the intensity scattered by particle α_i at θ_j

m is the number of size classes in the spray.

The above formulation assumes, first, that the particles are sufficiently far apart that the intensity signature for each particle, as formulated by Mie, is unaltered. Secondly, no substantial secondary scattering occurs within the suspension. In most practical cases of interest these limiting conditions can be avoided. It has been proved that the maximum allowable number density for a typical cloud lies between 10^9 and 10^{13} particles/cc[20]. This is adequate for most practical purposes.

To gain some insight into the effect of the size distribution width, shape, and the position of the modal mean of the particle suspension, on the scattered light, intensity functions were calculated in the i_1 plane using Mie theory for several particle distributions. To ascertain the effect of shape two standard distribution functions were assumed. The calculations are for water having refractive index m = 1.33.

(1) Normal distribution

$$n(\alpha) = \frac{1}{(2\pi)^{\frac{1}{2}}\sigma} \exp\left[- \frac{(\alpha - \bar{\alpha})^2}{2\sigma^2} \right]$$

α = non-dimensional size ($\pi D/\lambda$)

$\bar{\alpha}$ = mean size parameter ($\pi \bar{D}/\lambda$)

σ = standard deviation

(2) Zeroth order logrithmic distribution (Z.O.L.D.)

$$n(\alpha) = \exp\left[- \frac{(\log\alpha - \log\alpha_m)^2}{2\sigma_o^2} \right] / (2\pi)^{\frac{1}{2}}\sigma_o\alpha_m \exp[\sigma_o^2/2]$$

where $\sigma = \alpha_m \left[\exp(4\sigma_o^2) - \exp(3\sigma_o^2)\right]^{\frac{1}{2}}$ α_m = modal mean

The normal distribution is not a realistic representation of a naturally occurring distribution as negative values of α are possible. However, being symmetric, it provides a useful contrast with the Z.O.L.D., which is a skewed distribution. In both cases the modal value remains the same if the standard dviation is changed. The range of particle sizes of interest in this investigation was approximately 2-100μm. However, preliminary computations were limited to sizes between, α = 2-300 (diameters of 0.4-60μm with a light source of λ = 0.6328μm). Figures 4, 5, 6 and 7 show intensity signatures of normal distributions and zero order log distributions of various standard deviations, σ, and mean diameters, α. These were calculated from a set of individual intensity functions which had been computed beforehand and stored in a computer disc file. The size range restriction mentioned above was imposed by the available file capacity. Each distribution intensity signature was calculated from a large number of discrete sizes spaced at intervals of α = 2 (0.4μm for λ = 0.6328μm). Increasing the number of size classes so this interval became less than α = 1 made no apparent difference to the computed signatures. Increasing the size of the interval beyond α = 2, however, made a considerable difference; the computed signatures became more structured. It was assumed that the spraying systems of interest would generate relatively dense particle distributions. Therefore small intervals were used to compute the intensity signatures throughout the theoretical investigation. Subsequent practical work proved that this assumption was correct.

The curves in Figures 4-7, reveal that the distribution mean size and standard deviation has a considerable effect on the

scattered light polar diagrams. The shape of the forward scatter lobe was evidently dictated almost exclusively by the modal size of the distribution. Its width was relatively unaffected by the standard deviation of the distribution. However, the distribution width affects the degree of structure in the intensity function and tends to change the intensity of light scattered at the forward angle ($\theta = 0°$). A broadening distribution showed increasing loss of structure and more light being scattered forward. Comparison of equivalent normal and log distributions showed that skewed distributions have less structure than symmetric ones. If a rig were available for measuring the angular variation of scattered light from a suspension and provided a Z.O.L.D. or normal distribution was representative, particle size could be obtained by comparing the data with curves similar to those in Figures (4-7). The potential of this method is explored later.

Several design criteria for a light scattering experimental apparatus can now be established. The importance of the forward scatter cone meant it must be possible to obtain intensity measurements very near to the zero scatter angle. In practice the light scattered directly forward is superimposed on the main beam and is, as a consequence, unmeasurable. However, large particles (α >150) have a very narrow forward lobe and for a determination of size would require intensity measurements within 0.5° of the forward direction. The angular range of data necessary to characterise a distribution need not be greater than that shown in the accompanying figures for the range of sizes of interest. This is because the structure and absolute intensity of the scattered light signature diminishes beyond 15°. Measurements in this region would have been difficult in practice because the scattered light is

several orders smaller than the forward scatter. If the structure in the signature is to be detected an angular resolution of approximately 15 minutes of arc would be necessary. Finally, the light detection system must be capable of monitoring accurately changes of intensity which can cover several orders of magnitude.

A system of particle sizing in which experimental data in the sensitive forward scatter region is compared to a series of computed theoretical overlays is possible. It is flexible and does not require the insertion of a probe into the spray or suspension. The zero order log distribution function has been shown to be representative of many real distributions[6]. This is probably one of the best functions to use as a basis of comparison for obtaining particle size information. The technique has been applied experimentally to a variety of systems and the results are discussed in a later section.

If the comparison of theory and experiment could be automated, the sizing technique would assume much greater value. The following chapter describes several methods of data inversion tried by different research workers. This is a prelude to a description of the least squares inversion technique which constitutes a large part of this thesis.

1.3 A Review of Techniques for Obtaining Distribution Information from Light Scattering Data

Particle sizing techniques used by previous workers have generally fallen into one of four categories.

(1) Polarization techniques

(2) Turbidimetric methods

(3) Large angle variation of light scatter

(4) Measurements in the forward scattering cone.

The first three of these methods required the 'a priori' assumption of a specific distribution function. In many cases the zero order log distribution was used. Another distribution function which has had wide use is defined by,

$$p(\alpha) = C(\alpha - p) \exp\{-|(\alpha - p)/q|^3\}$$

where $p = 2\pi a_o/\lambda$

$\alpha = 2\pi a/\lambda$

$q = 2\pi s/\lambda$

C = normalisation constant

a_o = radius of the smallest particle

a_m = modal radius

a = particle radius

$a_m - a_o = 3^{-1/3} S$

S = determines the modal diameter of the distribution

1.3.a Polarization methods

Polarization techniques require the measurement of the scattered light in each of the two planes which constitute the solution of the Mie theory. The ratio of the light scattered in the two planes at the same angle of scatter is a unique measure of particle size. Measurements taken at several angles provide enough information to establish the mean size and distribution width of the particles under investigation.

For a polydisperse the polarization ratio is defined at a specific angle, θ, by,

$$p(\theta) = \frac{I_2(\theta)}{I_1(\theta)} = \int p(\alpha) i_2(\theta, \alpha) d\alpha / \int p(\alpha) i_1(\theta, \alpha) d\alpha$$

i = intensity function (Mie theory)

$p(\alpha)$ = number density function

The characteristics of the suspension are ascertained by comparing the angular experimental data with a series of computed figures evaluated for a set of distributions of various means and widths[7]. The technique is only useful for particles of submicron size where the differences between the two planes, i_1 and i_2 are large.

An alternative polarization method involves measuring the polarization ratio at one angle but for a variety of illuminating beam wavelengths (the polarization spectra method, ref (8)). The size dependent parameter is called the scattering ratio and incorporates the distribution function defined at the beginning of this section as follows.

$$\rho(p, q) = \frac{I_2(p, q)}{I_1(p, q)} = \frac{\int_0^\infty i_2(\alpha)(\alpha - p)\exp(-|(\alpha - p)/q|^3)d\alpha}{\int_0^\infty i_1(\alpha)(\alpha - p)\exp(-|(\alpha - p)/q|^3)d\alpha}$$

This technique has been used successfully to size particles around one micron in diameter[9] with small errors well within the range experienced in electron microscope techniques. In order to use the method, however, extensive calculations of the pertinent parameters had to be undertaken for a large range of refractive index and the previously defined quantities q and p. The angle of scatter commonly adopted was 90°. As before, the distribution information was obtained by comparing experimental results with a large series of theoretical equivalents.

The two techniques can, if required, be combined; measurements being taken simultaneously at several wavelengths and scatter angles.

1.3.b Turbidimetric techniques

These methods involve the measurement of attenuation of an illuminating source. This attenuation arises because light is intercepted and scattered out of the beam by the particle suspension. The transmission, T, of light at one wavelength can be expressed as

$$T = \frac{I_i}{I_o} = \exp(-\tau \ell)$$

τ = turbidity

ℓ = path length

I_i = intensity of attenuated beam

I_o = intensity of beam at input.

For a polydisperse the turbidity is,

$$\tau = (\lambda^2/2\pi) \int_o^\infty p(\alpha) \sum_{n=1}^{\infty} (2n+1)\{|a_n|^2 + |b_n|^2\}\, d\alpha$$

where λ = wavelength of illuminating beam

a_n and b_n are constants derived in the Mie theory.

Turbidimetric measurements taken at various wavelengths can produce detailed distribution information. Here again it is necessary to define a particular quantity which can be both measured, and predicted with Mie theory.

The non-dimensional quantity used is,

$$\frac{\lambda\tau}{\phi} = 3\pi \frac{\int_p^\infty \Sigma_{sca}(\alpha - p)\exp\{-|(\alpha - p)/q|^3\}\, d\alpha}{\int_p^\infty \alpha^3(\alpha - p)\exp\{-|(\alpha - p)/q|^3\}\, d\alpha}$$

$$\Sigma_{sca} = \sum_{n=1}^{\infty} (2n+1)\{|a_n|^2 + |b_n|^2\}$$

ϕ is the volume fraction of scattering material,

$$\phi = \int_{a_o}^\infty (4\pi a^3/3)\, p(a)da$$

a = particle radius

α = non-dimensional parameters ($2\pi a/\lambda$)

All other quantities are as defined earlier. The distribution derived at the beginning of the chapter is incorporated in the $\lambda\tau/\phi$ quantity.

The droplet or particle distributions are ascertained by direct visual comparison of experimental data with theory. A comparison of the polarization spectra method, the last-mentioned technique and electron microscopy proved that the two light scattering methods were capable of excellent results[10]. Particle measurement, in both techniques is again limited to the sub-micron range where the measured and computed parameters are sensitive to particle size, α.

Particles have been sized successfully in a moving stream using the multi-wavelength turbidity approach[11]. The transmission through wet steam flows was measured and compared with a suitable set of theoretical results to obtain the Sauter Mean Diameter of the fog.

The attenuation was expressed as,

$$\frac{I}{I_o} = \exp\left\{-\frac{3}{2}\left(\frac{E}{D_{32}} C_v t\right)\right\}$$

where t = optical path length

D_{32} = sauter mean diameter

C_v = volume fraction of suspension

E = particle extinction coefficient.

The parameter used for characterising the suspension was the wave number (π/λ) dependence of the attenuation. No assumption of distribution shape was made, but only a mean size was obtained from the data.

The Sauter Mean diameter is also known as the volume-surface mean diameter and can be expressed as,

$$D_{32} = \frac{\sum_{i=1} n_i D_i^3}{\sum_i n_i D_i^2}$$

n_i = number density

D_i = particle size

If the particles transmit all incident energy and absorb none as heat, the extinction coefficient E is equivalent to the scattering cross section C_{sca} given by

$$C_{sca} = (\lambda^2/2\pi)\ \Sigma_{sca}$$

All the previously described techniques are suitable for the sizing of particles whose refractive indices are real. Certain types of material, soot and TiO_2 for example, have refractive indices which under certain conditions, i.e. high temperature, can assume complex values. In this case the analysis must be modified to account for the additional energy which is absorbed by the particle as heat. In the presence of absorption the extinction cross section can be calculated from Mie theory as

$$E = C_{ext} = \lambda^2/2\pi \sum_{n=1}^{\infty} (2n+1)\ \{Re(a_n + b_n)\}$$

For non-absorbing particles

$$C_{ext} = C_{sca}$$

The absorption cross section can be calculated from

$$C_{abs} = C_{ext} - C_{sca}$$

If it is required to calculate the angular variation of light intensity for polarization measurements it is only

necessary to apply a complex refractive index to the Mie theory. The intensity solutions can be used directly in the polarization and scattering ratios.

1.3.c Large angle variation of light scatter

It has already been shown that the variation of light scattered radially by a particle is a unique indication of its size. If the particles are very small ($\alpha < 5$) the lobes of the intensity signature extends gradually over the whole angular range of 0-180°. As the particle size is increased the lobular structure becomes compressed, the peaks and troughs migrate slowly towards the forward ($\theta = 0$) direction. Generally a large quantity of light is scattered forward in the form of a pronounced lobe. This lobe, which is symmetric about $\theta = 0°$, is highly characteristic of the mean particle size. To obtain accuracy from an angular scattering technique it is advisable to make measurements in this lobe. If distribution detail is required the angular measurements should be extended to include the secondary structure which exists beyond the forward scatter lobe.

Mie theory can predict the light scattered in any direction by a particle of known size and refractive index. However, the computations associated with measurements are simplified if measurements are confined to one of two planes. These are perpendicular and parallel to the electric vector of the illuminating beam and are respectively the i_1 and i_2 intensity solutions which constitute the Mie theory. These are the same planes which are used to calculate the aforementioned polarization and scattering ratios. The compression of the structure toward the forward angle, as the particle size

increases, occurs in both planes. This dictates that the choice of angular range of measurement be tailored to the particle size under investigation. Sub-micron particles require measurements over the whole angular range (0-180°). Particles greater than $\alpha = 20$ can be measured from angular data taken over 0-15°. The next chapter describes a technique in which data taken over 0-3° is sufficient to size particles over $\alpha = 25$ ($d = 5\mu m$, $\lambda = 0.6328\mu m$). The need to establish accurately the detailed lobular structure of the intensity signature dictates that the measurement of scattered light be made at a large number of angular stations. With small particles, $\alpha < 5$, the angular interval can be quite large ($\sim 5°$). For larger particles the interval may have to be as small as a few minutes of arc.

A technique using the angular variation of light intensity has been suggested to measure the distribution of particle sizes in condensing and evaporating aerosols[12]. The particles were generally sub-micron although there was no reason why the technique should not be extended to larger particles. Measurements were made at a large number of angular stations between $\theta = 8-175°$. A zero-order log distribution form was assumed. A theoretical intensity signature was calculated for a distribution of arbitrary mean and width and the new signature was compared with the experimental data. The assumed distribution was progressively altered until the sum of the squares of the differences between theoretical and experimental distribution intensity data were minimised.

The large angle scatter method, discussed in section 1.2, which uses theoretically derived intensity signatures as comparative overlays, falls into this category of scattered light sizing techniques. The method discussed in the previous paragraph is an

attempt to automate the purely visual comparative technique for obtaining particle size.

1.3.d Measurements in the forward scatter cone

As already stated, the shape of the forward scatter lobe is highly representative of particle size[13]. In recent years several techniques have been suggested which require detailed measurements to be taken within this forward scatter region[14]. The light scattered forward is primarily due to diffraction and is relatively independent of the optical properties of the particle. The intensity function in this region can be calculated from an approximation of the Mie theory. In the approximation the intensity at any angle β around a particle a is written

$$I = I_o\, a^2\, J_1(Ka\beta)/\beta^2$$

providing the approximation $\sin\beta = \beta$ is acceptable and that the true particle size $a >> \lambda$.

a = particle size

K = $2\pi/\lambda$

J_1 = is a bessel function of the first kind, first order

I_o = input intensity of the beam.

If a distribution of particles is present and is represented by a function f(a), the number density in the interval a to a + da is f(a)da. The light scattered at β is,

$$I = \frac{I_o}{\beta^3} \int_o^\infty f(a)\, a^2\, J_1^2(Ka\beta)da$$

This integral can be inverted by applying a theorem due to Titchmarsh[15], to provide an expression for f(a).

$$f(a) = \frac{-2}{Ka} \int_0^\infty \beta \, J_1(Ka\beta) \, Y_1(Ka\beta) \, \phi(\beta) d\beta$$

Y_1 is a Newmann function

and

$$\phi(\beta) = \frac{d}{d\beta} \left| \pi K^3 \beta^3 \frac{I}{I_o} \right|$$

A further approximation makes the computation of f(a) from experimental intensity data relatively straightforward. The exact procedure is outlined in ref.(16) and results in the expression,

$$f(a) = \frac{-2K}{a^2} \sum_{\beta = \beta_{min}}^{\beta = \beta_{max}} Ka\beta \, J_1(Ka\beta) \, Y_1(Ka\beta) \, D(\beta^3 \frac{I}{I_o})$$

The rather unrealistic integration limits have been replaced by practical limits dictated by the $\beta = \sin\beta$ approximation and the physical restraint which disallows measurement at $\beta = 0$. This apparently drastic reduction of the integral range has little effect as the intensity equation is only valid over a limited angular range from the forward direction.

Measurement of intensity variations at small (3') intervals over an angular range of three degrees can be applied to the equation to produce the distribution function, f(a). No assumption of the form of the distribution is necessary. The analysis will reconstruct accurately a distribution of arbitrary shape for particles between 5 and 60μm. The assumption of diffraction dominated scatter fails below a = 5μm and above 60μm.

This method has been used by the author to measure the sizes of glass beads contained in a resin block. The results were relatively accurate, comparing well with the size

distribution as measured by microscope. The data is shown on Figure 8.

In an alternative technique measurements are made of the transmission of light through a suspension in which the detector simultaneously measures some of the forward scattered light[17]. The effective cross section of the particle is apparently reduced because of the inclusion of this extra light.

The scattering cross section efficiency term is defined by

$$Q_{sca} = \frac{\text{Effective cross section of the particle}}{\pi\alpha^2}$$

where $\alpha = \pi D/\lambda$

This can be re-expressed as:

$$Q_{sca} = {}^{1}/\alpha^2 \int_0^{\pi} (i_1 + i_2)\sin\theta \, d\theta$$

i and i_2 are the Mie solution intensity functions mentioned previously in chapter (1.2).

When some of the forward scatter is included, the efficiency is reduced by the light scattered in the acceptance cone of half-angle, ω.

$$Q_{eff} = Q_{sca} - ({}^{1}/\alpha^2) \int_0^{\omega} (i_1 + i_2)\sin\theta \, d\theta$$

The term $R = Q_{eff}/Q_{sca}$ can be approximated, for particles greater than $\alpha = 20$, by,

$$R = \tfrac{1}{2} \left|1 + J_0^2(\alpha\omega) + J_1^2(\alpha\omega)\right|$$

where J_0 and J_1 are Bessel functions of order zero and one.

From the expression for transmission,

$$\ell n \frac{I}{I_o} = \pi \ell \int_R Q_{sca} \alpha^2 p(\alpha) d\alpha$$

where ℓ = path length

an expression for the distribution function can be derived,

$$p(\alpha) Q_{sca} \alpha^2 = 2\pi \int_o^\infty M(\omega) \left| -J_1(\alpha\omega) N_1(\alpha\omega) (\alpha\omega) \right| d\omega$$

$$\text{where } M(\omega) = \frac{4}{\ell \lambda^2} \frac{d}{d\omega} \left(\omega^2 \frac{d(\ell n\ I)}{d\omega}\right)$$

J_1 and N_1 are Bessel and Neumann functions. $M(\omega)$ can be calculated from experimental values of I obtained by varying ω in known fashion. $p(\alpha)\ Q_{sca}\ \alpha^2$ can be obtained by integrating the whole of the equation graphically. This technique has produced accurate reconstructions of distributions of particles around 20μm where the limiting value $Q_{sca} = 2$ can be adopted. The term Q_{sca} increases with α to a maximum value of approximately 5 and then oscillates about and eventually approaches a value of 2 in the limit of large particles.

1.3.e Practical considerations in the use of scattering techniques

Of the techniques discussed in this section only one has the potential to size particles of both submicron dimensions and the much larger diameters associated with sprays, namely the large-angle scatter technique using Mie theory as the comparative standard. The polarization methods are size limited because of their relative insensitivity at particle sizes above 1μm. The small angle diffraction theories are valid for particles between 5 and 60μm.

Each method has its own practical peculiarities which must be considered when a choice of technique has to be

made. The particle size range aspect has already been discussed. A further consideration concerns the nature of the measuring volume. The polarization spectra method has a fixed volume; however, if the measuring angle is fixed at 90° as is recommended in the literature, the scattered light levels experienced will be very low. The angular polarization method suffers from a problem common to most angular measuring techniques; that is, as the observation angle is altered, the scattering volume observed by the detection optics changes in proportion to the reciprocal of the sine of the scatter angle, θ. This effect is particularly powerful at small scatter angles, where the measuring volume is large and changes considerably in size as the observation angle is altered. The particle suspension must be either very much larger than, or smaller than, the measuring volume irrespective of the angular range of measurement of light scatter. The large angle scatter method shares this problem, but because there is not a requirement for measurements at very small angles, the scattering volumes observed by the receiving optics never become excessively large.

Light intensity measurements performed at scattered light angles less than $\theta = 1°$ are known to encounter problems of scattered light noise and poorly defined measuring volumes. The apparatus (similar in concept to that described in section 1.6.b) which was used by the author to obtain data for the Shrifrin technique (described above), was intended to overcome these difficulties. However, problems with background noise and secondary scatter were severe, particularly at angles less than $\theta = 0.5°$. As measurements were ultimately to be made in a hot gas rig of restricted dimensions

where secondary scatter was a particular problem it was decided not to adopt a small angle method. In addition, at this stage in the project it was hoped that a single technique to cover the entire range of particle sizes of interest ($\bar{d}$ = 1-100μm) in the envisaged heat transfer experiments would be found. As it transpired the large angle scattering method finally proved to have a similar range of applicability as the 'Shifrin' small angle method. However, the new technique required less data and did not need measurements to be made at very small angles ($\theta < 0.5°$). In addition, an alteration in the range of data collected offered the possibility of extending the range of sizes that could be measured to larger or smaller particles. The small angle methods described offered no prospect of extending their range of applicability.

The large angle measurement of light scatter appears to offer many practical advantages over the alternative techniques. The measuring volume is confined to a reasonable size allowing measurement in a small part of a large system. The change in volume did not at this stage seem excessive. The possibility of sampling a different distribution with a change of angle appeared small. The avoidance of practical problems was not in itself sufficient to allow the measurement of particles over the range of sizes required. The existing techniques for processing scattered light data to give mean size and standard deviation of the distribution were regarded as unsatisfactory. For example, it has been found in previous work that it is possible to obtain a seemingly plausible result from totally inaccurate data.

Least squares analysis provides a technique for extracting distribution data from large angle data. No 'a priori' assumption of distribution shape is necessary; a true distribution shape is obtained from the experimental data providing the data is truly representative of the suspension.

The basic theory is defined in the next section.

1.4 The Application of Least Squares Fitting to Particle Sizing

1.4.a Least squares theory

The method of least squares fitting is one of a family of techniques which constitute the more general subject of 'Approximation of Functions'.

If f(x) is the function to be approximated and F(A, x) is a linear approximating function, the best fit is achieved by minimising the 'distance function', $\bar{E}(f(x), F(A, x))$. For the most part these functions are norms which have the form[18],

$$L_p(f) = \left|\int_o^{'} [f(x)]^p dx\right|^{1/p} \quad p > 1 \quad - \quad 1.4.1$$

or for approximation purposes

$$L_p(F(A, x) - f(x)) = \left|\int_o^{'} [F(A, x) - f(x)]^p dx\right|^{1/p} \quad - \quad 1.4.2$$

In most instances the pth root can be deleted[18] when obtaining the best fit without affecting the solution. The function to be minimised then becomes,

$$L_p = \left|\int_o^{'} [F(A, x) - f(x)]^p dx\right| \quad - \quad 1.4.3$$

Choice of the value of p has a profound effect on the nature of the achieved approximation. The value p = 2 is the least squares norm. The other norms commonly used are those of p = 1 and p = ∞. In the case of p = 1 the area difference between f(x) and F(A, x) is minimised, and for p = ∞ the maximum differences are minimised. Rice[18] describes the L_2 approximation as having the least 'moment of inertia' about f(x). The L_2 norm is that

most universally used as it offers the least involved way of obtaining a good approximation. The basic theory is well developed and minimisation of the distance function involves simple calculus operations. The result is a matrix of easily calculable coefficients. In many cases exploitation of the unique characteristics of orthogonal functions is possible, considerably simplifying the solution procedure.

To consider a general case, suppose $y(x)$ is to be approximated by the general function $\phi(A, x)$,

where $\phi(A, x) = a_1\phi_1(x) + a_2\phi_2(x) + \ldots a_n\phi_n(x) = \sum_{i=1}^{n} a_i\phi_i(x)$

$\phi_i(x)$ are linearly independent functions.

The best L_2 approximation is achieved by minimising

$$\left| \int_o^{'} (y(x) - \phi(A, x))^2 dx \right| \qquad - \qquad 1.4.4$$

The pth root has been deleted as suggested earlier. A minimum occurs where all the derivatives $\partial / \partial a_i = 0$. Subsequent differentiation of the above function i times produces the normal equations,

$$\sum_{i=1}^{n} a_j \int_o^{'} \phi_i(x)\, \phi_j(x)dx = \int_o^{'} y(x)\, \phi_i(x)dx \quad i = 1, 2 \ldots n \quad - \quad 1.4.5$$

Where the functions are expressed as a set of finite points the normal equations have the form,

$$\sum_{i=1}^{n} a_j \sum_{k=1}^{m} \phi_i(x_k)\, \phi_j(x_k) = \sum_{k=1}^{m} y(x_k)\, \phi_i(x_k) \quad i = 1,2 \ldots n - \quad 1.4.6$$

These result from the minimisation of the distance function

$$\left| \sum_{k=1}^{m} y(x_k) - \phi(A, x_k))^2 \right|$$

The normal equations can be solved simultaneously to give the coefficients a_i directly.

When the functions are expressed as finite point sets

$$\begin{bmatrix} \sum_{k=1}^{m} \phi_1(x_k)^2, & \sum_{k=1}^{m} \phi_1(x_k)\phi_2(x_k) \ldots \Sigma\phi_1(x_k)\phi_n(x_k) \\ \sum_{k=1}^{m} \phi_2(x_k), & \phi_1(x_k) \qquad\qquad \Sigma\phi_2(x_k)\phi_n(x_k) \\ \vdots & \\ \sum_{k=1}^{m} \phi_n(x_k)\phi_1(x_k) & \ldots\ldots\ldots\ldots \sum_{k=1}^{m} \phi_n(x_k)^2 \end{bmatrix} \begin{bmatrix} a_1 \\ a_2 \\ \vdots \\ ak \end{bmatrix} = \begin{bmatrix} \sum_{k}^{m} y(x_k)\phi_1(x_k) \\ \sum_{k}^{m} y(x_k)\phi_2(x_k) \\ \vdots \\ \sum_{k}^{m} y_k(x_k)\phi_n(x_k) \end{bmatrix} \quad - 1.4.7$$

The resulting accuracy of the computed function $\phi(A, x)$ will depend on several factors:

(1) The choice of the functions $\phi_i(x)$.

Ideally these should have properties which are shared by the function being approximated.

(2) In the case of finite points sets the available number of data points for each function $y(x)$ and $\phi_i(x)$ should be appreciably greater than the number of functions ($m >> n$).

(3) The resulting matrix must be soluble.

If the normalised determinant of the matrix is appreciably less than unity, the matrix is ill conditioned. In this case the resulting solution is totally unrepresentative of the original function $y(x)$. Much of the following text describes methods of avoiding ill conditioning in the normal equations. It became apparent early in the development work

that the least squares matrices used for obtaining size information were badly ill conditioned.

1.4.b Orthogonal functions and least squares

Many of the computational difficulties associated with the solution of large matrix equations can be avoided if the approximating functions $\phi_i(x)$ are orthogonal functions. The system of equations $[\phi_i(x)]$ is orthogonal on the interval a, b if

$$\int_b^a \phi_i(x)\,\phi_j(x)dx = 0 \qquad i \neq j \qquad - 1.4.8$$

or $\sum_{k=1}^{m} \phi_i(x_k)\,\phi_j(x_k) = 0 \qquad i \neq j$ for finite point sets. $a < xk < b$

Should the normal equations be derived for an approximating function made up of orthogonal functions the result is a coefficient matrix whose off-diagonal values are all zero.

$$\begin{bmatrix} \sum_{k=1}^{m} \phi_1(x_k)^2, & & & \\ & \sum_{k=1}^{m} \phi_2(x_k)^2 & & \\ & & \ddots & \\ & & & \sum_{k=1}^{m} \phi_n(x_k)^2 \end{bmatrix} \begin{bmatrix} a_i \\ a_2 \\ \cdot \\ \cdot \\ a_n \end{bmatrix} = \begin{bmatrix} \sum_{k=1}^{m} \phi_1(x_k)y(x_k) \\ \cdot \\ \cdot \\ \cdot \\ \sum_{k=1}^{m} \phi_n(x_k)y(x_k) \end{bmatrix} \qquad - 1.4.9$$

The coefficients are obviously given by

$$a_i = \sum_{k=1}^{m} \phi_i(x_k)y(x_k) \Big/ \sum_{k=1}^{m} \phi_i(x_k)^2. \qquad - 1.4.10$$

The advantages of approximation with orthogonal functions are readily apparent. Complicated elimination schemes of solution are avoided, and problems with ill conditioning do not arise. Typical orthogonal functions used for approximation are Chebyshev and Legendre polynomials. The schemes are described in detail in reference 19.

1.4.c Estimation of size distributions using least squares theory

The intensity of light at any angle, θ_j, scattered by a particle suspension can be expressed as,

$$I_{exp_j} = \sum_{i=1}^{n} n_i I_{ij} \qquad 1.4.11$$

As I_{ij} are known functions provided by Mie theory, an L_2 distance function can be formed over the set of arguments $j = 1,2,\ldots M$, i.e. all the observation angles θ_j.

$$L_2 = \left| \sum_{j=1}^{m} (I_{exp_j} - \sum_{i=1}^{n} n_i I_{ij})^2 \right| \qquad 1.4.12$$

Differentiation of the distance function yields the normal equations from which the number densities (n_i) for each size class, α_i, can be derived.

In earlier research Vardon[20] explored the possibility of using this technique for reconstructing distributions from synthesized experimental data. The research showed that a distribution consisting of a limited number of size classes, about eight, could be reconstructed accurately. Basic error analysis showed that experimental accuracy in the measurement of intensity at a fixed angle, had to be better than 1%. In addition the number of angular measurements, θ_j, had to exceed the number of size classes, α_i, by at least a factor of three. Application of this method of analysis to real data, however, proved unsatisfactory for two main reasons:

(1) For the most part a real spray or suspension consists of an infinite number of size classes, not a limited number of

discrete sizes.

(2) The normal equations were invariably ill-conditioned and produced erroneous results.

Several other practical problems also became apparent. The original researcher[20] had the benefit of foreknowledge of the distribution and this was used to make an accurate choice of the size classes which were applied to the analysis. In practice the contributing classes are unknown and the correct choice of the approximating functions, I_{ij}, must be obtained by trial and error. The computation time required to calculate the theoretical intensity functions also became a problem. For large particles (say >50) up to 100 seconds of computer time was necessary. The following is a description of the developments and considerable modifications that were necessary to overcome all of these problems.

The excessive time involved in calculating the intensity function was reduced relatively easily. A family of intensity functions was computed in the range $2 < \alpha < 300$, at intervals of 2, and was permanently stored in a disc file. Once the initial lengthy procedure of computing and storing the data was complete the scattering functions could be rapidly recalled in any order with the minimum delay. The same file was used throughout the investigation. The data was stored at scatter angle intervals of 0.125° and covered an angular range of 15°.

In theory, increasing the number of size classes to a level more representative of a real distribution can be done simply by increasing the size of the normal equation matrix. A distribution consisting of 100 individual size classes would

result in a normal equation matrix which has 100 x 100 elements. When a matrix of this size was used the results became hopelessly ill-conditioned making an accurate solution impossible. The problem was partly overcome by blocking together the intensity functions of adjacent sizes as one size class. In effect this was reconstructing the original distribution as a histogram rather than a continuous curve. In general fifteen blocked size classes were used, each consisting of five intensity functions for individual size classes spaced at intervals of $\Delta\alpha = 2$. The maximum width of distribution that could be accommodated was $\Delta\alpha = 150$ (30μm, $\lambda = 0.6328$μm). This could be extended by including more than five sizes in each size class.

Three overlapping sets of fifteen size classes were applied in the analysis of a set of scattering data. The minimum size in each range was $\alpha = 2$, 74 and 150 respectively (4, 15 and 30μm, $\lambda = 0.6328$μm). The computer programme which was written to test the least squares theory began its operation by reading intensity data from an input file, or computed synthetic data, as required. This data was then applied to the analysis with each of the three sets of overlapping size classes.

Overcoming ill-conditioning of the normal equations proved difficult. One possible method is to scale the normal equations. One of the most elegant ways of scaling is to transform the equations to produce a matrix of simple correlation coefficients[21]. The normal equations then become,

$$\sum_{j=1}^{n} n_i^* \left[\frac{\frac{1}{m-1} \sum_{j=1}^{m} (I_{ij} - \bar{I}_{ij})(I_{kj} - \bar{I}_{kj})}{\frac{1}{m-1} \sum_{j=1}^{m} (I_{ij} - \bar{I}_{ij})^2 \frac{1}{m-1} \sum_{j=1}^{m} (I_{kj} - \bar{I}_{kj})} \right]$$

$$= \left[\frac{\frac{1}{m-1} \sum_{j=1}^{m} (I_{exp_j} - \bar{I}_{exp_j})(I_{kj} - \bar{I}_{kj})}{\frac{1}{m-1} \sum_{j=1}^{m} (I_{exp_j} - \bar{I}_{exp_j}) \frac{1}{m-1} \sum_{j=1}^{m} (I_{kj} - \bar{I}_{kj})} \right]$$

$$k = 1,2,....n \qquad 1.4.13$$

n_i^* = transformed solution for the number density of size α_i

$\bar{I}_j = \frac{1}{m} \sum_{j=1}^{m} I_j$

The matrix consists of simple correlation coefficients between all pairs of the independent variables. The right hand side is made up of correlation coefficients between the independent and dependent variables. The coefficient matrix is characterized by a diagonal of unity which represents perfect correlation between pairs of identical intensity functions. All other coefficients lie within the limits +1 and -1.

The solution of these equations can be transformed back to the solution of the original normal equations, through the expression

$$n_i = \frac{S_{exp}}{S_i} n_i^* \qquad i = 1,2,....n \qquad 1.4.14$$

S_i and S_{exp} represent the standard deviations of the ith independent variable (I_{ij}) and the dependent variable (I_{exp}) respectively.

These equations were used to obtain distribution reconstructions from synthetically derived intensity signatures

similar to those in Figures (4-7). The data was synthesized and then inverted back to a distribution within the same computer programme. The intensity signature and subsequent inversion were both obtained using the disc file of individual size class intensity functions described earlier.

To ensure maximum accuracy the equations were solved with a sophisticated Gauss elimination and back substitution technique. This included pivotal condensation, or row interchanging, and iteration on the residuals between the right and left hand sides of the equations. All computation was undertaken in double precision arithmetic.

1.4.d Discussion of results of the transformed least squares normal equations

Theoretically derived intensity functions for both Z.O.L.D. and Gaussian normal distributions were used as input data for testing the least squares analysis. Generally an accurate reconstruction of the original distribution was obtained. Examples of these are shown in Figures 9 and 10. The computer programme solved the least squares normal equations with each of the three overlapping size ranges in turn. Figure 11 shows a set of typical results obtained for each of the size ranges. Only when a size range included the size classes which constituted the distribution being reconstructed was a plausible distribution solution, as demonstrated in Figures 9 and 10, obtained. This was a particularly important discovery. The large positive values of number density which were predicted below $\alpha = 20$ arose continuously during the theoretical study. The reason for this is that the characteristic structure in the intensity function of an individual particle migrates to larger angles as α decreases.

The angular range of data used for this study covered a maximum range of 0-15°. For most particles of interest the characteristic structure exists within these limits. However, at $\alpha = 2$ for example the intensity signature over this angular range is a monotonic decay of a small fraction of an order of magnitude. Any attempt to find a least squares solution for a set of data that changes over several orders of magnitude with a function which changes by so little will invariably lead to errors. If distribution information is required on such small particle sizes the angular range of data should be increased. For particles less than $\alpha = 2$ measurements from 0-180° are probably necessary. It would also be necessary to increase the number of, and decrease the range of sizes in the sets of size classes applied to the analysis. However, where a distribution is so broad that large and small particles are included, errors of the kind experienced and illustrated at the low α range on the upper curve on Figure 11 are inevitable unless high resolution data is collected over a large range of angles. Practically, this would be both time-consuming and costly, with the probability of any real gain being uncertain. It is interesting to note that Abbiss[16] experienced similar problems with the Russian small angle diffraction technique for obtaining distribution data from light scattering. Here again the angular range was limited to a range of less than 4° from the forward direction. The minimum size limit in this case was 5μm, equivalent to $\alpha = 25$ with a helium-Neon illuminating beam. For the most part the problems associated with these small particles were not important, because the majority of distributions investigated did not include the small particle size classes.

The value of using a blocked intensity function as one size class can be assessed from Figure 12. Two reconstructions have been attempted using identical data, one with blocked intensity functions as mentioned previously, the other with a limited number of discrete functions. The blocked-functions least squares solution produced a reasonably accurate reconstruction of the original distribution and is shown in Figure 12(a). The solution obtained with discrete size classes is barely relateable to the original distribution. The large positive and negative excursions below $\alpha = 60$ arise because the analysis is attempting to minimise the difference between the smooth set of experimental data and a linear combination of a small number of highly oscillatory functions. Had the experimental data comprised a suspension of discrete sizes then a solution could have been obtained. However, most sprays consist of a continuous envelope of particle sizes, in which case the use of blocked functions becomes a necessary expedient.

In an experiment the range of angular measurements which it is possible to make is subject to practical limits. First, the sensitivity of the collecting optics dictates the minimum measureable intensity, and hence the maximum angle of scatter. Secondly, the forward scattered light is orders of magnitude weaker than, but is superimposed on, the main illuminating beam; the two are indistinguishable. Therefore, it was important to find out how the least squares solution was affected by the absence of data at the extreme ends of the angular range. It was not surprising to find that distributions with relatively small mean sizes ($\alpha < 90$) were sensitive to the loss of data at the larger angles but insensitive to the absence of data near 0°.

These points are adequately demonstrated in Figures 13 and 14. The former shows reconstructions obtained after deleting input data up to 1.25° from the forward direction. Figure 14 shows reconstructions of the same distribution after deleting scatter data at angles above 8.625°. The loss of accuracy, although not great, is more significant with the loss of large angle data rather than that at small, forward angles. Conversely, if the distribution is centred around particle means in excess of $\alpha = 150$, the least squares reconstruction is affected most by the loss of forward scatter angular data. It was found necessary to provide data to within 0.5° of the forward direction if an acceptable reconstruction was required. Extending this limit beyond 0.5° resulted in a rapid loss of accuracy such that no recognisable solution was obtained. An additional, important parameter was the choice of angular intervals used to characterize the intensity signature. The value used in this investigation, $\Delta\theta = 0.125°$, was chosen following a close inspection of theoretical intensity signatures such as those in Figures 4, 5, 6 and 7. The major criterion was the necessity of containing sufficient detail in the scattered intensity diagram. Increasing this interval to 0.25° resulted in no change in the reconstructions of distributions below $\alpha = 150$, providing the number of angular points exceeded the number of size class by a factor of four. In all cases reducing this factor below four caused a complete loss of accuracy; this complied with the findings of a previous worker[20]. Distributions centred around the nominal value of $\alpha = 200$ could not be reconstructed with an angular interval of $\Delta\theta = 0.25°$. As in the previous cases the transition from an acceptable to

an unacceptable solution appeared to be relatively sudden. The lobular structure in the intensity signatures of individual particles above α = 200 is too detailed to be captured by an angular interval of this size.

An ability to measure three orders of magnitude change in light intensity over an angular range of 0.5°-9° would allow the estimation of particle sizes from α = 20-200 (4-40μm, λ = 0.6328μm). This size range would be increased substantially if measurements over the whole spectrum of scattering angles were possible (0-180°). In theory it would then be possible to extract distribution information from scattered light from particles in a size band in the submicron (α < 5) range. The lower band limit is the Rayleigh region where the particle signatures are of the same form irrespective of size. This precludes measurements of particles in the region of interest to researchers in the nucleation field, (α = 0-0.07). No currently available light scatter technique can produce size distribution information in this area.

The upper limit is less easy to establish but is certainly in excess of α = 300, the self-imposed limit in this work. However, at some large particle sizes the forward scatter cone must assume proportions comparable to the beam dimensions. The loss of detail in the forward lobe must inevitably affect the accuracy of an attempted distribution inversion using the least squares method.

The ultimate aim of the technique is to process experimental data to obtain distribution information of a real suspension. The analysis should be capable of providing an accurate result despite the presence of experimental error.

However, whenever a least squares solution was attempted the normalised determinant of the normal equations was typically between 10^{-40} and 10^{-60}. The equations are still very ill-conditioned. When the synthetic input data was truncated from the full range of digits available in the computer to three, a solution proved impossible. The sensitivity of the right hand side of the equations to small changes in value is a classic manifestation of ill-conditioning. Any attempt to process experimental data, where the best apparatus would only provide data accurate to three places of decimals, will inevitably fail. However, the problem is purely associated with the solution procedure. If accurate data is available the proper solution of the equations can be made to provide the required information. Ill-conditioning of the least squares normal equations has been the subject of much research in recent years as it severely limits the usefulness of the technique. The equations are ill-conditioned by their very nature[22]. During the triangularising stage of Gauss elimination, numbers in the matrix are successively reduced in value until they are comparable with the computer round-off error. From that point on the loss of accuracy is dramatic. As the unknowns are then computed successively by back substitution the accumulated error affects all of the solution values. The following section describes a technique for solving the normal equations which avoids these problems. It allows acceptable solutions to be obtained from data of whose accuracy is comparable to that obtained experimentally. It is a matrix decomposition technique based on orthogonal transformation of the independent variable.

1.5 Least Squares Approximation with Gram-Schmidt Orthonormalisation

If the normal equations include a large number of unknowns a solution often becomes impossible using standard matrix decomposition methods. The problem arises because the decomposition techniques which are most often used involve successive subtractions which invariably produce very small numbers. These numbers are, as a consequence, badly influenced by computer round-off error. The least squares normal equations are particularly susceptible to this problem because of their close similarity to the troublesome Hilbert matrix. This has been adequately discussed by Golub[22] and Osborne[23]. An alternative scheme of matrix decomposition has been suggested by Davis and Robinowitz[24] using orthonormal transforms of the independent variables. The course of the computational procedure is altered such that small number computations are avoided and accuracy is maintained.

1.5.a The Gram-Schmidt orthonormalisation procedure

As discussed previously, the approximation problem is considerably eased if the approximating functions are orthogonal. The normal equations resolve into a form where all but the main diagonal elements of the coefficient matrix have a coefficient value of zero. The diagonal values can assume unity value if, in addition, the functions are orthonormal rather than orthogonal. Orthonormal functions, which are expressed as a set of finite points, have the property,

$$\sum_{j=1}^{N} (\phi_{ij} \times \phi_{kj}) = \begin{cases} 0 & i \neq k \\ 1 & i = k \end{cases} \qquad 1.5.1$$

A least squares approximation of a function can be easily obtained in the same way as with orthogonal functions, i.e.

$$Ie_j = \sum_{i=1}^{m} n_i \phi_{ij} \qquad 1.5.2$$

where the coefficients are given by,

$$n_i = \sum_{j=1}^{N} (Ie_j \times \phi_{ij}) \qquad 1.5.3$$

This has the same form as equation 1.4.10 except for the denominator which is now unity. This results from the condition, shown in (1.5.1), that occurs when two identical orthonormal functions are multiplied vectorally.

In many cases the approximating functions are not orthonormal. However, it is possible to produce an equivalent set of functions, which are orthonormal, using the Gram-Schmidt procedure. These are obtained by linearly combining the original functions in the form,

$$\begin{aligned}
\phi_{1_j} &= a_{11} I_{1_j} \\
\phi_{2_j} &= a_{21} I_{1_j} + a_{22} I_{2_j} \\
\phi_{3_j} &= a_{31} I_{1_j} + a_{32} I_{2_j} + a_{33} I_{3_j} \qquad 1.5.4 \\
&\\
\phi_{mj} &= a_{m_1} I_{1_j} + a_{m_2} I_{2_j} + \ldots . a_{mm} I_{mj}
\end{aligned}$$

where I_{ij} are the original, non-orthonormal functions, and where ϕ_{ij} now depicts the orthonormal equivalents. The least squares approximation using the new functions, ϕ_{ij}, has an identical form to that of equation 1.5.2. However, this can be re-expressed in terms of the original functions by substituting ϕ_{ij} in (1.5.2) and (1.5.3), with (1.5.4), i.e.

$$Ie_j = \sum_{i=1}^{m} (Ie_j, \phi_{ij}) \sum_{k=1}^{i} d_{ik} I_{kj} \qquad 1.5.5$$

$$= \sum_{k=1}^{m} n_k I_{kj} \qquad 1.5.6$$

where $$n_k = \sum_{i=k}^{m} (Ie_j, \phi_{ij}) d_{ik} \qquad 1.5.7$$

and where (Ie_j, ϕ_{ij}) denotes the vector product $\sum_{j=1}^{N} (Ie_j \times \phi_{ij})$

It is not difficult to see that n_k are the coefficients which minimise the least squares distance function,

$$L_2 = \sum_{j=1}^{N} |Ie_j - \sum_{i=1}^{m} n_i I_{ij}|^2 \qquad 1.5.8$$

The coefficients n_k are the coefficients for an approximation using the non-orthonormal functions I_{ij}.

The orthonormalisation procedure required to transform the original functions to the form shown in (1.5.4) can take the following form[24].

$$\phi_{ij} = I_{ij}/D_1 \text{ where } D_1 = (I_{ij}, I_{ij})^{\frac{1}{2}} \qquad 1.5.9$$

where again $(I_{ij}, I_{ij}) = \sum_{j=1}^{N} (I_{ij} \times I_{ij})$

$$\phi_{ij} = \{I_{ij} - (I_{ij}, \phi_{ij})\phi_{ij} - (I_{ij}, \phi_{2j})\phi_{2j} - \ldots (I_{ij}, \phi_{i-1,j})\phi_{i-1,j}\}/D_i \qquad 1.5.10$$

where

$$D_i = \{(I_{ij}, I_{ij}) - |(I_{ij}, \phi_1)|^2 - |(I_{ij}, \phi_2)|^2 - \ldots |(I_{ij}, \phi_{i-1,j})|^2\}^{\frac{1}{2}} \qquad 1.5.11$$

It can easily be shown that,

$$\sum_{j=1}^{N} (\phi_{ij} \times \phi_{kj}) = \begin{cases} 0 & i \neq k \\ 1 & i = k \end{cases}$$

A new procedure for evaluating the coefficients in a least squares approximation using non-orthonormal functions

has been described. It requires that the functions be transformed into an equivalent orthonormal set using equations (1.5.10) and (1.5.11). It is then possible, using (1.5.7), to evaluate the coefficients for an approximation using the non-orthonormal functions.

The discrepancy between the function being approximated and the least squares expansion is given by,

$$\delta_j = Ie_j - \sum_{i=1}^{m} (Ie_j, \phi_{ij})\phi_{ij} \qquad 1.5.12$$

The following section describes the way in which the residuals (δ_j) and the coefficients in the orthonormalisation equations (a_{ik}) are calculated automatically by modifying the input data.

Close analysis of this least squares technique reveals very close similarity with the very techniques it is supposed to supercede. This has prompted much discussion regarding the actual benefit of obtaining a solution by this method. Winch[25] has shown that when compared to Crouts method of matrix decomposition the Gram-Schmidt technique is uncannily similar. However, Fougere[26], in his answer to Winches criticism, pointed out correctly that the claimed advantages of the method were justified on the basis of computational accuracy rather than purely algebraic grounds. The erosion of accuracy by successive subtractions is avoided and accuracy maintained by altering the sequence of the calculations. In this case the similarity with other methods of solution is irrelevant. Certainly, in the case of this research work enormous improvements in stability were obtained by assuming an orthonormal basis for the approximating functions.

1.5.b Least squares distribution reconstructions using Gram-Schmidt orthonormalisation

The Gram-Schmidt scheme adopted for this work followed that suggested by Davis and Rabinowitz. The computer programme was written such that all of the pertinent parameters could be calculated from a limited equation set. If additional values were added onto each set of approximating function discrete points, the orthonormalising equations provided the a_{ik}'s in addition to orthonormalising the original functions. Calculation of the residuals, δ, can be made to include evaluation of the n_i coefficients by an appropriate choice of additional values of I_{exp_s}.

The programme input data must take the following form.

	Weights	I_1	I_2	....	I_m	I_{exp}
	W_1	I_{11}	I_{21}		I_{m_1}	I_{exp_1}
	W_2	I_{12}	I_{22}		I_{m_2}	:
N	.	I_{13}	I_{23}		.	.
	.	.	.		.	.
	.	.	.		.	.
	.	.	.		.	.
	W_N	I_{1_N}	I_{2_N}		I_{m_N}	I_{exp_N}
	0	1	0		0	0
	0	0	1		0	0
m	.	0	0		0	0
	.	.	.		.	.
	.	.	.		.	.
	.	.	.		.	.
	0	0	0		1	0

The N values of each vector have been extended with m additional values most of which are zero's.

m = number of size classes assumed to represent the distribution under investigation.

N = number of angular measurements, θ_j.

The programme output is then,

	ϕ_1	ϕ_2	.....	ϕ_m	δ
	ϕ_{11}	ϕ_{21}		ϕ_{m_1}	δ_1
	ϕ_{12}	ϕ_{22}		ϕ_{m_2}	δ_2
N	.	.		.	.
	.	.		.	.
	.	.		.	.
	.	.		.	.
	ϕ_{1_N}	ϕ_{2_N}		ϕ_{m_N}	δ_m
	a_{11}	a_{21}		a_{m_1}	$-n_1$
	0	a_{22}		a_{m_2}	$-n_2$
m	0	0		.	.
	.	.		.	.
	.	.		.	.
	.	.		.	.
	0	0		a_{m_m}	$-n_m$

The number densities (n_m) are included in the residual array, the coefficients a_{ik} are in the orthonormalised functions array, ϕ_{ij}. Adoption of this computing scheme resulted in an extremely compact and fast, least squares approximation programme. Store was reduced by more than half and run time by more than three quarters by comparison with the previously used techniques. The programme listing is shown in Appendix A.

The accuracy and stability of the new technique was evaluated in exactly the same way as that of the more conventional method described earlier. Synthetic data was calculated from an assumed distribution and then used to obtain a least squares reconstruction within the same programme. The disc file of intensity functions was again used. Unlike the previous method, however, all computation was undertaken in single, rather than double, precision arithmetic. The computation of distributions from ideal data was in no way affected by this loss of significant digits. This was an early indication of the improved

stability of the orthonormal method.

Examples of distributions reconstructed using Gram-Schmidt orthonormalisation are shown in Figures 15, 16. These show various widths of distribution at two means, α = 80 and 150 (16μm and 30μm; λ = 0.6328μm). Both narrow and wide distributions can be accommodated without appreciable loss of accuracy. Fifteen size classes were used, each $\Delta\alpha$ = 10 wide. However, if the distribution being reconstructed is wider than the range of sizes applied to the analysis, no recognisable distribution reconstruction will be obtained. Therefore, care must be taken when a set of data of an unknown suspension is applied to the analysis.

The major test of the least squares method was its sensitivity to error in the experimental data. Figure 17a shows a reconstruction of a Z.O.L.D. where the synthetic intensity data has been truncated to three figures. No rounding up or down of the numbers was made. Each simply had all digits after the third significant digit deleted. In one of the two cases shown the forward data from 0-0.5° has also been deleted to simulate a practical set of empirical data. In all cases the reconstruction is a good representation of the original. The discrepancies that exist are relatively small and do not prevent a meaningful interpretation of the result. A significant improvement in stability had been achieved even in the presence of simulated experimental error.

A final test made before the experimental verification of the technique, established that the least squares method could be used to analyse submicron distributions. The Gram-Schmidt Orthonormalised least squares technique has been used to reconstruct submicron distributions from synthesized data.

An example of one of these is shown in Figure 17b. As anticipated the angular range of data had to be extended to 180°. The angular interval was also increased to $\Delta\theta = 3°$, and the number of angular stations was 60. It was not found necessary to alter the number of sub-sizes in each major size class, but the range of particle sizes was compressed to match the width of the distributions.

1.5.c Summary of the theoretical results

Although of limited practical use, the standard least squares method provided useful information regarding the sensitivity of a solution to the absence of data over some ranges of scatter angles. It had shown that scattered light data collected between 0.5 and 10° at intervals of 0.125° will allow the measurement of distributions containing particles between 5 and 60μm.

The Gram-Schmidt orthonormalisation least squares technique overcame the ill-conditioning problem. The new scheme was compact and fast and proved capable of accommodating errors in the angular intensity data. Finally, it indicated that extending the angular data to 180° will allow the analysis of submicron particle distributions.

The next section describes the experimental verification of the method.

1.6 Experimental Verification of the Least Squares Distribution Inversion Technique

1.6.a Introduction

The final stage in the development of the least squares data processing technique was the testing of the method using experimental light scattering data. The sizing technique was being developed to measure the vaporisation rate of water droplets in a high temperature, high pressure air stream. Theoretical calculations had revealed that the probable range of mean droplet sizes that would be encountered in the envisaged heat transfer experiments was 5.0-100.0μm. It was expected that the vaporisation rates would be such that the droplets would soon be of 50μm or less in diameter. Calculations[27] showed that this size would occur approximately adjacent to the first observation port in the experimental duct. Therefore, the range of sizes likely to be encountered, 5-50μm complied with the practical range over which the calculations described in the previous section had shown the least square method to be most applicable. As a preliminary step it was decided to test the technique using sprays exhausting directly into the laboratory. A series of sprays producing different particle sizes were obtained and an optical particle size apparatus was built around the spray system. The light scattering rig was very simple and was based on a concept originally devised by Moore and Carabine[12]. The severe restriction on the time available for development of the apparatus meant that it had to be very quickly manufactured and the design had to afford a high chance of success.

From the outset it was assumed that, in order to ensure the applicability of Mie theory, the incident light field should be planar throughout the measuring volume. To aid this

it was decided not to focus the illuminating laser beam but to maintain it as nearly parallel as was practically possible. Similarly, the light collection optics were designed to accept a near parallel column of scattered light. The measuring volume was then simply defined by the intersection of two parallel sided cylindrical beams of light that were joined at any arbitrary angle, Figure 19. The method of changing the scatter angle (θ) involved bending the laser beam through an observation point viewed by a stationary photomultiplier. The new apparatus differed from that of Moore and Carabine in being optimised for the measurement of light scattered over the range $\theta = 0.5°-10°$. In accordance with the theoretical results the system was designed to accommodate an angular interval of $\Delta\theta = 0.125°$. The original system used by Moore and Carabine was designed for the measurement of submicron particles and involved measurements over $\theta = 3°-180°$. Their apparatus involved rotating the laser beam with a complicated system of fixed and rotating front silvered mirrors. The apparatus described in this thesis was much simpler to build and align. The design did not prove to be optimum from the point of view of light collection efficiency and methods of improving it are described in a later section. However, its simplicity was an essential advantage while the use of a high powered laser overcame the problems of the inefficient light collection system.

1.6.b A description of the light scattering apparatus

Schematics of the two pieces of equipment used are shown in Figures 18a and 18b. In both of the systems the variation of the scatter angle, θ, was achieved by directing a laser beam via a front silvered mirror onto the face of a plano-

convex lens. The mirror bent the beam of light, taken directly from the laser, through 90° and directed it along a line parallel to the axis of the main lens. A traversing mechanism was used to travel the beam across the face of the lens resulting in the beam being rotated about its focal point. The angle of the beam relative to the lens axis was simply the arc-tangent of the distance between the incoming beam and the lens axis, divided by the lens focal length. To counteract the beam convergence imposed by the main lens, a further lens of equal focal length was mounted in the beam path between the laser and the right angle mirror. This focussed the laser beam onto the face of the mirror such that the beam entering the main lens was diverging. This divergence was cancelled by the main lens so that an essentially parallel ray of light was directed through its focal point. Some control of the final diameter of the light beam was theoretically possible through a careful choice of focal lengths of the two lenses. The relationship between the laser beam diameter, the focal lengths of the lenses and the beam diameter at the main lens focal point is simply,

$$\frac{d_f}{d_\ell} = \frac{f_f}{f_\ell} \qquad 1.6.1$$

where d_f = diameter at the main lens focal point

d_ℓ = laser beam diameter

f_f = Main lens focal length

f_ℓ = focal length of the lens following the laser.

An attempt to reduce the size of the beam emerging from the main lens was made by using a short focal length main lens (5 cm) and a relatively long lens (15 cm) immediately after the laser. Although this should have reduced the beam size to

a third of that emerging from the laser source, the practical result was a diffuse beam of no value to the planned experiments. This probably occurred because of the severe aberrations generated by the poor quality, thick, short focal length laboratory lens used to deflect the laser beam. As the range of angles and beam sizes required by the experiments could be met using two then available 10 cm focal length lenses this configuration was adopted and used throughout the experimental period. No further attempts to use lenses of different focal lengths to reduce the beam size were made or found necessary. On occasions, however, the beam size was reduced by placing a 500μm pinhole between the laser and the first lens. The slight divergence introduced into the laser beam by the diffraction at pinhole could, if required, be calculated using the formula for the angular position of the first zero in the Airy pattern,

$$\sin \theta = \frac{1.22 \lambda}{\Delta} \qquad 1.6.2$$

where θ = angular position of the first zero

Δ = aperture diameter

λ = wavelength of light.

In general, however, it was found that careful positioning of the two lenses in the beam deflecting optics could ensure that a near parallel ray of light was produced at the measuring volume. This could be checked by projecting the beam emerging from the main deflecting lens across the length of the laboratory.

To reduce the effect of lens aberrations and the problem of curvature of the focal plane only the central portion of the main deflecting lens was used. In the case of a 5 cm

diameter, 10 cm focal length lens, the use of the central ±1.25 cm from the lens axis made available a range of light scattering angles of $\theta \sim 0°$-14.25°. As the majority of lens aberrations are functions of the distance of the incoming beam from the lens axis raised to some power, the use of the central portion of the lens reduced any possible effects to a minimum. In addition, plano-convex lenses were used for all optical components to minimise spherical aberrations. These were used to meet as closely as possible the condition for lens surface curvature given by Bergmann and Schaefer[43]. This has the form,

$$\frac{r_1}{r_2} = (2\,m^2 - m - 4)/(2\,m^2 + m) \qquad 1.6.3$$

r_1 = radius of lens face through which the parallel beam passes first

r_2 = radius of second face

m = refractive index

Of the lenses available those that gave the nearest to the optimum value of r_1/r_2 (0.1667 for m = 1.5) were plano-convex lenses ($r_1/r_2 = 0$). These were used throughout the experimental programme.

The beam of light produced by a laser yields a Gaussian light intensity distribution. The focussing of 'Gaussian' light beams has very special problems which have been the subject of considerable study in recent years. The propagation of such beams through lenses has been analysed by Kogelnik and Li[41]. Relationships between the radius of curvature of the incoming beam, the position of the waist and the waist diameter of the focussed beam have been derived.

The relationship between the beam waist within the lasers optical system (σ) and that at a lens (σ_L) is given by,

$$\sigma_L = \sigma \left[1 + \left(\frac{\lambda\delta}{4\pi\sigma^2}\right)^2\right]^{\frac{1}{2}} \qquad 1.6.4$$

where λ = wavelength

δ = distance of the lens from the beam waist in the laser.

The beam wave curvature at the lens (P_{L_1}) is given by

$$P_{L_1} = \delta \left[1 + \left(\frac{4\pi\sigma^2}{\lambda\delta}\right)^2\right] \qquad 1.6.5$$

The effect of the lens on the wave curvature as the beam propagates through the lens is given by[41]:

$$\frac{1}{P_{L_2}} = \frac{1}{P_{L_1}} - \frac{1}{f} \qquad 1.6.6$$

where P_{L_2} = curvature of the wave after the lens

f = lens focal length

These values of beam radius (σ_L) and wave curvature (P_{L_2}) can be used to calculate the position of the focussed beam waist relative to the lens (z) and the new waist diameter (σ_f), using the general expressions,

$$\sigma_f^2 = \sigma_L^2 / \left|1 + \left(\frac{\pi\sigma_L^2}{\lambda P_{L_2}}\right)^2\right| \qquad 1.6.7$$

$$z = P_{L_2} / \left|1 + \left(\frac{\lambda P_{L_2}}{\pi\sigma_L^2}\right)^2\right| \qquad 1.6.8$$

Substitution of real values into equations 1.6.4 and 1.6.5 and using the resulting values of P_{L_1} and σ_L in 1.6.6-1.6.7 shows that the beam waist will not be coincident with the lens focal length, f. In practice this means that a small diameter

Gaussian beam traversed across the face of a lens would not rotate about the centre of the beam waist. This creates particular problems with the two beam Laser Doppler Anemometers where the two beams, although they cross at the lens focal point, do not have coincident beam waists. This problem is overcome by placing a positive and negative lens between the laser and the transmitting lens. In this case the 'Gaussian' divergence is cancelled out by focussing the beam and then using the second lens to make the beam more nearly parallel prior to the beam splitting. This system can be used to move freely the beam waist positions around the focal length of the lens used to cross the two initially parallel beams. The beam deflection system used in the apparatus shown in Figures 18a and 18b uses the same principles. The adoption of a two lens system ensures that the main beam is parallel, and that problems of aligning a beam waist with the focal point of the lens and the collection optics system are avoided. However, as will be demonstrated, this method of minimising the problems of alignment by avoiding the use of a focussed beam, aggravated the problem of spatial resolution and measuring volume size. The system did have the major advantage, however, that the collection optics system always viewed a near planar light field. This generated angular scattered light distributions from particles which were accurately modelled by Mie theory. Initial tests with the beam bending apparatus showed that this method of rotating the laser beam around a fixed point was capable of providing a closely controlled change in light scattering angle.

Two light collection optic systems were used in conjunction with the previously described beam bending apparatus.

Early experiments used two pinholes of equal size to define a near parallel light acceptance column. The pinholes were typically 300μm in diameter and were usually between 40 and 60 cm apart. The detector, a photomultiplier was contained in a holder with a 1 mm orifice admitting light. This was placed approximately 5 cm behind the second pinhole. The angular resolution of this system was limited by the effects of diffraction at each pinhole. This angle, which can be calculated using equation 1.6.2, defines the light collection solid acceptance angle subtended at the first pinhole. If a blue (0.488μm) laser beam intersects with the collection optics column 20 cm from the first pinhole then the width of the column at the crossing point is approximately 0.8 mm. This size increases strongly as the pinhole size is reduced, for example a 100μm pinhole produces a column width of 2.4 mm. Divergence in a light collection system using 300μm pinholes results in an angular uncertainty, given by equation 1.6.2, of 0.11°. This limits the resolution of the instrument and restricts its ability to resolve the detail in a polar scattering experiment in which the particles produce a series of closely packed lobes of light intensity. However, this scheme was used with some success to measure the angular variation of light intensity for a series of water droplet sprays of different mean sizes. These results are discussed in the following section.

The problems encountered while using the twin pinhole collection optics system included limited angular resolution and the systems poor discrimination against background light noise. In an attempt to overcome these a second optical system was constructed using a small grating spectrometer, Figure 18b.

The basic design was based on an optical arrangement described by Chu[42]. In this scheme a single lens was placed one focal length away from a pinhole placed in the entrance to the spectrometer. An additional aperture was placed in front of the focussing lens. This latter aperture dictated the size of the light acceptance column within which the scattered light would be measured. The Gaussian beam equation for calculating the size of a spatial filter for diffraction limited operation was used to fix the size of the spectrometer pinhole[42]. This is very similar to the equation for calculating the diameter of the first Airy disc, derived from equation 1.6.2, and has the form:

$$d_p > \left(\frac{4}{\pi}\right) \frac{\lambda f}{\Delta} \qquad 1.6.9$$

d_p = spatial filter pinhole diameter

λ = wavelength of light

Δ = aperture size in front of the lens

f = lens focal length.

The angular uncertainty of the system is given by,

$$\delta\theta = \frac{d_p}{f} \qquad 1.6.10$$

Using a 10 cm lens and an aperture of 500μm equation 1.6.9 predicts that a 125μm pinhole is required producing an angular uncertainty, $\delta\theta$, of 0.07°. This represented a substantial improvement in resolution compared to the early twin pinhole system. In practice a pinhole of 150μm was available and this was used throughout the experimental period. The angular uncertainty of this arrangement was considered adequate for the envisaged series of experiments as theory had implied that a resolution of around 0.125° was required. The introduction of

this system made the experiments much easier to conduct as they could now be carried out in a fully lit laboratory without the need for light shielding. The spectrometer was used for the bulk of the experiments following initial testing when the twin pinhole system was used.

The size and shape of the measuring volume was dictated by the nature of the intersection of the parallel laser beam with the nearly parallel light acceptance column. The simple schematic in Figure 19a demonstrates one of the problems of this type of angular light intensity experiment. A change in light scatter measurement angle θ is accompanied by a change in measuring volume. For parallel sides beams size of the measuring volume is directly proportional to the reciprocal of the sine of the scatter angle (θ). In order to normalise all measurements to a scatter volume of constant size it was necessary to multiply all scattered light intensity measurements by sine (θ). The increase in measuring volume with a reduction in θ raised two additional problems. Firstly, the intensity of the light collected by the photomultiplier covered a much greater range than that implied by Mie theory. In practice the collected light variation was found to exceed more than three orders of magnitude and was greater than the resolution of the photomultiplier (an E.M.I. 9658B) allowed for accurate measurements. In the second place the measuring volume became physically large compared to the system under investigation for the smallest values of θ.

The first of these problems was simply overcome by using carefully calibrated neutral density filters to attenuate the light at small scatter angles. This meant that the measurements could all be taken at a constant photomultipler supply voltage and with the tube always operating over a range where

output current was linearly related to the incident light intensity. The second problem, however, was not so easily solved and in fact a fully satisfactory solution was never implemented although schemes for improving this situation are discussed in a later section. The length of the illuminated observation volume (Y in Figure 19) can be expressed approximately as:

$$Y = \frac{B}{\sin \theta} + \frac{\Delta}{\tan \theta} \qquad 1.6.11$$

where B = beam diameters

Δ = collecting optics diameter

θ = scatter angle.

For small angles, say $\theta < 5°$, the above equation simplifies to the following form where θ is expressed in radians:

$$Y = \frac{B + \Delta}{\theta} \qquad 1.6.12$$

Assuming a parallel laser beam of diameter = 0.5 mm and a receiving optics column of diameter Δ = 0.5 mm, Y is 28 mm at $\theta = 2°$ and 57 mm at $\theta = 1°$. These values were typical of those used during the experiments. To ensure that the optical system was sampling a homogeneous section of the spray under investigation, the atomizers were positioned so that the spray dimensions exceeded the sample volume at the measurement point. This was achieved by moving the atomizer away from the sampling point until the plume width was four or five times the maximum size of the measuring volume. For the limited range of experiments eventually undertaken this method was reasonably successful.

The light intensity was measured using an E.M.I. 9658B photomultiplier suitable for use throughout the visible part of

the spectrum. The tube was placed behind the second pinhole in the scheme of Figure 18a or at the exit of the spectrometer in the system of Figure 18b. The short term variation in the intensity of the scattered light was damped out using a low pass filter. The output signals were output to a digital voltmeter and were continuously monitored on an oscilloscope.

The light source was a Coherent Radiation 52G Argon/ Krypton laser with a total output power of 2 watts. This unit was capable of operating at a variety of wavelengths between the strong line limits of $\lambda = 0.488\mu m$ to $\lambda = 0.657\mu m$, blue through to red. The wavelengths outside this range were too weak in power to be useful. Most data was taken at the blue line as it was the strongest; the photomultiplier was also more efficient at this wavelength.

The laser output was stabilised with a small solid state detector mounted at the laser head. A small fraction of the output was directed at the detector which was part of a closed loop power control system. The large power potential of the laser partly contributed to the success of the simple optical systems used in the experiments. The monochromatic, planar light beam generated by the laser was a major asset in the generation of data for use with the Mie theory based inversion technique.

The method of using the apparatus involved aligning the collection optics along the laser beam at one extreme of the range of deflection angles which could be induced by the main deflecting lens. This was done by removing the photomultiplier tube, dynode chain and base, and replacing them with a sheet of semi-transparent paper. The collected light could then be viewed on the paper and the optics aligned to maximise intensity

and centralise the disc of light at the centre of the PM housing. This position was noted as the zero scatter point and all subsequent measurements were referred to it. With the spectrometer system scatter angles of $\theta \sim 0.5°$ were then possible without meeting too many secondary light or background light noise problems. The detector was returned to its housing after aligiment and following the removal of the beam from the detector housing inlet aperture. The spray system was then activated and directed toward the intersection point of the illuminating beam and collection optics column. The polar diagram was measured by traversing the laser beam across the main deflecting lens in small increments and noting the PM output on the digital voltmeter. It was important to ensure that the gas supplied to the pneumatic spraying systems was accurately regulated to eliminate drift in the performance of the spray. This was essential because the design of the 'first generation' experimental rig resulted in a full traverse taking up to five minutes. If conditions were not maintained constant the drift in the electronic apparatus and in the range of spray droplet sizes generated could destroy the validity of the test. These problems were largely overcome by the use of a long time constant low pass filter on the input of the digital voltmeter which monitored the PM tube output, and by the adaption of a pressure regulator and the use of bottled gas (N_2) to generate the spray. However, problems of drift were often encountered during these exploratory experiments and would have to be more adequately countered in any later work.

1.6.c The experimental programme

Measurements were made on a variety of atomizing devices producing water sprays of diameters between 20 and 60μm. These included simple air blast devices, hydraulic nozzles and lubricating nebulizers. For the most part the work was confined to water sprays as these were readily available and did not require special extraction facilities in the laboratory.

Initial tests were conducted simply to establish that the apparatus performed satisfactorily and also to check the viability of a sizing technique based on the shape of the forward scatter lobe. This technique was discussed in section 1.2 and involved comparing the light measurements with a series of theoretically derived overlays. Three spraying systems were chosen for this purpose, each of which produced a different particle size. The performance of the sprays was known approximately from manufacturers data. The angular light intensity distribution of each of the sprays was measured using the previously described apparatus and the results are all plotted on the graph in Figure 20. These were then compared to overlays similar to those in Figures 5 to 7 but computed for a much wider range of sizes. The mean sizes of the sprays deduced from this crude comparison are also shown in Figure 20. These means are modal means and represent the particle size which has the maximum number of particles in the distribution. Reference to Figures 5 to 7 show that the width of the forward scatter lobe varies little with distribution width but is a good indication of the modal mean of the distribution. In general the measured means compared favourably with the available manufacturers data. These results indicate that the simple light scattering apparatus was performing with reasonable accuracy. A more rigorous test of the apparatus

was made, however, in which the overlay technique was used to measure droplet size in a high pressure, high temperature duct. This was part of an experimental programme mentioned earlier and funded by Rolls-Royce (1971) Ltd. to investigate the rate of evaporation of water droplets in an environment similar to that in gas turbine compressor bleed air passages. The test duct, constructed under this contract, consisted of a 3.8 cm diameter stainless steel tube along whose length was situated six pairs of diametrically opposed windows. To withstand the high temperatures (773 K) the windows were manufactured from transparent fused silica. They were mounted on silver plated stainless steel 'O' rings to accommodate any differential expansion between the tube and the quartz. The high pressure air, from a dried supply, was heated in an electrical resistance heater designed and built for the purpose[27]. The optical apparatus of Figure 18 was mounted on a moveable optical bench with the test duct aligned to coincide with the measuring volume of the apparatus. The beam was rotated about the axis at the centre of the tube without the spray activated to determine the effects of secondary scatter from the windows and the polished surfaces of the duct were. The photomultiplier registered very little noise until scatter angles of less than $\theta = 1°$ were reached. Here the noise built up rapidly toward $\theta = 0.5°$. The formula, outlined in section 1.6.a, for predicting the size of the measuring volume indicated that at $\theta < 1°$ the measuring volume was longer than the duct diameter. Various minor modifications to the apparatus were tried to allow the measurement of scattered light at smaller angles, but to no effect. It was rapidly concluded that, in order to make more accurate measurements at the small angles that would

be necessary. In spite of this, however, results were taken with the apparatus at positions 30 cm and 60 cm from the point at which the spray was injected into the hot air stream. The heater was set to deliver gas at 300°C and at 8 atmospheres. The average velocity in the duct prior to evaporative cooling was 10 m/sec. The spray used to cool the gas was generated from a C.T. Spraying Company, hydraulic atomizer which, according to the manufacturer's data, delivered particles of 20μm mean diameter. The light scatter data measured between $\theta = 1°$ and $6°$ is shown in Figure 21. The nearest equivalent theoretically derived scattering signatures for zero order log distributions are also shown in the figure. This relatively crude comparison showed that the particles had vaporised to 12.0μm after 30 cm and 6.0μm after 60 cm in the air stream. These results compared reasonably well with the results from the theoretical model of the vaporisation process[27] mentioned earlier. However, the recognition of the shortcomings of the simple light scattering apparatus, and the need to test the least squares technique in controllable, predictable conditions, prompted a return to a further phase of laboratory bench testing at this stage. The apparatus was re-assembled in the laboratory and an attempt was made to obtain data from a small airblast atomizer and to invert the data using the least squares analysis. In parallel with this experimental effort a complete re-appraisal of the suitability of the existing light scattering rig was made and a new design prepared. In the event it was not possible to build the new rig as the time for development and research ran out.

The airblast atomizing device was supplied by the C.T. Spraying Company and, when operated in the syphon mode, produced a fine plume of particles with a mean size between 10 and 12μm diameter. To accommodate the large measuring volumes inherent with the existing scatter apparatus, measurements were made where the plume appeared to be a finely dispersed cloud of about 40 cm overall diameter. This allowed the measurements of scattered light down to $\theta \sim 0.5°$ without the measuring volume length exceeding the size of the spray. The method of collecting the data was the same as that used in the earlier experiments. The beam was rotated in steps of $\Delta\theta = 0.125°$ from $\theta = 0.5°$ to $10.0°$.

The method of least squares analysis used was similar to that used for the theoretical study described in an earlier section. No foreknowledge of the size distribution was assumed and three sets of overlapping size classes were applied in turn as approximating functions to each set of data. The ortho-normalised least squares method was used exclusively for the analysis and to save computation time the disc file of intensity signatures was again used. The range of sizes investigated and programmed into the file was $\alpha = 2$ to 300 (0.3 to 45μm with $\lambda = 0.488\mu m$).

The method of generating the experimental data was described earlier. It required that the mirror be traversed in closely defined steps across the face of the deflecting lens. A vernier traverse was used for this purpose. In practice it proved time consuming and difficult to generate pre-determined scatter angles identical to those stored in the computer disc files. This problem was overcome by modifying the least squares

computer analysis. A cubic spline fitting routine was added to the computer programme and this was used to fit a curve to the measured set of experimental data. This allowed the data to be collected at an arbitrary set of angles. Scattered light intensities at the angles stored in the disc file were then obtained from the spline interpolation procedure. A modification which simplified the experimental procedure considerably. However, the technique was not used to relax the requirement for a sufficient number of data points to characterize the intensity signatures. The angular intervals used were those the theoretical work had indicated were necessary to capture sufficient of the detail of the polar diagrams. The procedure was used simply to interpolate between the measured angular data points.

A series of experimental data sets were applied to the least squares analysis with varying degrees of success. Unfortunately only a limited number of experiments were possible before the period available for development had to cease. In many of the cases in which the least squares analysis was used a very poor distribution reconstruction was obtained. However, in an isolated number of cases a very good reconstruction was obtained which compared favourably with the data available from the atomizer manufacturers. An example of one of the more successful inversions is shown in Figure 22. A comparison of the original light scatter data with the least squares approximation obtained from the reconstructed distribution is shown in Figure 24. The distribution has a characteristic log normal shape with a modal peak at about 11μm. In order to achieve a smooth distribution with a least squares fitted intensity distribution which compares well with the original it was found

necessary to increase the number of subsizes in each major size class to ten. The degree of structure in both the derived number distribution and the angular intensity signature gradually decreased as the number of subsizes increased and the size interval decreased from $\Delta\alpha = 2$ toward $\Delta\alpha = 1$, Figure 23. The final smooth distribution had a zero order log normal form. The reconstructed polar scattering diagram compared closely to the original except at the extreme angles where the theoretical function showed an oscillatory form.

1.6.d Discussion of the experimental results

The amount of experimental work to investigate the potential of the least squares method was very limited and of insufficient quantity to demonstrate the true value of the technique. However, the basis of a practical method was developed and the technique was used to obtain some apparently successful inversions from experimental data. In order to achieve these reconstructions several modifications were necessary before the least squares analysis would work. These modifications were to accommodate the following:

1) A distribution would only reconstruct if the range of sizes used in the least squares analysis encompassed the range of sizes in the original distribution.

2) As mentioned previously the reconstruction conformed to a recognisable distribution only after the interval between the subsizes was decreased from $\Delta\alpha = 2$ to $\Delta\alpha \sim 1$.

3) The modification described in (2) above also involved a parallel increase in the number of subsizes in each major approximating size class function from five to ten.

As the development proceeded the problems outlined

above were progressively overcome. In the case of (1) above the number of size ranges with which a fit was attempted was increased from the three used in the theoretical work to a maximum of ten. The problems implicit in (2) and (3) involved decreasing the non-dimensional size interval $\Delta\alpha$ from 2 down to 1. This was done, however, at the expense of the total range of sizes that could be covered as the computer disc file. As a result this was reduced from 0.3-45μm to a range of 0.3-25μm. This was necessary because of the limited size of the then available computer disc files used to store the data used by the least squares programme. The application of ten overlapping size ranges to this limited total number of particle subsizes gave a high probability that the condition in (1) above was met. Despite these additional modifications the results proved to be extremely variable. Different sets of apparently acceptable data could produce inversions or distribution reconstructions of widely different quality. In some cases an acceptable distribution was obtained whereas on other occasions the solution collapsed to large positive and negative particle number density values. The major source of error was traced to the accuracy of the experimental apparatus. The inversion proved to be extremely sensitive to small changes in the intensity values at angles between $\theta = 5°$ and 10°. Equally, the accuracy of the data recorded at small angles could also influence the solution. The reason for the sensitivity of the solution to the accuracy of these ranges of data was simply that they represented the areas of least experimental accuracy and consistency. Data recorded in the forward direction continually ran into the problem of the measuring volume assuming proportions which were

large compared to the particulate system. This fact plus the non-homogeneity of the spray system under investigation was assumed to be the major contributing factor to errors in the forward direction. At the large angles the source of error simply stemmed from the relatively low scattered light intensities that were small compared to the ambient noise level particularly at angles near $\theta = 10°$. Both of these problems would have been most readily overcome by a suitable redesign of the optical apparatus. Insufficient time was available to carry out the modifications but a new arrangement has been designed and is described in a following section. The full potential of the method described in this chapter will only be properly assessed if these experimental deficiencies are eliminated and the sizing tests repeated.

1.7.a General discussion of the least squares evaluation and recommendations for further work

The theoretical programme was successful in proving the potential of the least squares method in ideal circumstances. The simple transition of the derived scatter data proved that the Gram-Schmidt solution procedure was capable of generating solutions which were less sensitive to the accuracy of the experimental data. Previous solution procedures including Gaussian elimination had produced an ill conditioned matrix that made a practical solution using raw experimental data impossible to obtain. The basis of a practical scheme for a general method of sizing particles was developed around the Gram-Schmidt procedure and using the previously described disc file. This latter modification allowed the use of a large number of individual intensity functions in the analysis while avoiding the problem of inordinately long computer times and large demands on storage. In practice, however, a full appraisal of the least squares technique was not possible because of a basic lack of time and because of deficiencies in the experimental apparatus. These deficiencies were largely confined to the variable and large size of the measuring volume at small light scatter angles ($\theta < 3°$). This could be overcome by a more careful consideration of the optics design incorporated in the experimental rig. A suitable set of optics are discussed in the following section.

Any future work in this area should undoubtedly be carried out with a more suitable light scattering apparatus. In addition to reducing the measuring volume size the problem of potential drift both in the electronics and in the nature of the spray must be accommodated more effectively than was managed in this study. This could possibly be done by using a rapid

scan apparatus to traverse the illuminating beam around the measuring point over a short time scale. An accurate mean intensity function could be built-up by accumulating angular data from a series of these traverses. In this way data at all angles would have approximately the same time history and the effect of drift would be minimised. Data would have to be recorded continually in a fast response storage system. A multi-channel instrument such as that supplied by Malvern Instruments for accumulating photon counts could provide a suitable means of achieving this. The beam could be traversed or rotated by using a rotating mirror or prism device.

Any further work to develop the theoretical method must, to a large extent, depend on the completion of a more extensive practical study. Only then would a full appreciation of any practical difficulties be obtained. However, in view of the non-linear relationship between the optical diameter of the particles and the angular period of the lobular structure in the intensity function, some potentially desirable modifications can be anticipated. The particle size interval between each major size class was constant throughout the whole size range used in the analysis. An investigation of Figures 2 to 7 shows that as α tends to small values the change in the size and number of scattered light lobes becomes progressively less pronounced. A rough plot of the angular width of the first lobe as a function of particle diameter reveals an inverse dependence with respect to $\alpha(\pi d/\lambda)$. The possibility of using a criterion of the following form to decide the size interval between adjacent size classes could be worth exploring,

$$\Delta\alpha_i = \frac{k}{\alpha_i} \qquad 1.6.14$$

The value of k will be chosen to give a sensible range of values for $\Delta\alpha$ over the total range of sizes of interest. For a size range α = 5-100 a major size interval given by $\Delta d = 50/\alpha$ may provide a starting point. The value of k could be experimented with over a broad range. It is not anticipated that blocked size classes of the type used in the previously described study will still be required. However, the potential of non-combined single unit size classes can be retested if desired. A similar form of relationship as that of equation 1.6.14 can also be used to define the required angular range of data for a given particle size study and to fix the angular resolution. It is suggested that for the angular resolution the form be

$$\Delta\theta^\circ = \frac{25}{\alpha} \qquad 1.6.15$$

and for the total angular range of data required

$$\theta^\circ = \frac{500}{\alpha} \qquad 1.6.16$$

These values have been chosen following a close inspection of the theoretical data such as that in Figures 4-7. They predict an angular range and resolution which will capture adequate angular detail to characterise a suspension of a prescribed size. The problem with using a variable angular range and resolution is that it requires a foreknowledge of the distribution of sizes. In addition it would put a greater emphasis on the computational aspect of the method. The range of intensity functions of the calculated angular range and resolution would probably have to be calculated, using Mie theory, as required. This would make the method very time consuming

with all but the most powerful computers. This would be particularly true for large values of distribution mean size. A major advantage of the technique described earlier was that it allowed the convenient use of the pre-programmed disc file of intensity functions which dramatically reduced data processing times. It may be possible to programme the disc file in accordance with the criterion of equations 1.6.15 and 1.6.16 above. However, the range of angular data and resolution would have to be carefully chosen so that they were compatible with the least squares method whatever the range of particle sizes under investigation. In particular, the need for each Mie function to have the same angular resolution and total range of intensity data as the experimental data must be accommodated. However, the criterion implicit in equation 1.6.14 is much easier to apply. It only dictates the interval between each approximating Mie function and allows the use of the same resolution and angular range in each subsize class stored in the disc file. This would seem a modification worth testing at an early stage in any future work. In the event of a transfer of interest to smaller or larger particles then a re-appraisal of the method of application would be desirable. For large particles the use of long wavelengths to reduce the value of α may be necessary. Small particles may be easier to analyse by monitoring the variation of light transmission with changes in illuminating beam wavelength rather than the variation of scattered light with wavelength. In this case the approximating function would represent the effect of wavelength on the scattering cross section of each subsize class.

1.7.d A design for a more appropriate apparatus for light scattering measurement

The problems associated with the simple optical apparatus have been touched on in previous sections. This apparatus was designed to meet the need for simplicity and ease of construction and to generate a planar light scattering field. This latter requirement was to ensure the full applicability of Mie theory. However, the use of a parallel light beam and light collection optics column resulted in impractically large measuring volumes at small scatter angles ($\theta < 3°$). In any future experiments this problem can be overcome by using focussed light beams and collection optics in the manner illustrated on Figure 18c. These new optics must be carefully designed and aligned to ensure that the light is scattered and collected from the planar light field at the centre of the laser beam waist. As before the Gaussian beam relationships can be used to design an optimum system.

The proposed system uses the same method for changing the scatter angle as in the previous scheme. However, the first focussing lens is, in effect, deleted and the bending lens deflects and focusses the beam at the lens focal point. Assuming the lens was 5 cm in diameter and that the maximum angular range to be accommodated was approximately 15° an optimum lens focal length was 10 cm. As before the lens would ideally be plano-convex and to minimise aberrations only the central 2.5 cm at most would be used. Spherical aberrations are a function of the cube of the distances between the incoming beam and the lens axis. The necessary degree of rotation of the light beam can be minimised if a series of equally spaced light detectors are used, Figure 18c.

In this case the maximum required angle of beam rotation is equivalent to the angular interval between the detectors..

The angular resolution and minimum forward scatter angle at which measurements can be made can be calculating using the Gaussian beam relationships. The divergence introduced into the beam at source can be eliminated if necessary by using two lenses in series, one to focus and the other to remake a parallel beam. This would then be redirected onto the main bending lens, as before, by a front silvered mirror. The now parallel beam will be focussed at, and deflected through, the lens focal point. The beam waist at the focal point can be calculated from the equation 1.6.7

$$\sigma_f^2 = \sigma_L^2 / \left[1 + \left(\frac{\pi\sigma_L^2}{\sigma P_{L_2}}\right)^2\right]$$

σ_L = beam radius at the lens

P_{L_2} = beam wavefront radius at the emergent side of the lens.

If the beam has some divergence prior to meeting the lens then equation 1.6.6 can be used to calculate P_{L_2};

$$\frac{1}{P_{L_2}} = \frac{1}{P_{L_1}} - \frac{1}{f}$$

P_{L_1} = radius of curvature of incoming beam

f = lens focal length.

If the two lens system described in the previous section is used to cancel the laser beam divergence then $P_{L_1} = \infty$ and $P_{L_2} = -f$ where the negative sign denotes that the curvature is convex relative to the direction of travel. If P_{L_1} is finite then, as mentioned in a previous section, a problem is encountered in aligning the beam waist with the main lens focal

point. The two lens system allows the beam waist generated by the third lens to be moved and aligned relative to the lens focal point with a high degree of control.

With a lens of 10 cm focal length and a parallel beam of 1 mm diameter at the lens then equation 1.6.7 predicts that $\sigma_f = 39.4\ \mu m$. The far field diffraction angle, Figure 19b which dictates the minimum measurable scatter angle is given by:

$$\delta\theta \doteq \frac{\lambda}{\pi\sigma_f} \qquad 1.6.17$$

This gives a minimum measurable scatter angle of $\theta = 0.22°$ using the components described above. This ensures the full range of angles required for the successful use of the least squares analysis (0.5°-15°) is achievable.

In order to achieve the full benefit from the focussed light beam, some modifications to the collection optics are also required. To allow some control of the measuring volume dimensions and to allow an optimum choice of optical components the two lens scheme shown in Figure 18c is proposed. The aperture between the two lenses and the carefully designed pinhole in the photomultiplier system dictates the light collection efficiency and angular uncertainty. The aperture size should be chosen to produce a measuring volume matched to the focussed beam diameter. The ideal aperture size is also affected by the focal length of the first lens used in collection system. The second lens, nearest the photomultiplier, should be chosen such that the light entering through the pinhole expands to cover the whole of the photomultiplier detection face.

The diameter of the light collection optics column (d_o) at the focal point of the first lens is given by an equation of the form of 1.6.9

$$d_o = \frac{4}{\pi}\frac{\lambda_f}{\Delta} \qquad 1.6.18$$

Δ = chosen aperture diameter

f = lens focal length.

Equation 1.6.9 is used to calculate the pinhole diameter in the face of the photomultiplier housing. In the case of the second lens being of a shorter focal length than the collecting lens the angular uncertainty will be dictated mainly by the collecting lens. This is determined from equation 1.6.10,

$$\delta\theta = \frac{d_o}{f}$$

Using equations 1.6.18 and 1.6.10 the diameter of the aperture necessary to achieve a collection optic waist of the same diameter as the laser beam waist can be calculated. If a 30 cm lens is used to collect the light and it is desired to match the 78.8μm beam derived earlier then equation 1.6.18 predicts that an aperture of 2.5 mm is required. The angular uncertainty of this scheme is calculated, using 1.6.10, to have a value of 0.0149°. This is well within the angular resolution required to obtain accurate light scatter data suitable for use with the least squares analytical method.

The second lens should, as stated earlier, be chosen with a view to optimising the quantity of light falling on the photomultiplier face. If the second lens has a focal length of 10 cm equation 1.6.9 indicates that $d_o > 25\mu m$ for diffraction limited operation. If an EMI 6256S photomultiplier is used to detect the light then it should be placed 20 cm behind the pinhole

to ensure that the detector tubes 1 cm diameter light collection face is completely filled with light. In practice the several variable components will have to be optimised to meet the previously experimental requirements. The proposed scheme offers considerable scope for flexibility and adjustment.

This optical system should provide a substantial improvement in resolution and allow measurements to be made at forward scatter angles less than those possible with the previously described simple apparatus. The theoretical limit of $\theta = 0.22°$ will probably not be achieved in practice but angles of less than $\theta = 0.5°$, which was the minimum previously possible, should be attainable. A limitation will be imposed by the diverging laser beam approaching the collection optics and finally saturating the photomultiplier with noise.

This optical system can be combined with the modifications discussed earlier involving rotating prisms or mirrors to rotate the laser beam around the measuring volume, and multiple detectors to limit the extent to which the laser beam angle must be altered. In this way the time to collect the data can be reduced, the problems of drift eliminated and the effect of imperfections in the main beam bending lens minimised.

1.8 Conclusions and Recommendations

The work described in this report had its origins in an initial appraisal conducted by a previous worker and is still far from complete. However, several important conclusions can be drawn from the work and major advances toward the development of the technique as a practical system have been made. In addition certain experimental and practical advantages afforded by the least squares method over other techniques can be shown.

The method has the following advantages:

1) A particle size distribution of any arbitrary shape can be measured and reconstructed. Many of the alternative methods are only capable of fitting a log normal or other assumed distribution shape.

2) Any size of particle distribution can be measured in principle providing the correct angular range is used and that the approximating functions cover the particle sizes of interest.

3) Data is not required at extremely small forward scatter angles ($\theta < 0.5°$) for particle sizes between $\alpha = 25$–$20°$ and the angular resolution required is less than recommended with other techniques. If carefully designed optics are used the absence of a requirement for small angle data will help achieve good spatial resolution by minimising the size of the measuring volume.

4) It appears to be impossible to produce a plausible but erroneous result using a least squares method because an incorrect choice of approximating functions or alternatively inaccurate experimental data will result in a wildly oscillating distribution solution.

The work described in this thesis revealed that,

(a) In order to produce a meaningful solution from practical data the number of individual intensity functions used as approximating functions in the analysis must be increased from that originally recommended[20]. This can be accommodated without disadvantage by grouping together adjacent size class scatter functions to form a series of averaged size groups. These can then be applied as approximating functions in the least squares analysis.

(b) In order to accommodate the error inherent in experimental data the Gram-Schmidt method of matrix decomposition must be used. Any other method (such as Gaussian elimination) will become ill-conditioned and a meaningful solution will be impossible.

(c) To ensure the most accurate solutions the range of approximating function size classes must totally encompass the range of sizes in the spray. This requires a carefully designed search routine to obtain a distribution reconstruction.

(d) The method used in this work proved incapable of working with particle sizes giving α less than 2.5. This problem can probably be overcome using a more appropriate range of angular data. This requirement for a varying range of angular data depending on size may possibly be accommodated if the suggestions in 1.7.a are adopted.

(e) The experimental apparatus used towards the end of this work was inadequate in fully and accurately assessing the true practical value of the least squares technique. However, it was shown to be possible to achieve meaningful size distribution data, and further work is desirable.

In any future work the following recommendations should be followed.

(i) Only the Gram-Schidt method should be used to obtain a solution.

(ii) The disc file should continue to be used to store computed intensity functions in order to minimise computer time requirements. For sprays the interval between sizes should be $\Delta\alpha = 1$. Some refinement in this criterion along the lines discussed in 1.7.a may be possible.

(iii) If the grouped size class approach is continued then each group should consist of ten (summed) adjacent size classes from the computer disc file.

(iv) For water sprays giving $\alpha = 25$ to 300 data between $\theta = 0.5\text{-}15°$ at intervals of about $0.125°$ should be collected.

(v) For an automated search for a solution a fixed interval of sizes should be scanned at small increments throughout the whole size range accommodated in the disc file or, if required, over a range specified in advance. This will increase the probability that one of the applied size ranges will encompass the true range of sizes present in the spray. In the event of a solution not being achieved the width of the applied size range can be altered. This latter facility can be incorporated into the computer search routine described in the thesis.

(vi) A set of optics along the guidelines described in section 1.7.b should be constructed to improve optical resolution and reduce measurement volume size.

PART 2. CROSSED BEAM PARTICLE SIZING

2.1 Introduction to Part 2

The experimental programme described in the previous section in addition to proving the viability of the least squares technique, also highlighted several practical shortcomings of the single beam apparatus. The most predominant of these was the variation of the measuring volume with changes in the observation angle and the inaccessibility of the forward scatter data. The combined effect of these problems was to minimise the range of particle sizes that could be measured. In an attempt to overcome these problems a new method was devised for illuminating the particles, using crossed laser beams. Although it was soon discovered that the new method possessed limitations of a different kind, it was a sufficiently promising technique to warrant further investigation. The programme involved the development of a new light scattering theory together with a preliminary evaluation of the accuracy of a new technique for measuring submicron particles.

2.2 The Potential Advantages of Crossed Beam Illumination

When a particle is situated within a single plane wave light beam the most intense components of scattered light are projected along the propagation direction of the illuminating beam. Normally this light cannot be measured as it is many orders weaker than the light upon which it is superimposed. If, however, the particle is placed within the intersection region of two crossed beams a substantial change in the direction of the most intense scatter can result. The two main beams combine such that the effective direction of propagation within the intersection region lies along their bisector. Providing the particles are

sufficiently small the forward and back scatter is projected into free space between the beams where it can be readily measured. Unfortunately this phenomenon only occurs for a specific range of particle sizes beyond which the scattered light re-orientates itself such that two primary peaks occur each aligned along a different main beam. The intersection region of two coherent, monochromatic plane waves resolves itself into a set of fringes[3], causing a sinusoidal variation in light intensity. The forward and back scatter is redirected into free space when the particles under investigation have a diameter smaller than the width of a single fringe.

The fringe spacing can be calculated from the equation,

$$\lambda^* = \frac{\lambda}{2\sin\theta}$$

λ = wavelength of the light

θ = half angle between the intersecting beams.

Figure 25 shows the basic differences between single beam and twin focussed beam systems. The single beam system has a large irregular measuring volume and forward scatter directed along the main beam. With two crossed, focussed beams the measuring volume is small and for small particles the forward scatter can be easily measured. Lens abberrations result in an intersection volume of finite proportions with virtually parallel fringes.

The fringe dimensions can be increased by using an illuminating beam of longer wavelength or reducing the angle between the beams. As a particle traverses the fringe region it is subject to a continuously varying incident light field. This modulates the scattered light sinusoidally at a frequency

which is a function of the fring spacing and the particle velocity. The crossed beam laser doppler anemometer utilises this signal to monitor the velocity of particle seeded gas flows. In the context of particle sizing, the modulation frequency can be used to isolate the light scattered from the intersection region from that scattered by particles situated elsewhere in the beams. It also provides a means of discriminating the required light scatter from light noise. This would be particularly valuable in measurements being made in reacting systems with appreciable levels of combustion light emission. In practice the modulated signal can be isolated using phase sensitive detection or a simple narrow band filter. The method has the additional advantage of possessing a small measuring volume which is invariant in size, a feature which aids measuring resolution.

Preliminary theoretical investigations, using plane wave theory, revealed that the ratio of forward to back scattered light was a monotonic function of particle size, between the nominal limits of 0.015-0.5μm. This is the range of sizes of interest in investigations of particle nucleation and growth. In view of the interest in soot and titanium dioxide particle formation within the Department of Aeronautics and Astronautics at this University the ratio technique was explored further. The measurement of large particles was abandoned so that the more immediate potential of the small particle technique could be explored.

It was soon realised that plane wave theory was not applicable to the crossed beam case and a new theory was derived. This is described in the next section.

On further problem concerned the measurement of stationary particles, because under normal circumstances these

would not give rise to a modulated scattered light signal. One example of a situation where it is desirable to make such a measurement is in the reflected shock region in a shock tube. This practical difficulty was overcome by applying an opposing doppler shift on each of the two main beams. This caused each beam to have a slightly different light frequency so that when they were crossed the resulting fringes moved continuously through the intersection region. A stationary particle situated in the measuring volume was then subject to a sinusoidally changing light field. As a result the scattered light was modulated at a frequency dependent on the spacing and translational velocity of the fringes. As in the case of moving particles, this frequency can be isolated and the signal amplitude equated to particle size. The doppler shift can be imposed on the beams in a variety of ways. These include splitting the single laser beam with a rotating diffraction grating, and the electro-accoustic Bragg cell.

The following section describes briefly the theory of crossed beam light scattering by a spherical particle. Single beam plane wave scattering is well described theoretically with Mie theory[1]. Light scattering from particles in the intersection region of two laser beams is not amenable to such a simple treatment. This is because the fringe field, which is the real part of the product of the electric and magnetic vectors, $\underline{E} \times \underline{H}$, is non-planar.

The development of the crossed laser beam technique was undertaken on a joint basis with a colleague, Mr. Chou. The original idea and the experimental development was the responsibility of this writer. The derivation of the theory

was the entire responsibility of Mr. Chou. Full accounts of the theory are available[28,29].

2.3 Crossed Laser Beam Scattering

The two main, intersecting, beams are assumed to be planar, coherent, monochromatic and of equal strength. The particles are spherical and of arbitrary diameter. A brief description of the theory follows.

The governing equation is derived from Maxwell's equations and is the potential field equation[30]. For a non-conducting sphere,

$$\nabla^2\psi(\underline{r}, t) - {}^1/c^2 \frac{\partial^2\psi(\underline{r}, t)}{\partial t^2} = 0 \qquad 2.3.1$$

where c is the speed of light, and $\psi(\underline{r}, t)$, a scalar potential, is related to the magnetic ($\underline{H}$) and electric ($\underline{E}$) vectors by the Lorentz condition,

$$\nabla \cdot A + {}^1/c \, \partial\psi/\partial t = 0 \qquad 2.3.2$$

$$\text{where} \quad \underline{H} = \nabla \times A \text{ and } \underline{E} = -\nabla\psi - {}^1/c \, \partial\underline{A}/\partial t \qquad 2.3.3$$

$\underline{A}$ is a vector potential uniquely related to $\underline{H}$ and $\underline{E}$[6]. The analysis is confined to a periodic field ($\psi(\underline{r}, t) = \Omega(\underline{r}) \exp(i\omega t)$, in which case (2.1) becomes,

$$\nabla^2\Omega(\underline{r}) = k^2\Omega(\underline{r}) = 0 \qquad 2.3.4$$

where $k = 2\pi/\lambda$ and λ is the wavelength of the incident light. Equation (2.3.4), the Helmholtz equation, can now be solved using classical methods and the following boundary conditions. These are that the tangential components of $\underline{E}$ and $\underline{H}$ are continuous, i.e.

$$(E_b - E_a) \times n = 0$$
$$(H_b - H_a) \times n = 0 \qquad 2.3.5$$

where the subscripts b and a represent media on each side of the scattering surface. The solution, described in detail in references 28 and 29, applies to a particle positioned anywhere within the intersection region of the beams. For this reason it is necessary to define two sets of co-ordinates; one centred on the intersection region of the incident light beams, Figure 26, while the other is positioned at the middle of the particle. The latter system is shown in Figure 27. The angular variation of light scatter is defined relative to those co-ordinates based on the particle centre, while the main co-ordinates define the particles position within the fringe field.

The general solution below is in the same form as that of the Mie theory solution descrided in section 1.2.

$$I_\phi = \frac{\lambda^2}{4\pi r^2} |E_\phi|^2$$
$$I_\theta = \frac{\lambda^2}{4\pi r^2} |E_\theta|^2 \qquad 2.3.6$$

These equations represent the intensities in two mutually orthogonal planes. The two main beams lie in the θ plane; the ϕ plane is perpendicular to the θ plane. Both of these are defined in Figure 26. The amplitude functions $|E_\phi|$ and $|E_\theta|$ are both functions of a particle non-dimensional size parameter, the particle medium relative refractive index and the particles position within the fringe field. As in the case of the Mie theory solution the size parameter (α) has the following form,

$$\alpha = \frac{2\pi r}{\lambda} \qquad 2.3.7$$

where r is the particle radius and λ the main illuminating beam wavelength.

Polar diagrams calculated using equation (2.3.6) are presented and discussed in the next section. In all cases the results were computed in either the $\phi = 0$ or $\phi = 90°$ planes. These are respectively, in the plane of the two main beams and perpendicular to the main beams but in the plane of their bisector.

2.4 Numerical Results

The new theory has been used to calculate polar diagrams of the light scattered in the two planes perpendicular, I_ϕ, and parallel, I_θ, to the electric vector of the main beams. The zero degree ($\theta = 0$) or forward direction lies along the bisector of the two incoming beams directed away from the light source. The backscatter also lies along the bisector and propagates at 180° ($\theta = 180°$) to the forward scatter direction. Figure 28 shows the angular variation of scatter for particles of two sizes situated at the centre of a bright fringe region, called here the symmetric case, with various beam intersection angles x. With a zero intersection angle the solution collapses to the same form as the Mie theory solution. When the fringe size is much larger than the particle diameter, the solution is very similar to that of Mie with the exception that the forward scatter lies between the main beams. As the intersection angle is increased the scattered light is attenuated evenly in all directions. The minimum in the I_θ plane occurs at the same angle of scatter irrespective of the intersection angle. For a particle whose diameter approaches the fringe spacing, in this

case $\alpha = 6$ (1.2μm, $\lambda = 0.6328$μm) and $x > 5°$ ($\lambda^* = 333$μm), the most intense scatter occurs as two peaks either side of bisector as shown in Figure 28(b). The scatter pattern assumes an increasingly unusual form as the intersection angle, x, is increased. The intense twin peaks migrate toward and through the incoming main beams and a considerable area of attenuation opens between the primary and secondary scattered light lobes on the polar diagram.

The modulated scattered light signal occurs when the particle migrates from a bright to a dark fringe region. Figure 29 shows a calculated polar diagram for light scattered by a 1μm particle within the dark region. This is the asymmetric case. The light has been strongly attenuated, in the forward direction. The amplitude of the modulated signal is the difference between the symmetric and asymmetric cases. The size of particles of interest in this study are sufficiently small that the scattered signal recorded at the forward point, $\theta = 0$, has optimum contrast. The signal amplitude in this case is given by equation (2.3.6) using co-ordinates which place the particle in the symmetric position. In practice the recorded scattered signal has far from perfect contrast. The existence of several arbitrary placed particles in the measuring volume, each with a slightly different velocity, will produce a signal of reduced contrast or visibility. The classical definition of visibility was first used in the field of holography to characterise hologram fringe field quality. It has the following form,

$$V = \frac{I_{max} - I_{min}}{I_{max} + I_{min}}$$

Ideally $I_{min} = 0$ and $V = 1$.

The visibility is a function of both the fringe width, particle diameter and the particle number density or spacing. The dependence of visibility on particle diameter has prompted the development of another sizing technique[31,32]. Jones[33] with an alternative analysis of crossed beam scattering, has pointed out the possible value of visibility polar diagrams in particle sizing field. This is certainly deserving of further attention. The visibility will in general be the same at $\theta \doteq 0°$ and 18° so the accuracy of the measurement of the ratio will be preserved. There must, however, be a practical minimum visibility below which measurements are not possible.

The calculations which were made using Mie theory to determine the forward to back scatter ratio were repeated using the new theory derived by Chou. The results confirmed the viability of the forward-back scatter ratio method. The new theoretical results are shown as continous curves in Figure 30. The ratio is a monotonic function of particle size between $\alpha = 0.1$ and 2.1 (0.02μm-0.35μm, $\lambda = 0.488\mu m$). The lower limit is imposed by the onset of the Rayleigh region in which the scatter ratio assumes a constant value of unity. Above $\alpha = 2.1$ the ratio begins to oscillate and loses its uniqueness. The practical lower limit has yet to be established in practice but is probably a larger size than suggested here because of the limitations of measuring accuracy. Another factor yet to be investigated is the effect of particle size distribution on the ratio. In the experiments described in the next section the effects of distribution width were ignored; the suspensions assumed to be mono-disperses.

2.5 The Particle Sizing Apparatus

A schematic of the apparatus is shown in Figure 31. The light source was an Argon-Krypton Ion laser of 4 watts total output. Most work was undertaken using the blue line, $\lambda = 0.488\mu m$, at which 800 mwatts of power was available. The laser beam was split with a rotating diffraction grating which had 10,800 lines/revolution, and which was spun with a phonograph motor at 1100 r.p.m. Sixty percent of the light was directed into the first two orders the remaining orders being blanked off with a black mask. The zero order beam was used to align the optical apparatus along a common axis. A lens focussed the laser light onto the grating and a further lens was used to cross the first order beams in the specimen suspension. Two small mirrors were placed between the beams, either side of the intersection point, which intercepted the forward and back scattered radiation and directed it through 90°. Two lenses made the light parallel and sharp edged orifices ensured that both signals were collected over identical solid angles. The light was then directed with further mirrors and lenses into a common spectrometer and photomultiplier apparatus. Great care was taken to keep the optical path of each scattered light beam identical. In order to monitor either of the signals one was temporarily obscured with a mask of black card. The output of the photomultiplier (E.M.I. 6256 S.A.) was displayed on an oscilloscope. The amplitude of the signal was measured directly from a photograph of the trace. The apparatus was designed to provide an accurate test-bed for the technique while avoiding unnecessary complications. One detector was used to overcome the difficulty of obtaining a matched pair necessary for simultaneous measurement of both scattered light components. No loss

of measuring accuracy was experienced because the specimens were static particulate suspensions. The modulated 'doppler' signals were obtained through the use of a rotating diffraction grating which imposed a doppler shift on each of the two beams and caused fringes to translate through the suspension. Typical signals were 50-200 mv in amplitude and had a frequency of 1 Mhz.

The suspensions, one of TiO_2 with a mean size of 0.3μm, the other colloidal silica of 0.04μm, were contained in a spectroscope cell which was suspended in the intersection region. The effective size of the intersection volume was 500μm x 100μm x 100μm. The intersection angle was 3° giving a fringe dimension of $\lambda^* = 4.18\mu m$. A variable band pass filter was incorporated into the plug-in amplifier used with the 'Tektronix' oscilloscope. This was used to filter-out unwanted low and high frequency noise. In general the signals observed were clearly defined sine waves. This would not happen in a flow situation where the particles possessed a range of velocities and arbitrary spacing, because these would result in a signal of low visibility which consisted of a narrow band of frequency. Under these circumstances more sophisticated instrumentation would be necessary.

The experimental results obtained using the apparatus yielded particle size estimates that agreed well with the information obtained from electron micrographs of the same two suspensions. These have been included on Figure 30, the points corresponding to particle diameters of 0.33μm (TiO_2) and 0.035μm (silica).

2.6 The Present State of Development

The preliminary experimental investigations described in 2.5 have served to prove the viability of crossed laser beam particle sizing. However, as already stated, the conditions in

which these results were taken were ideal; a low noise environment, and stationary particles diluted to give optimum signal visibility. Before the technique can be used with confidence it will be necessary to quantify the effect of the width of the size distribution on the calculated forward-back scattered ratio, and its relationship to the mean size. Similarly the effects of particle number density and velocity distribution must be ascertained. It is already known from Laser Doppler Anemometer work, that scattered light signals from seeded gas flows have far from ideal visibility. It is also known that Rayleigh sized particles (α <0.1) scatter light in proportion to a non-linear function of α. This means that the few particles in the coarse tail of a log normal distribution of particles would contribute the major proportion of the total scattered light. This has already proved a problem in several fundamental shock tube studies of soot formation[35,36]. A programme of work has been planned to provide answers to these remaining questions.

2.7 Current and Projected Work

At the outset it was intended to develop the forward to back scatter ratio technique to be used in shock tube studies of TiO_2 and soot formation. In order to demonstrate that the technique could work in an experimental situation the next stage in the development programme involved setting up a scattering experiment on a 2" diameter shock tube (Figure 32). A suspension of known size was used, in this case potassium iodide smoke. Only a limited amount of running was possible with the shock tube apparatus. However, one component of scatter was detected and monitored within the 800μsecs running time of the glass shock tube. The measurements were made in the reflected shock region

of the tube, and the frequency of the scattered light signal confirmed that the gas was effectively stationary. This was as it should be according to shock wave theory. It was not possible within the time available to attempt to measure the size of the KI smoke.

A comprehensive theoretical study of the potential of crossed beam sizing is planned for the future, with a view to finding new ways of using the light scattered from two crossed beams to obtain particle size.

2.8 Discussion

The basic principle of particle sizing using crossed laser beams has been tested. However, much further work is required before the method can be used with confidence. The principal experimental effort must be directed toward the development of suitable processing electronics. This must be backed up by appropriate mathematical studies. The work already conducted has served to prove the basic idea, and the validity of the new scattering theory.

The crossed laser beam technique has potential applications in many research and industrial process areas where the sizes of submicron particles are required. These include the monitoring of pigment quality, the monitoring of seed diameters in laser doppler anemometry, and others. The technique incorporates the advantages of a near point measurement and uses the most intense components of scatter to characterise the particle size.

In conclusion, it must be pointed out that only one method of using the modulated light scatter signal for particle sizing has been investigated. There may be other possibilities

including, for example, the angular variation of the visibility signal and its relationship to particle size parameters. This and other aspects of two beam particle illumination may be worthy of attention.

PART 3. OVERALL CONCLUSIONS

This thesis has described two methods of particle sizing using laser light scattering. Although the development of the method is incomplete both techniques have been shown to have distinct advantages that makes continued development attractive.

The adoption of the Gram-Schmidt orthonormalisation procedure and grouped size class approximating functions has transformed the least square method from one of only academic interest to a technique of potential practical value. The technique offers the advantage of being capable of accurately reconstructing distributions of arbitrary shape. In addition it may be possible to apply the technique to a wide range of particle sizes. This work demonstrated theoretically that both submicron and particles of 5 to 100μm diameter can be measured provided an appropriate range of angular theoretical and practical scattered light data is available. The practical work gave some initial proof of the technique's ability to work with experimentally derived data.

The two beam method originated from the desire to eliminate the problems of variable measuring volume encountered with the single beam system, and to make it possible to measure the light scattered at zero degrees. In practice the method was not suitable for the measurement of sprays as intended but proved most appropriate to the measurement of submicron suspensions. The modulated signal and the discrete but small measuring volume may be used to advantage when monitoring submicron particles in hostile environments.

The practical development of both methods should be continued with further testing of each technique using real sprays and suspensions. This additional work will prove, in the case of the least squares method, whether or not the technique is suitable for use in the vaporising droplet experiments described earlier. Further development of the experimental scattered light rig design is recommended.

The crossed beam technique requires a thorough study to establish its limiations and its strengths. The establishment of many of these can probably be accomplished using the newly derived theory of cross beam particle light scattering.[28]

REFERENCES

1. Mie G. (1908), Ann. Physik., 25, 377.
2. Kerber M. The Scattering of Light and other Electromagnetic Radiation, Academic Press, 1969.
3. Born M. (1933). 'OPTIK'. Springer, Berlin.
4. Kenyon A.S., and La Mer, V.K. (1949). J. Colloid. Sci., 4, 163.
5. Shifrin K.S., and Golikov V.I. (1961). 'Studies on Clouds, Precipitation and lightening electricity', pp.266-277. Inst. of Appl. Geophys. of the U.S.S.R. Acad. of Sci., Moscow.
6. Espensheid W.F., Kerber M., and Matijevic E. (1964). J. Phys. Chem., 68, 3093.
7. Kerber M., Matijevic E. et al. J. Colloid. Sci., 19, 213.
8. Sevenson A.F., Heller W., Wallach M.L. (1961). J. Chem. Phys., 34, 1789.
9. Heller W., Wallach M.L. (1963). J. Phys. Chem., 67, 2577.
10. Wallach M.L., and Heller W. (1964). J. Phys. Chem., 68, 924.
11. Wattens P.T. 'Conference on Heat and Fluid flow in steam and gas turbines'. Inst. Mech. Eng., Warwick, 1973.
12. Carabine M.D., and Moore A.P. Faraday symposium 7.
13. Hodkinson J.R. Appl. Optic., 5, 839, 1966.
14. Shifrin K.S., and Perelman A.Y. Opt. Spectroscopy (USSR). (English Transl.) 20, 75, 386.
15. Titchmarsh E.C. Proc. London Math. Soc. (2), 23, xxii-xxiv (1924).
16. Abbiss J.B. R.A.E. Tech. Report 70151 (1970).
17. Chin J.H. et al. J. Phys. Chem., 59, 841, 1955.
18. Rice J.R. The Approximation of Functions, Addison-Wetsley.

19. Schied. Numerical Analysis, Schaum Outline Series.

20. Vardon J.D.C., Ph.D. Thesis, University of Southampton, 1974.

21. Smillie K.W. An Introduction to Regression and Correlation, Academic Press (1966).

22. Golub G. Numerische Mathematik., 7, 206-216, 1965.

23. Osborne E.E. J. Assoc. Comput. Mach., 8, 628-636, (1961).

24. Davis P., and Rabinowitz. J. Assoc. Comput. Mach., 1, 183-191, 1954.

25. Winch D.E. J. Geophys. Res., Vol.71, No.21, 5165-5173, 1966.

26. Fougere F.P. J. Geophys. Res., Vol.68, No.4, 1131, 1963.

27. Waterston R.M. Progress Reports, RR (1971) Ltd., 1972-74.

28. Chou H.P. Ph.D. Thesis, University of Southampton

29. Chou H.P. and Waterston R.M. Laser Doppler Anemometer Conference, Copenhagen, 1975.

30. Stratton J. 'Electromagnetic Theory', McGraw-Hill, N.Y. (1941).

31. Farmer W.M. Appl. Optics, Vol.13, No.3, March 1974.

32. Fristrom R.M. et al. Faraday Symposia of the Chem. Soc., No.7, 1973.

33. Jones A.R. J. Phys. D. Appl. Phys., Vol.7, 1974.

34. Waterston R.M. and Chou H.P. 10th International Shock Tube Symposium, Kyoto, 1975.

35. Graham S.C., and Homer J.B. 9th International Shock Tube Symposium, Stanford University, California, 1973.

36. Graham S.C., and Homer J.B. Coagulation of Molten Lead Aerosols, Faraday Symp., 7, 1972.

37. Rizzo J. Ph.D. Thesis, University of Southampton, 1975.

38. Waterston R.M. B.Sc. Thesis, University of Southampton, 1969.

39. Waterston R.M. M.Sc. Thesis, University of Southampton, 1971.

40. Goodyer M.J., Waterston R.M. Mist Cooled Turbines. Inst. Mech. Eng. Conference Publication 3, Warwick, 1973.

41. Kogelnik H., and Li T. Applied Optics, Vol.5, No.10, 1966

42. Chu B. Laser Light Scattering, Academic Press, 1974

43. Bergmann L., and Schaefer C. Lehrbruch der Experimentalphysik, Band III Optik. Gruyter and Co., Berlin (1962)

APPENDIX A

```
0008            MASTER ORTHONORM
0009            REAL MEDIAN
0010            DIMENSION W(150)
0011            DIMENSION ALFA(20),XINT(150),ANG(150),R(20,21),DNOD(20)
0012            DIMENSION S(150),PHI(150,20),PMIE(150),CORTH(150),RESID(150)
0013            DIMENSION ENG(120),EPINT(120),AC(120),BC(120),CC(120)
0014            COMMON/THREE/ENG,EPINT,AC,BC,CC
0015            DEFINE FILE 4(151,120,U,IF)
0016            N1=120
0017            M=15   = number of size classes
0018            NINT=5 : number of subsections in each size class.
0019            MINT=1
0020            IF=1
0021            READ(4'IF)(ANG(J),J=1,N1)  N1= Number of angular measurements on the disc file. (ANG(S))
0022            READ(1,100) NDIST          Number of distributions investigated.
0023          100 FORMAT(I0)
0024              DO 1 J8=1,NDIST
0025              READ(1,400) N   number of experimental measurements
0026          400 FORMAT(I0)
0027              READ(1,401)(ENG(I),EPINT(I),I=1,N)  experimental angular (ENG) and intensity (EPINT) measurements.
0028          401 FORMAT(2F0.0)
0029              DO 402 J=1,N
0030          402 EPINT(J)=ALOG10(EPINT(J))
0031              CALL SPLINE(N)    spline coefficients subroutine.
0032            C=============================================================
0033            C============ RECONSTRUCT FUNCTION IN CORRECT INTERVAL ============
0034              N3=1          AT THIS POINT THE SPLINE PROGRAMME IS USED TO GENERATE DATA
0035              N2=0                    AT ANGLES STORED ON THE DISC FILE.
0036              DO 403 J=1,120
0037              IF(ANG(J).LT.ENG(1)) GO TO 405
0038              IF(ANG(J).GT.ENG(N)) GO TO 404
0039              N2=N2+1
0040              CALL SPLEV(N,ANG(J),XINT(N2))  Spline fitting Subroutine.
0041              XINT(N2)=EXP10(XINT(N2))
0042              GO TO 403
0043          405 N3=N3+1
0044          403 CONTINUE
0045          404 N=N2
0046              XDAT=XINT(1)
0047              DO 406 J=1,N
0048              XINT(J)=XINT(J)/XDAT
0049          406 ENG(J)=ANG(N3-1+J)
0050            C=============================================================
0051              WRITE(2,1010)(ENG(I),XINT(I),I=1,N)  Output of intensity data at angles on the disc file
0052              N2=N+N
0053           1010 FORMAT(5X,2(5X,F12.0))
0054            C============== WEIGHTS ==========================
```

```
0055              DO 121 J=1,N
0056            121 W(J)=1,
0057              DO 122 J=1,M
0058            122 W(N+J)=0,
0059          C-------------------------------------------------------
0060              DO 3 I8=1,5
0061              IF=14+(I8-1)*33
0062          C---------------- INITIALISE TO ZERO ----------------------
0063              DO 7 J=1,N
0064              DO 8 J1=1,M
0065            8 PHI(J,J1)=0,
0066            7 CONTINUE
0067          C-------------------------------------------------------
0068          C-------------------------------------------------------
0069              DO 5 K=1,M
0070              ALFA(K)=2*IF-2
0071              DO 12 J1=1,N
0072           12 S(J1)=0,
0073              DO 10 J=1,NINT
0074              READ(4'IF)(PMIE(I),I=1,N1)     input of Mie Theory Intensity for Particle Size ALFA(K)
0075              IF=IF+MINT=1                                  from disc file.
0076              FIND(4'IF)
0077              DO 11 I1=1,N
0078           11 S(I1)=S(I1)+PMIE(N3=1+I1)/1,E+7
0079           10 CONTINUE   — Loop 10 sums outbirges in each blocked sizeclass.
0080          C-------------------------------------------------------
0081                                ORTHONORMALISATION STARTS HERE
0082              DO 14 J=1,M
0083              XINT(N+J)=0,
0084           14 S(N+J)=0,
0085              S(N+K)=1,
0086              IF(K,GT,1) GO TO 201
0087              D1=0,
0088              DO 15 J=1,N2
0089           15 D1=D1+(S(J)*S(J)*W(J))
0090              D1=SQRT(D1)
0091              DO 16 J=1,N2
0092           16 PHI(J,K)=S(J)/D1
0093              GO TO 41
0094          C-------------------------------------------------------
0095          C---------------- PHI(I,J) J GT 1 -----------------------
0096            201 DN=0,
0097              DO 17 J=1,N2
0098              DN=DN+(S(J)*S(J)*W(J))
0099           17 PHI(J,K)=S(J)
0100              DO 18 I=1,K-1
0101              VECPROD=0,
0102              DO 19 J1=1,N2
```

```
0102              19 VECPROD=VECPROD+(S(I1)*PHI(I1,I)*W(I1))
0103                 DO 20 I1=1,N2
0104              20 PHI(I1,K)=PHI(I1,K)-VECPROD*PHI(I1,I)
0105                 DN=DN-ABS(VECPROD*VECPROD)
0106              18 CONTINUE
0107                 DN=SQRT(DN)
0108                 DO 21 J=1,N2
0109              21 PHI(J,K)=PHI(J,K)/DN
0110              41 CONTINUE
0111               5 CONTINUE
0112            C------------------- ORTHONORMAL COEFS --------------------
0113                 DO 22 I=1,M
0114                 CORTH(I)=0.
0115                 DO 23 J=1,N
0116              23 CORTH(I)=CORTH(I)+PHI(J,I)*XINT(J)
0117              22 CONTINUE
0118            C------------------- RESIDUALS AND NO DENSITIES ----------------------
0119                 DO 24 J=1,N2
0120                 RESID(J)=XINT(J)
0121                 DO 25 I=1,M
0122              25 RESID(J)=RESID(J)-CORTH(I)*PHI(J,I)
0123              24 CONTINUE
0124            C---------------- SAMPLE ORTHOGONALISATION -----------------
0125                 DO 26 J=1,M
0126                 VECPROD=0.
0127                 DO 27 I1=1,N
0128              27 VECPROD=VECPROD+PHI(I1,J)*PHI(I1,5)
0129              26 R(5,J)=VECPROD
0130            C------------------------- OUTPUT ------------------------------
0131                 WRITE(2,1000)((PHI(J,I),I=1,10),J=1,N2)
0132                 WRITE(2,1100)((PHI(J,I),I=11,15),J=1,N2)
0133                 WRITE(2,1000)(CORTH(I),I=1,M)
0134                 WRITE(2,1000)(RESID(J),J=1,N2)
0135                 WRITE(2,1000)(R(5,J),J=1,M)
0136           1000 FORMAT(10(1X,D11.5))
0137           1100 FORMAT(5(1X,D11.5))
0138                 DO 90 J=1,M
0139              29 DNOD(J)=RESID(N+J)
0140              90 WRITE(2,1000)DNOD(J),ALFA(J)
0141               3 CONTINUE
0142               4 CONTINUE
0143               1 CONTINUE
0144                 STOP
0145                 END
```

} ORTHONORMAL EQUIVELANTS OF INTENSITY FUNCTIONS

ORTHONORMAL COEFFICIENTS

RESIDUALS + PARTICLE NUMBER DENSITIES

SAMPLE ORTHONORMAL TEST OUTPUT.

OUTPUT OF NUMBER (DNOD(I)) OF PARTICLES OF SIZE ALFA(I)

END OF SEGMENT, LENGTH 819, NAME ORTHONORM

```
0146                    SUBROUTINE SPLINE(N)
0147                    DIMENSION H(120),E(120),F(120),G(120)
0148                    COMMON/THREE/X(120),Y(120),AC(120),BC(120),CC(120)
0149                    E(1)=0.
0150                    F(1)=0.
0151                    H(1)=X(2)-X(1)
0152                    N1=N-1
0153                    DO 1 I=2,N1
0154                    H(I)=X(I+1)-X(I)
0155                    A=H(I)/6.
0156                    B=(H(I)+H(I-1))/3.
0157                    C=H(I-1)/6.
0158                    D=(Y(I+1)-Y(I))/H(I)-(Y(I)-Y(I-1))/H(I-1)
0159                    E(I)=-A/(B+C*E(I-1))
0160                    F(I)=(D-C*F(I-1))/(B+C*E(I-1))
0161                  1 CONTINUE
0162                    G(1)=0.
0163                    G(N)=0.
0164                    DO 2 I=1,N1
0165                    J=N-I
0166                    G(J)=E(J)*G(J+1)+F(J)
0167                    AC(J)=(G(J+1)-G(J))/(6.*H(J))
0168                    BC(J)=G(J)/2.
0169                    CC(J)=(Y(J+1)-Y(J))/H(J)-H(J)*(G(J+1)*2.*G(J))/6.
0170                  2 CONTINUE
0171                    AC(N)=0.
0172                    BC(N)=0.
0173                    CC(N)=0.
0174                    RETURN
0175                    END

END OF SEGMENT, LENGTH   296, NAME  SPLINE
```

```
0176                  SUBROUTINE SPLEV(N,XV,Y)
0177                  COMMON/THREE/X(120), D(120),A(120),B(120),C(120)
0178                  IF((XV.LT.X(1)).OR.(XV.GT.X(N))) GO TO 2
0179                  DO 1 I=1,N
0180                  IF(XV=X(I))3,1,1
0181                1 CONTINUE
0182                3 I1=I-1
0183                  Z=XV-X(I1)
0184                  Y=A(I1)*Z**3+B(I1)*Z*Z+C(I1)*Z+D(I1)
0185                  RETURN
0186                2 Y=0.0
0187                  WRITE(6,4)
0188                4 FORMAT(///,47H SPLINE OUT OF BOUNDS Y=0.0,///)
0189                  RETURN
0190                  END

END OF SEGMENT, LENGTH   111, NAME  SPLEV
```

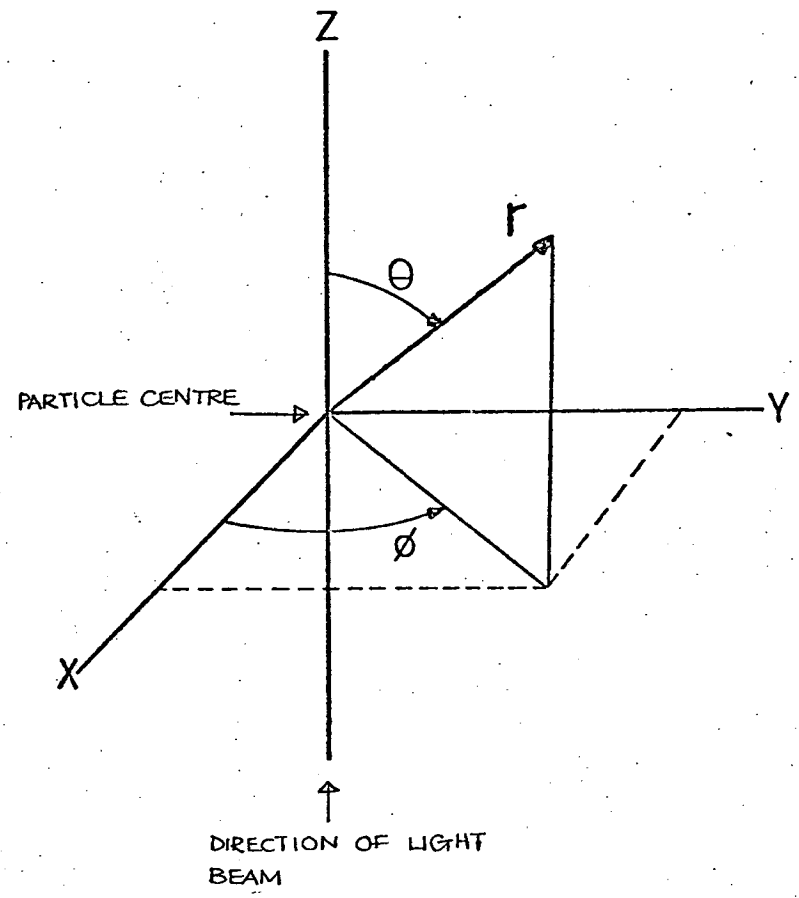

$$x = r \sin\theta \cos\phi$$
$$y = r \sin\theta \sin\phi$$
$$z = r \cos\theta$$

FIG 1. COORDINATE SYSTEM.

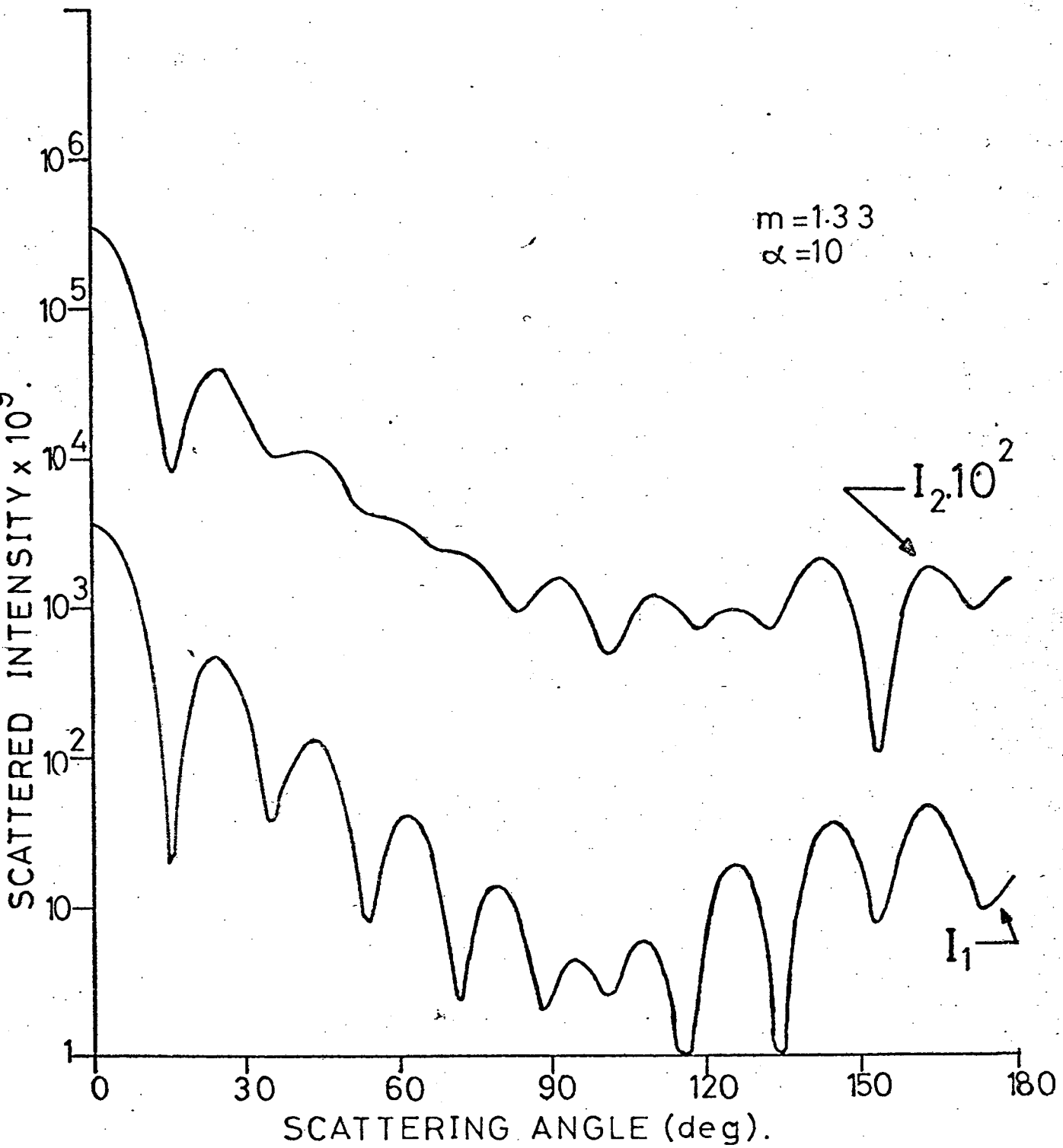

FIG 2. ANGULAR VARIATION OF SCATTERED INTENSITIES.

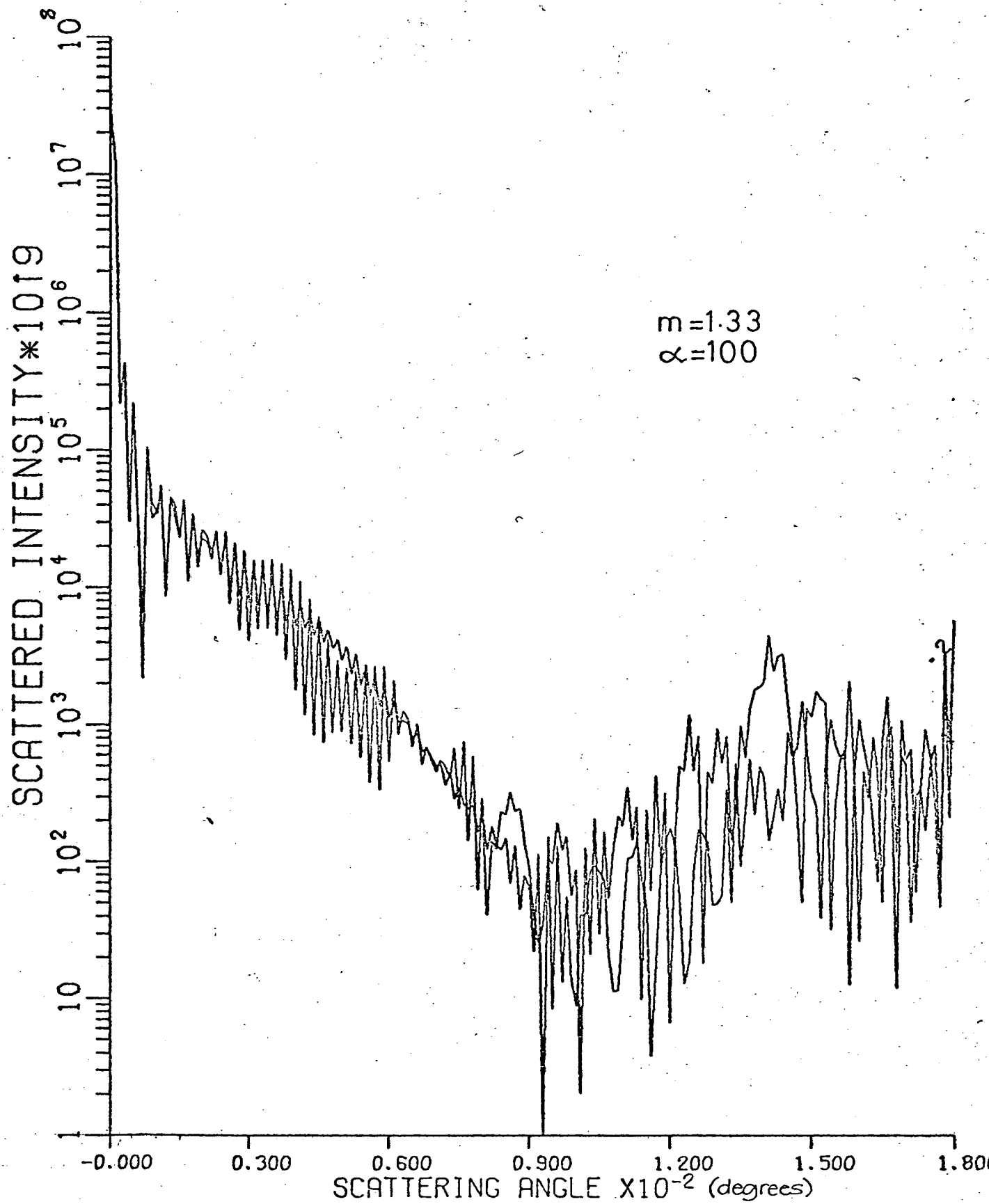

FIG 3. ANGULAR VARIATION OF SCATTERED INTENSITIES.

FIG. 4

SCATTERED LIGHT POLAR DIAGRAMS FOR GAUSS NORMAL DISTRIBUTIONS.

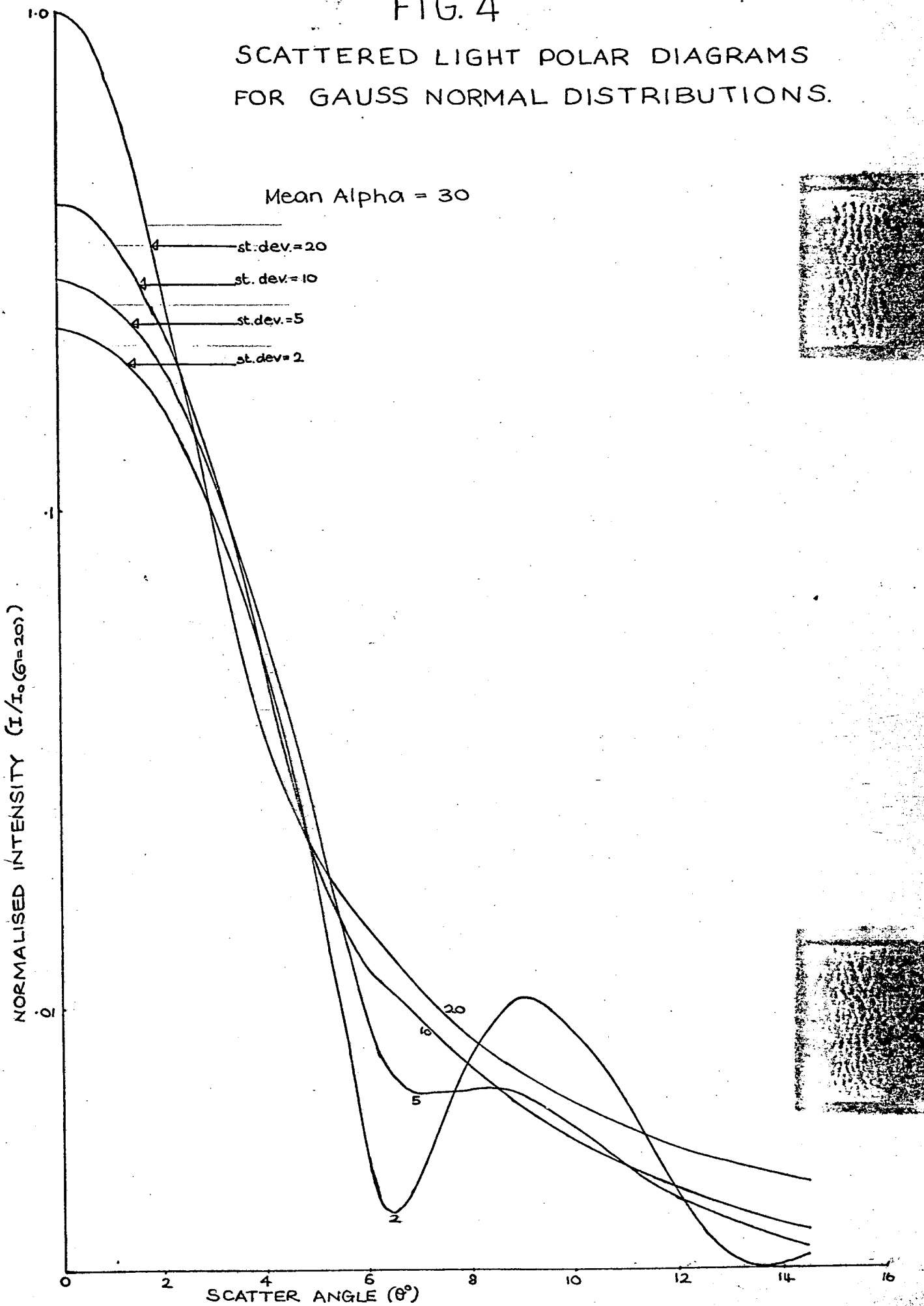

FIG. 5

SCATTERED LIGHT POLAR DIAGRAMS FOR GAUSS NORMAL DISTRIBUTIONS.

Mean Alpha = 100

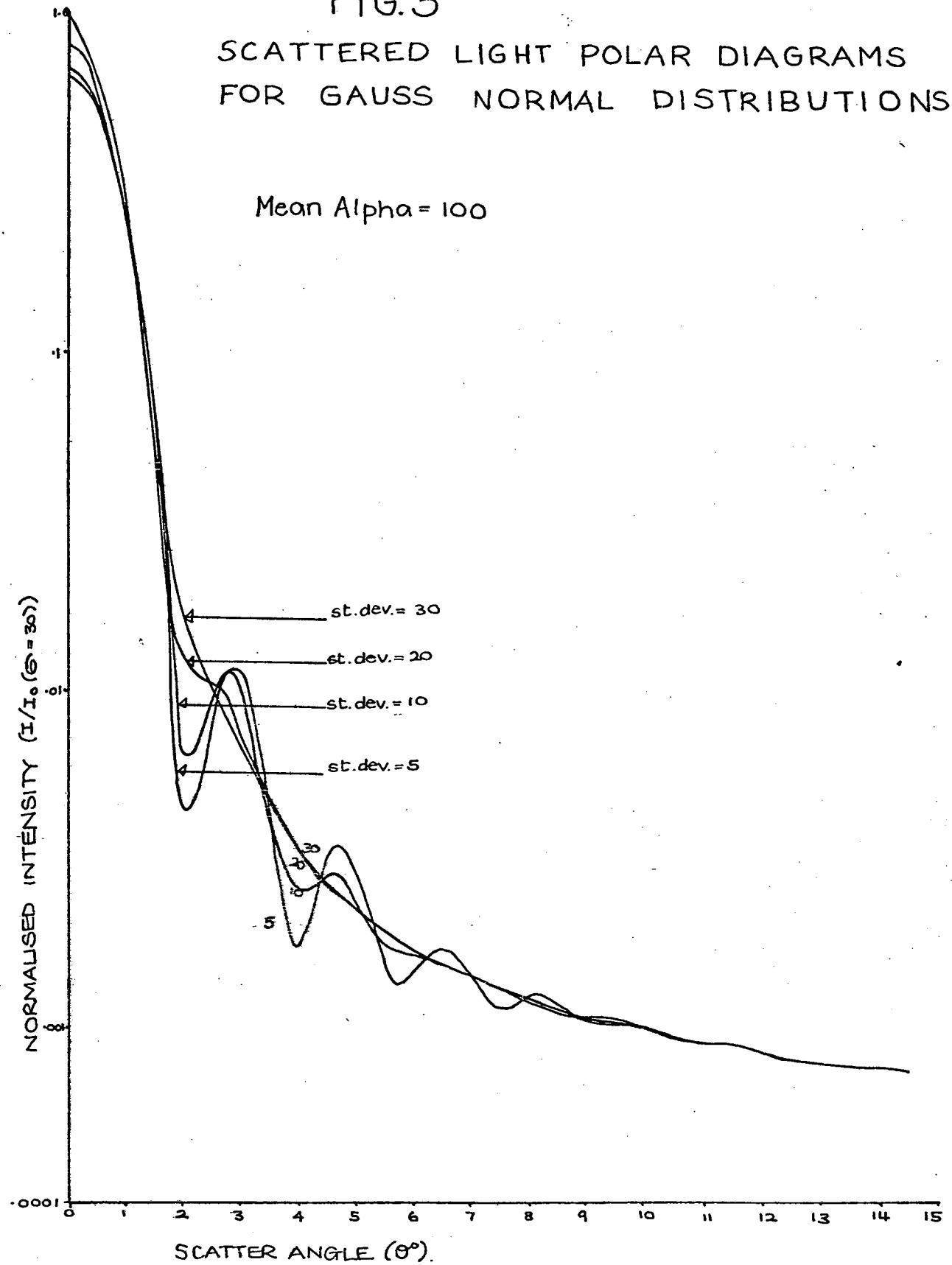

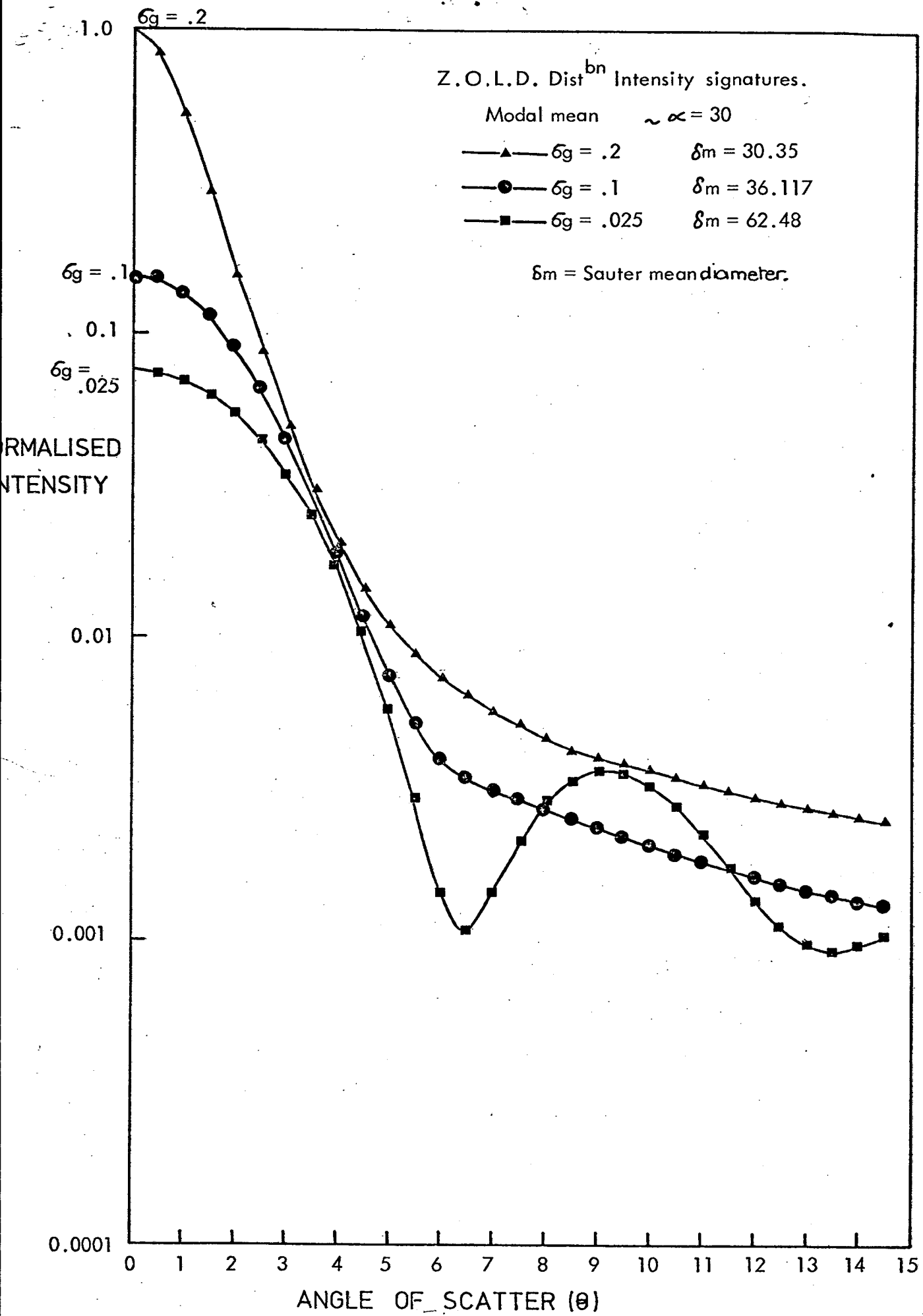
Z.O.L.D. Distbn Intensity signatures.
Modal mean ~ α = 30
σg = .2 δm = 30.35
σg = .1 δm = 36.117
σg = .025 δm = 62.48
δm = Sauter mean diameter.
σg = .2
σg = .1
σg = .025
1.0
0.1
0.01
0.001
0.0001
RMALISED
NTENSITY
0 1 2 3 4 5 6 7 8 9 10 11 12 13 14 15
ANGLE OF SCATTER (θ)

FIG.6

FIG.7

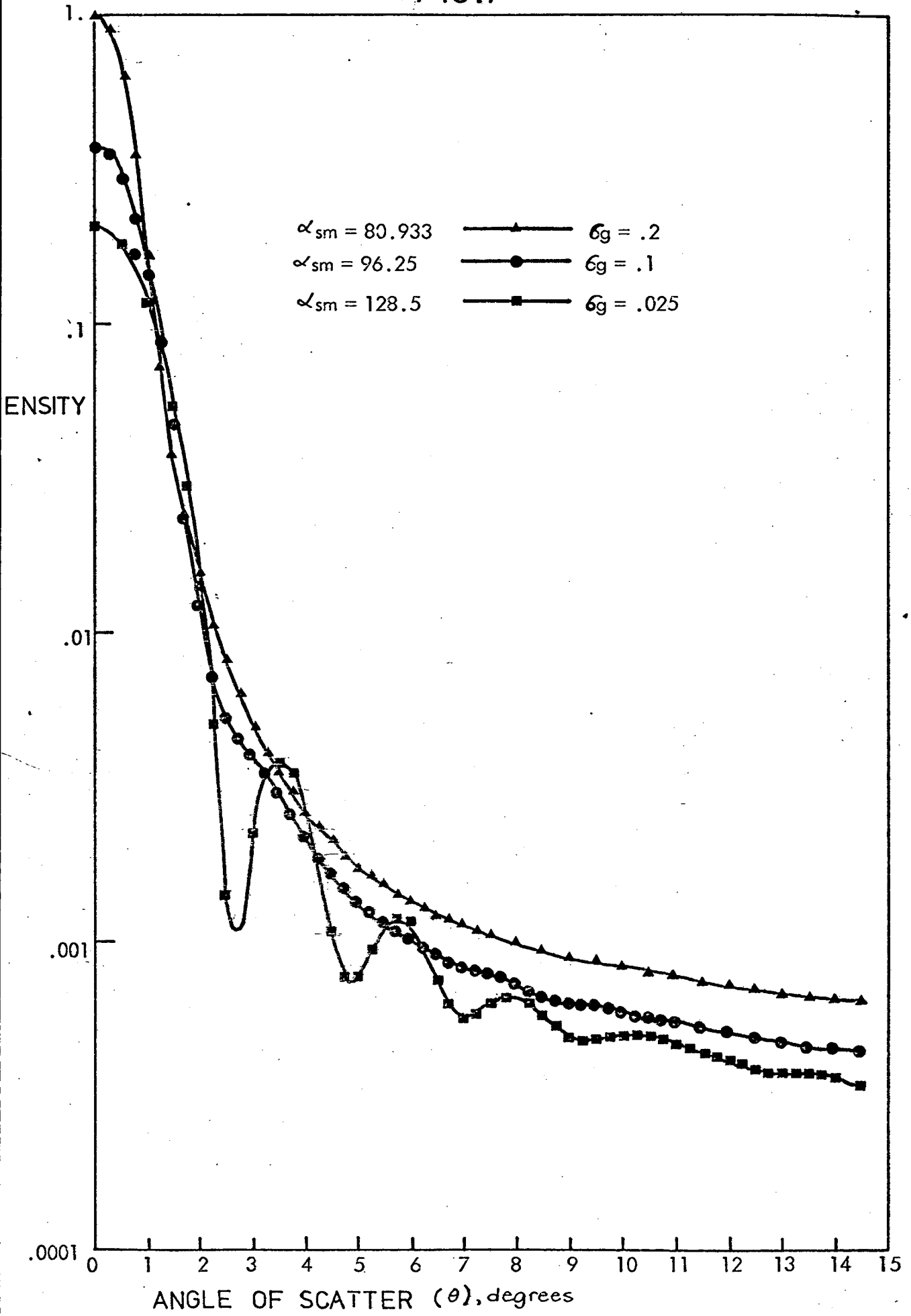

Z.O.L.D. INTENSITY SIGNATURES MODAL MEAN α = 80

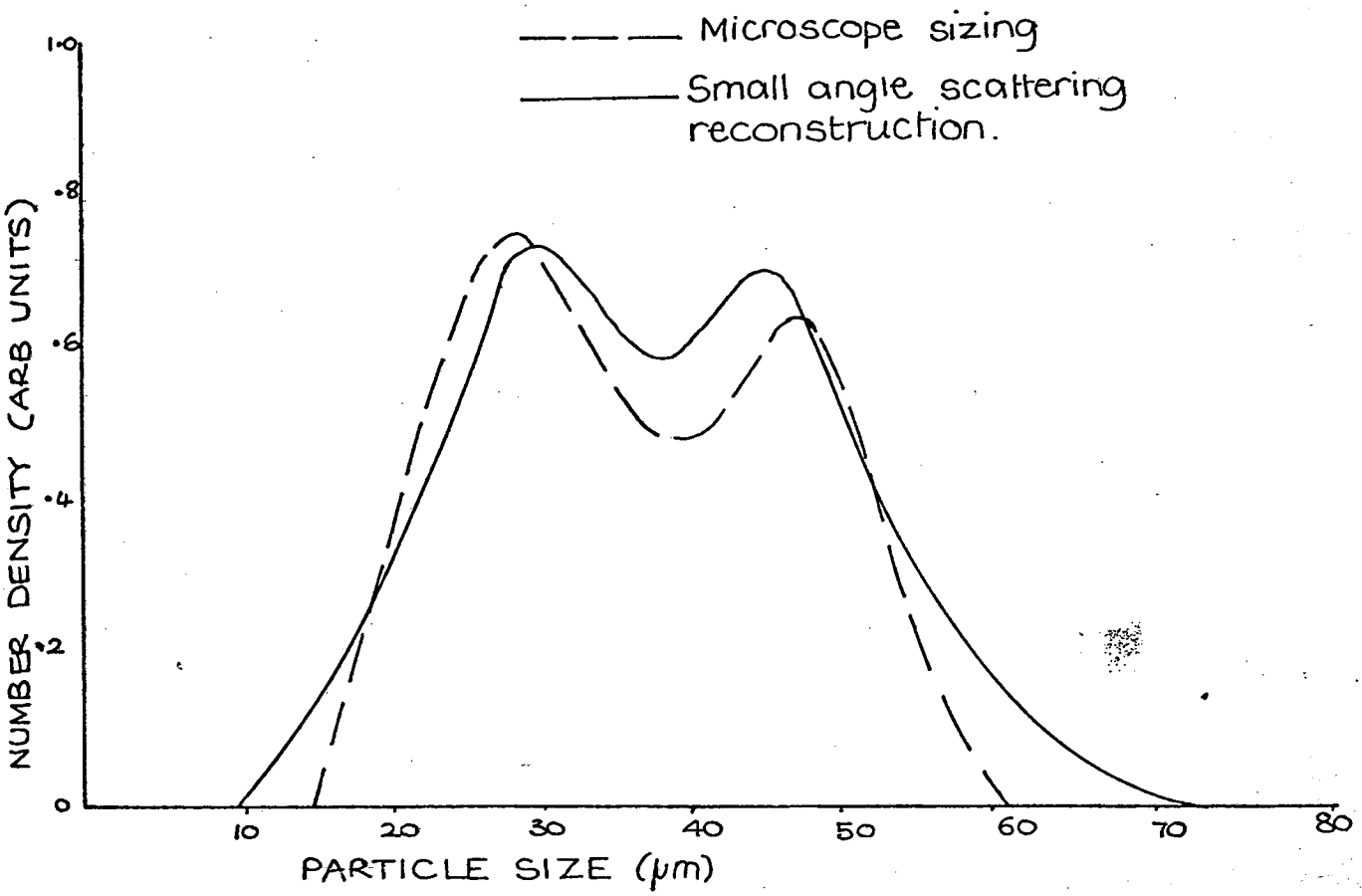

FIG. 8

SMALL ANGLE SCATTERING RECONSTRUCTION OF A DISTRIBUTION OF HOLLOW GLASS BEADS.

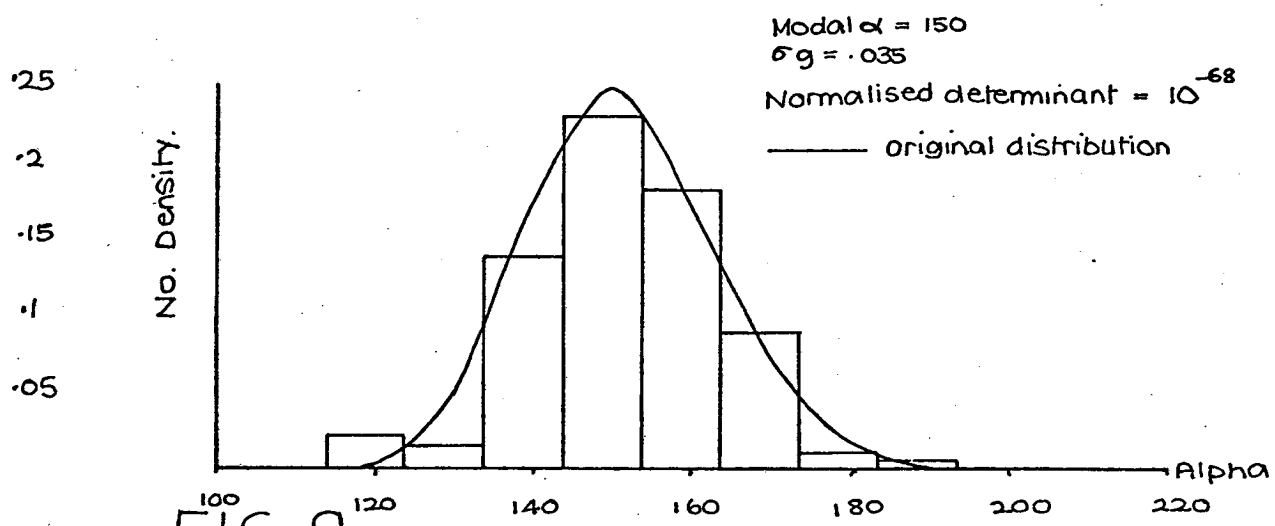

FIG. 9

LEAST SQUARES RECONSTRUCTION OF A ZERO ORDER LOG DISTRIBUTION.

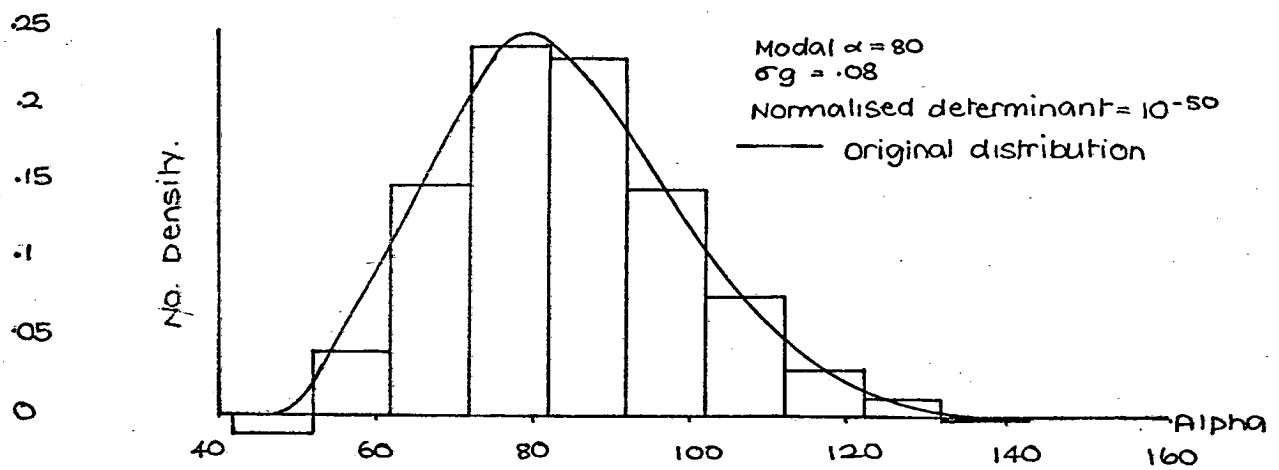

FIG. 10

LEAST SQUARES RECONSTRUCTION OF A ZERO ORDER LOG DISTRIBUTION.

1·0

FIG. 11

LEAST SQUARES SOLUTION OBTAINED WITH EACH OF THE THREE OVERLAPPING SIZE RANGES.

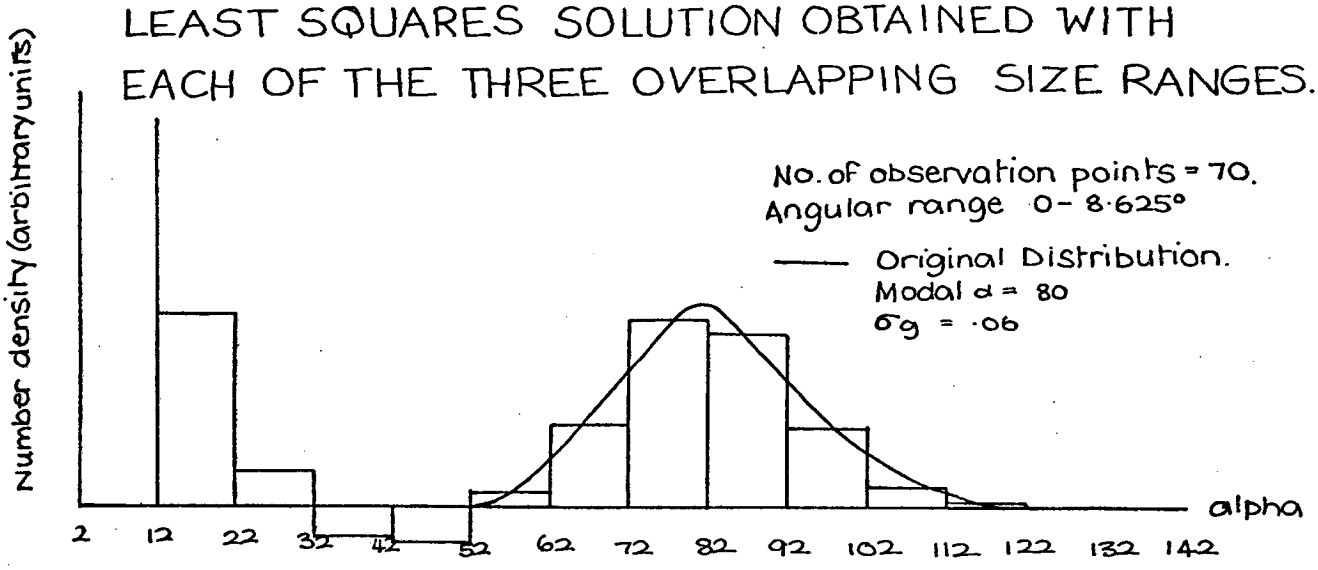

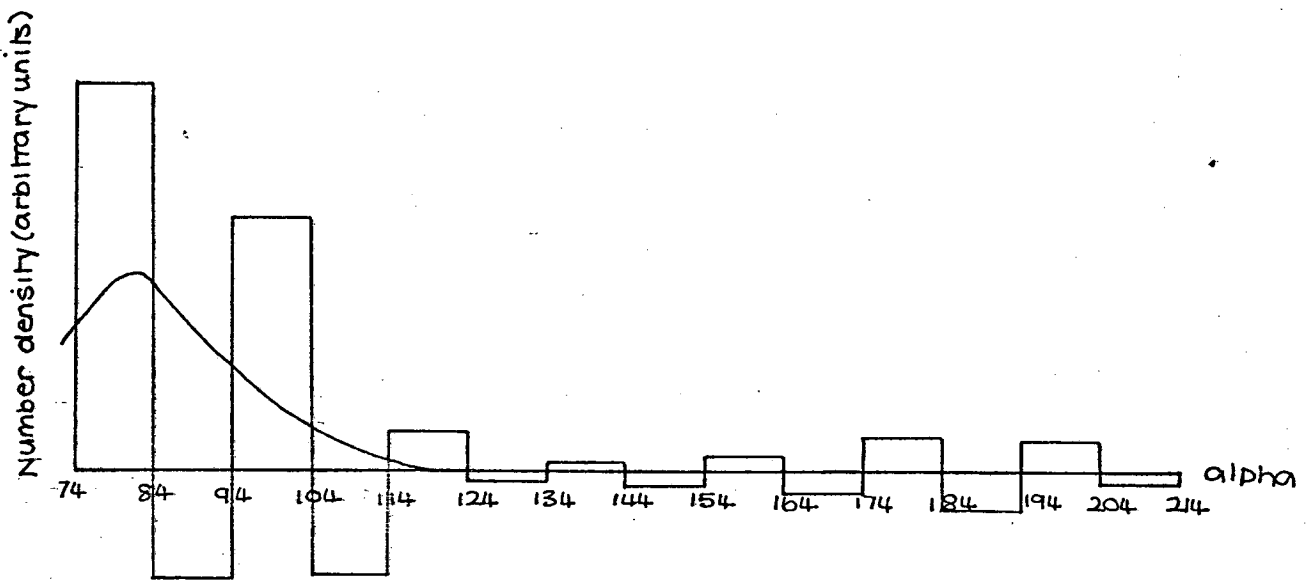

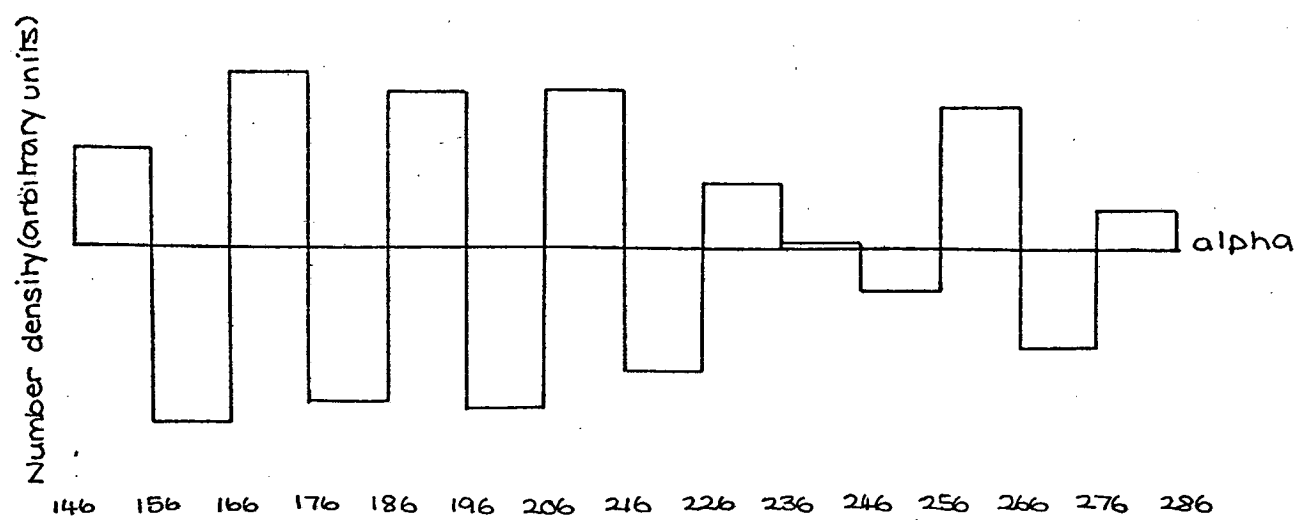

FIG. 12

COMPARISON OF LEAST SQUARES RECONSTRUCTIONS OF A Z.O.L.D. USING BLOCKED AND DISCRETE SIZE CLASSES.

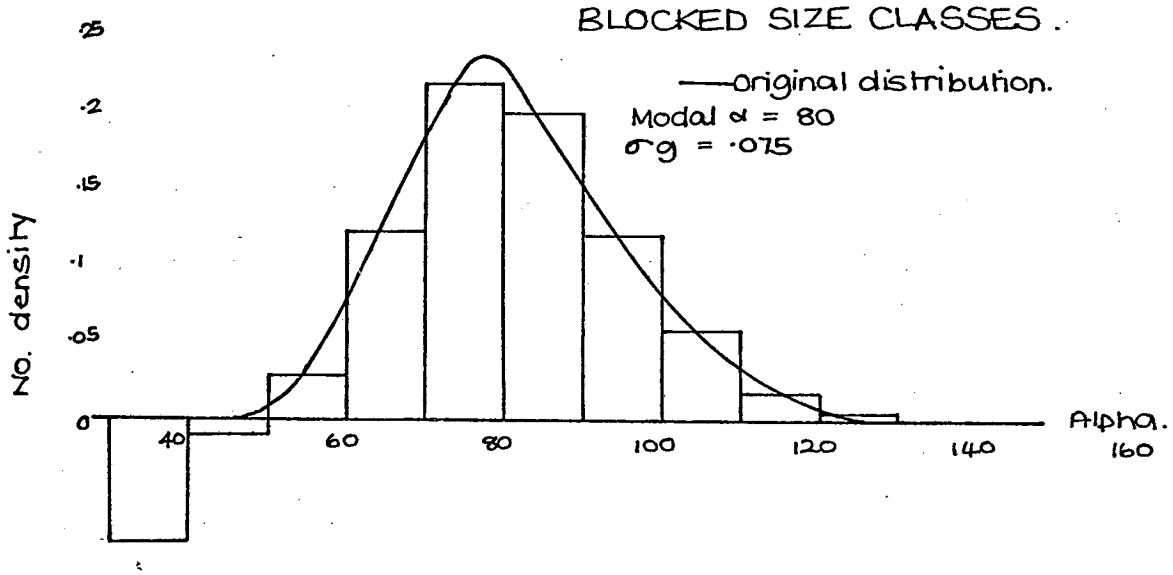

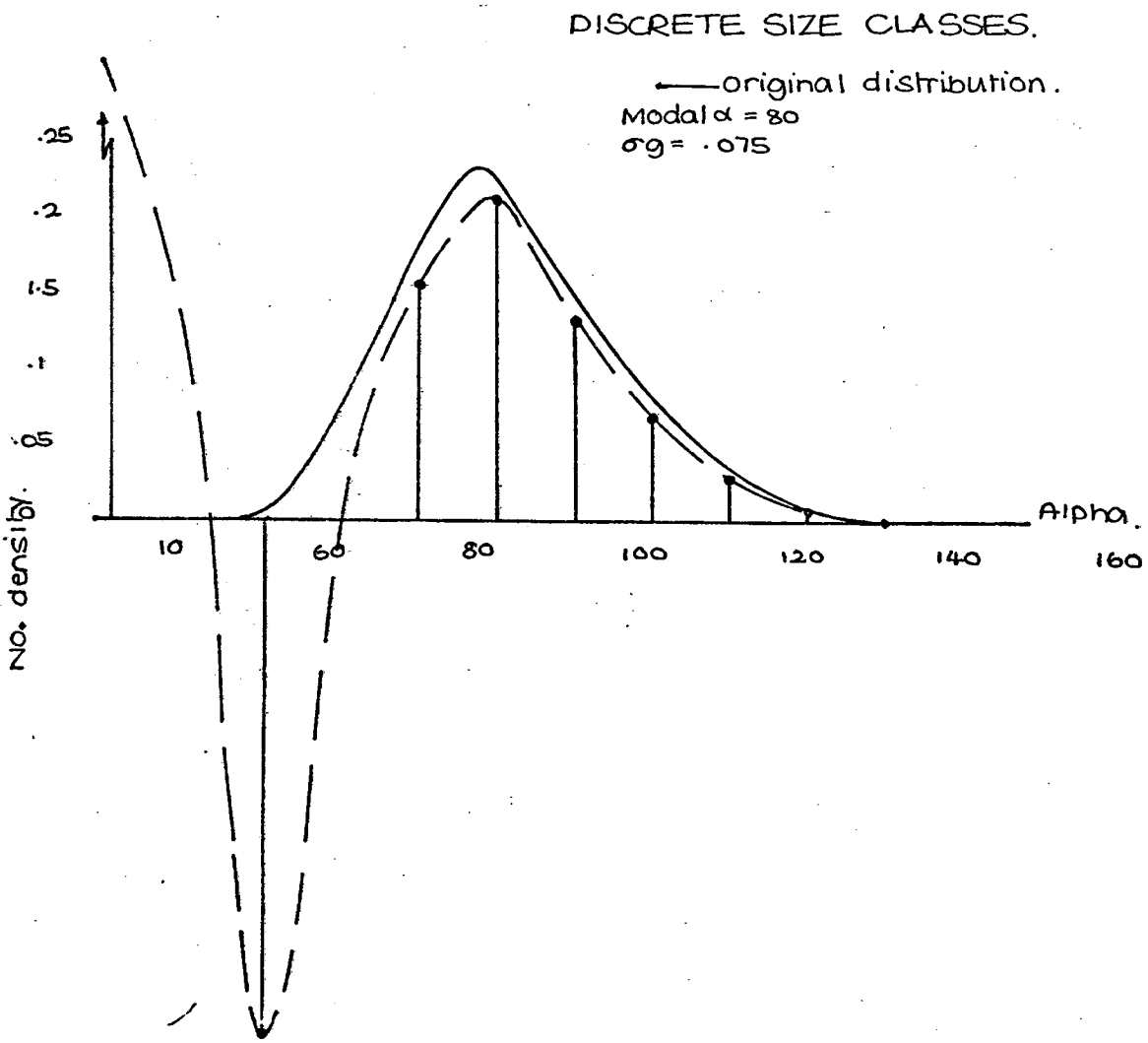

FIG 13

EFFECT OF TRUNCATION OF DATA IN THE FORWARD DIRECTION ON A LEAST-SQUARES CONSTRUCTION.

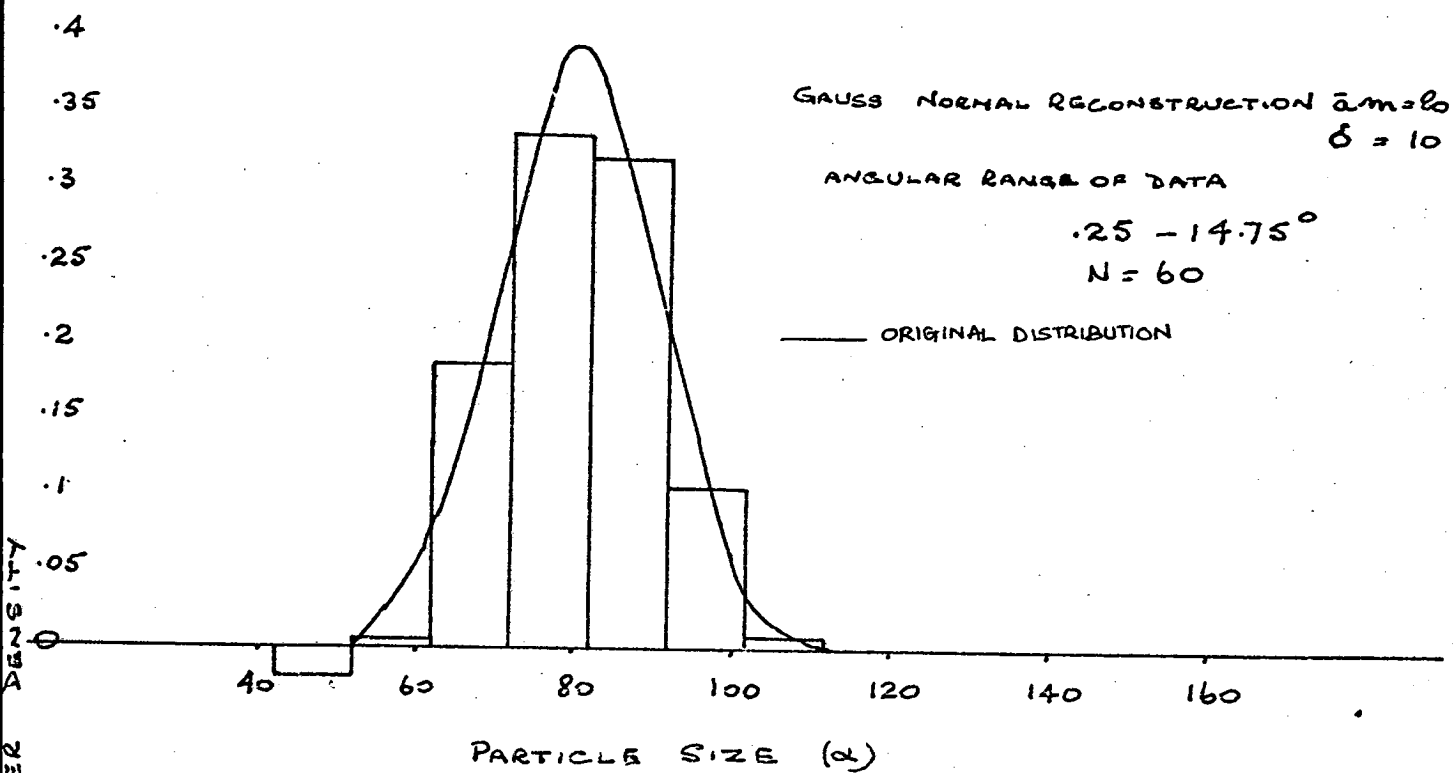

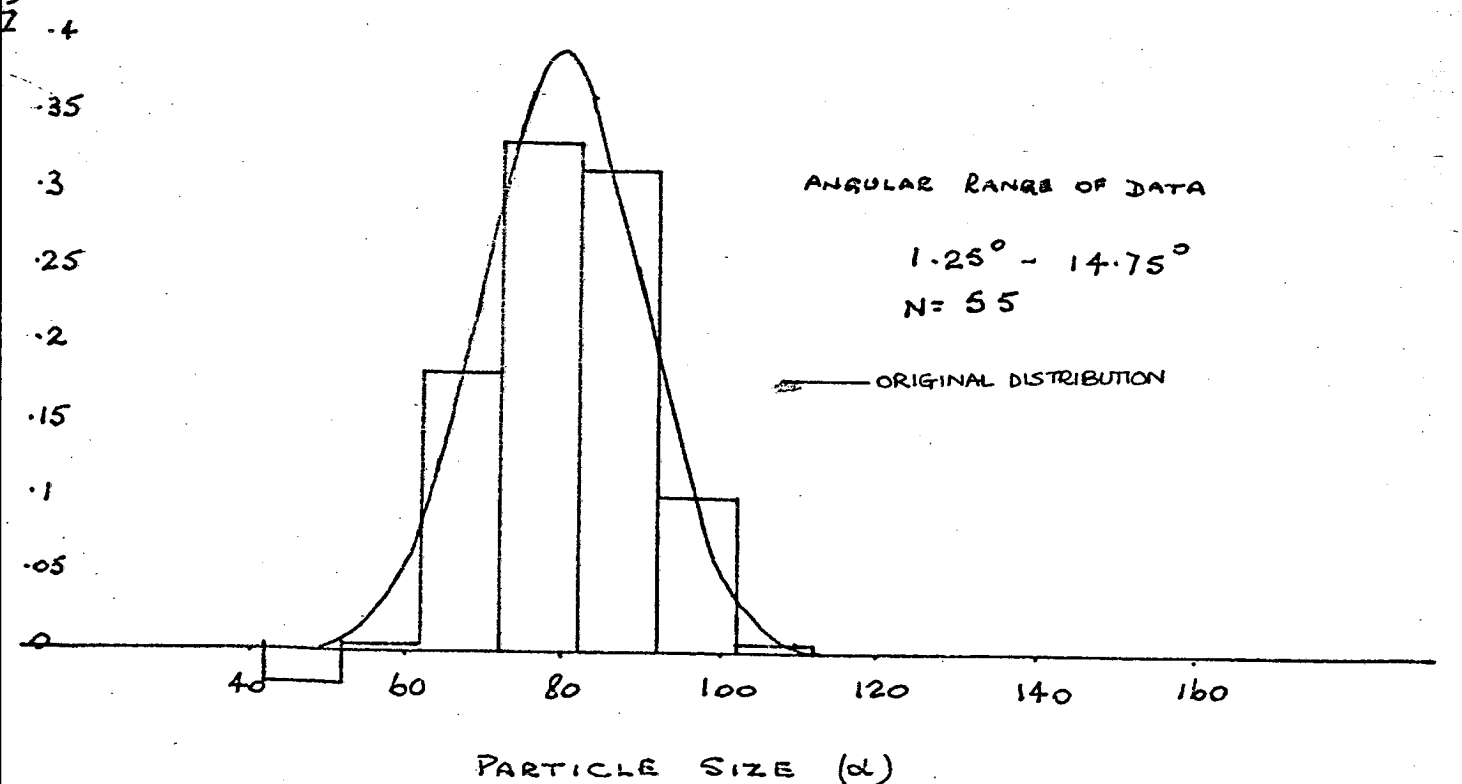

FIG 14

EFFECT OF REDUCTION OF NUMBER OF DATA POINTS AND TRUNCATION OF ANGULAR RANGE ON 2.O.L.D. LEAST SQUARES RECONSTRUCTION.

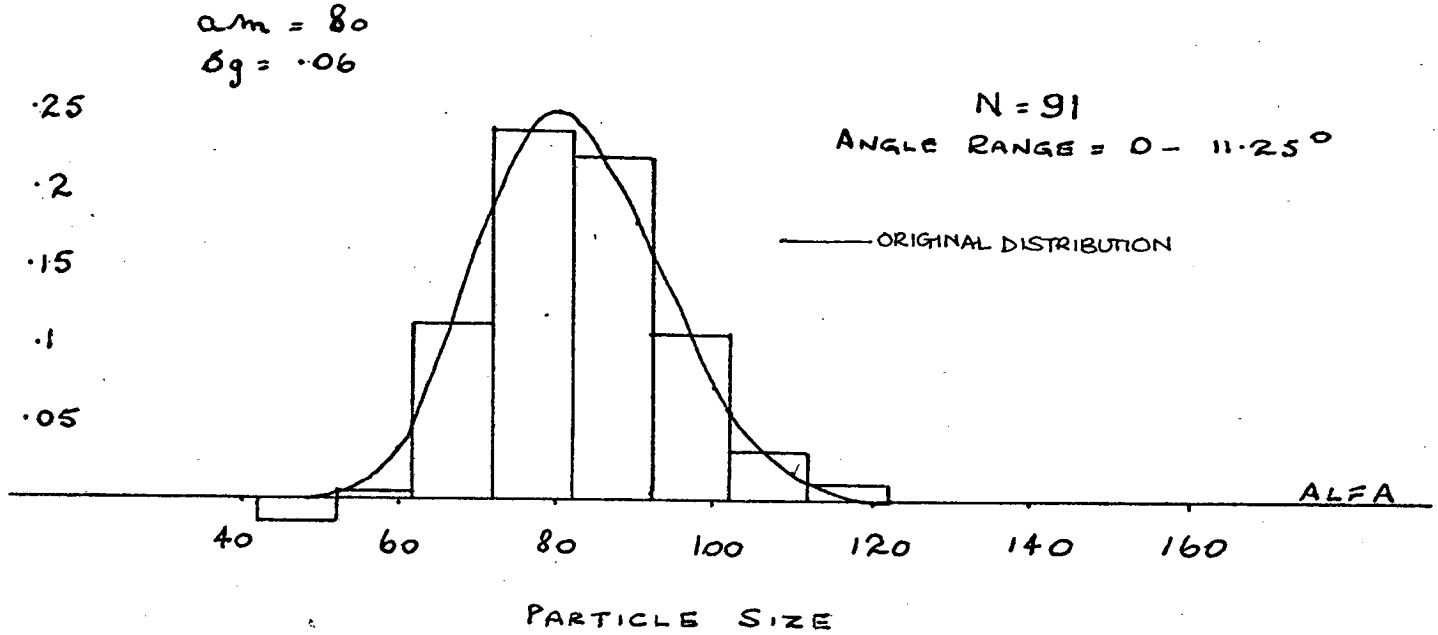

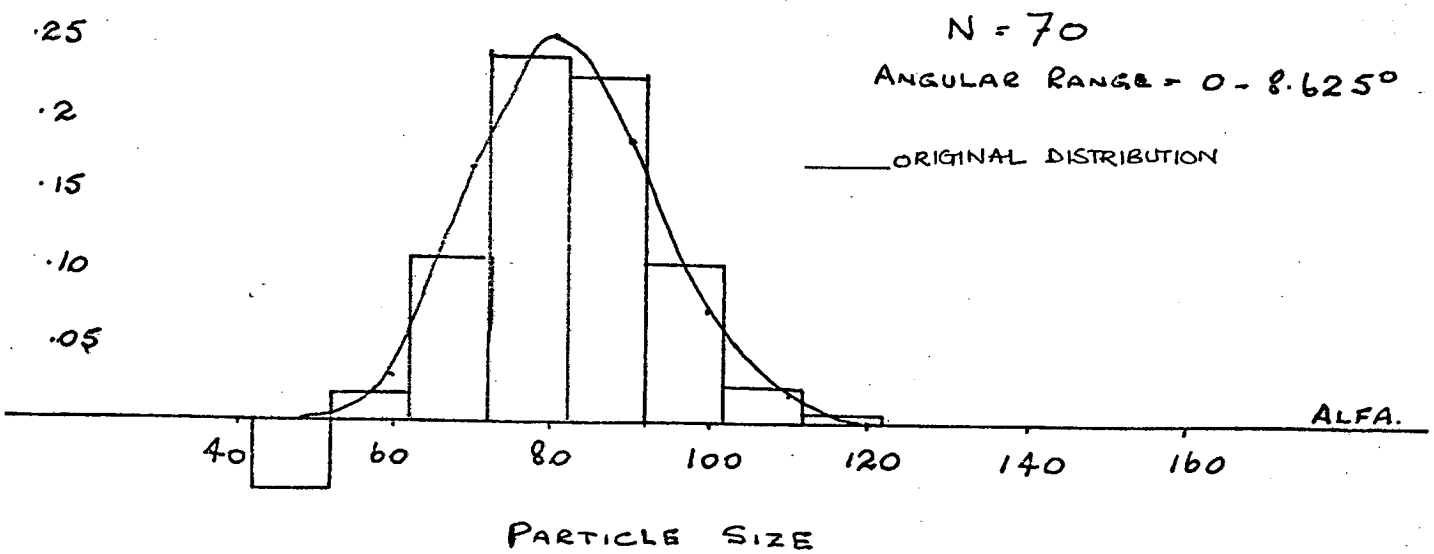

FIG 15

GRAM - SCHMIDT.

LEAST SQUARES RECONSTRUCTION OF ZERO-ORDER-LOG DISTRIBUTION.

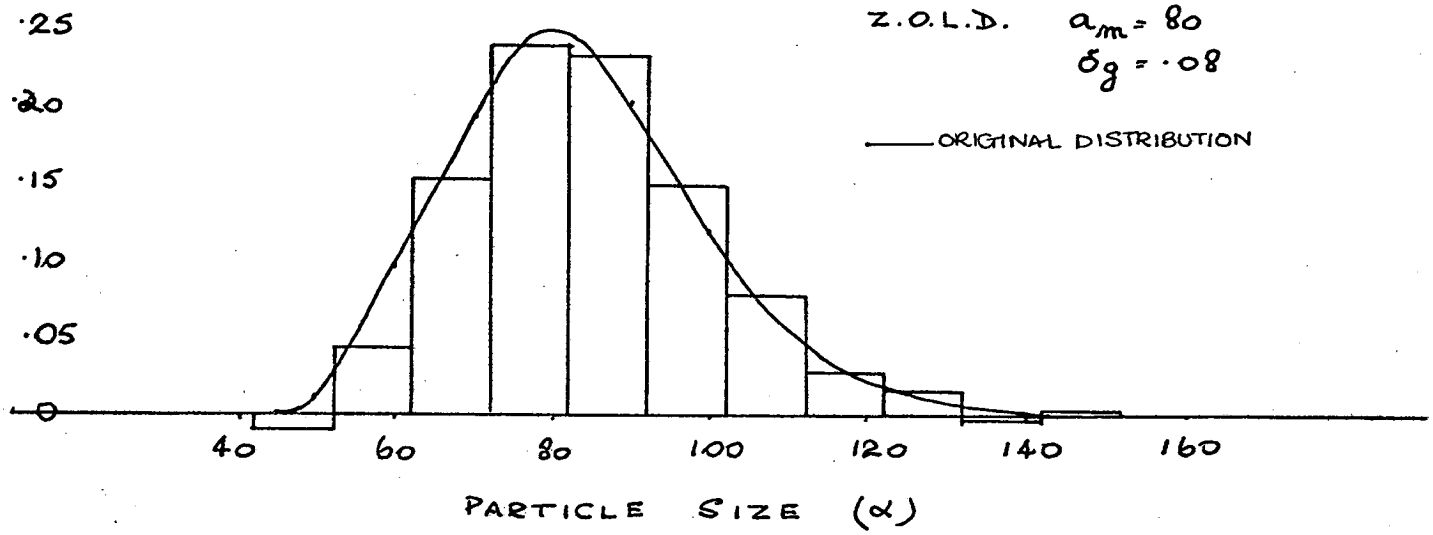

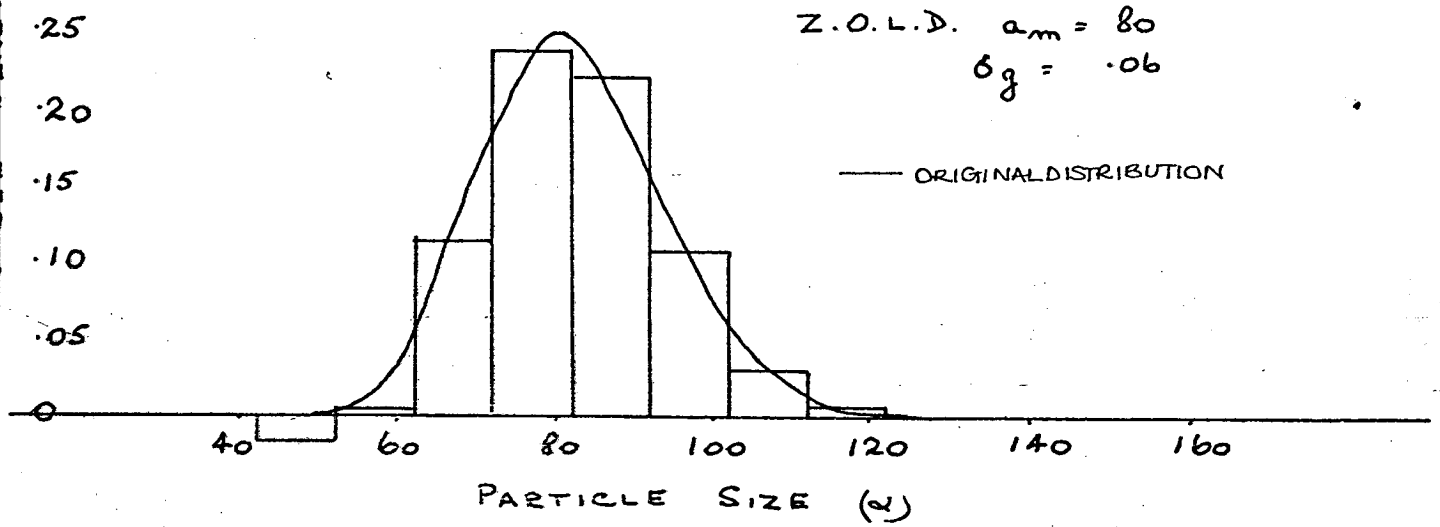

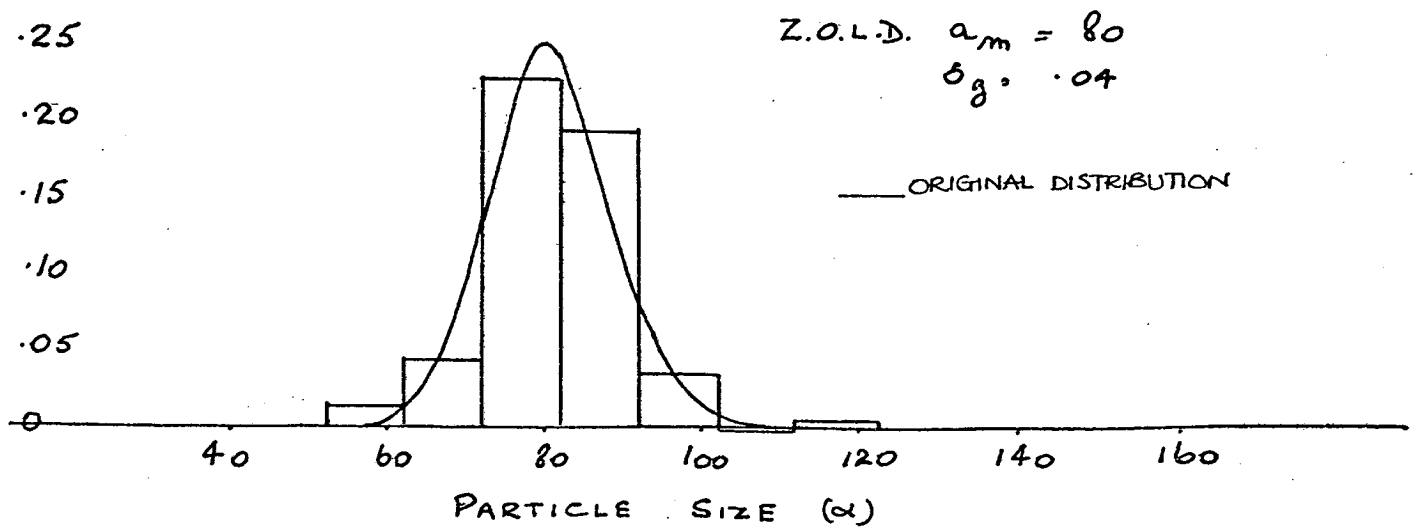

GRAM - SCHMIDT

LEAST SQUARES RECONSTRUCTION OF ZERO-ORDER - LOG DISTRIBUTIONS.

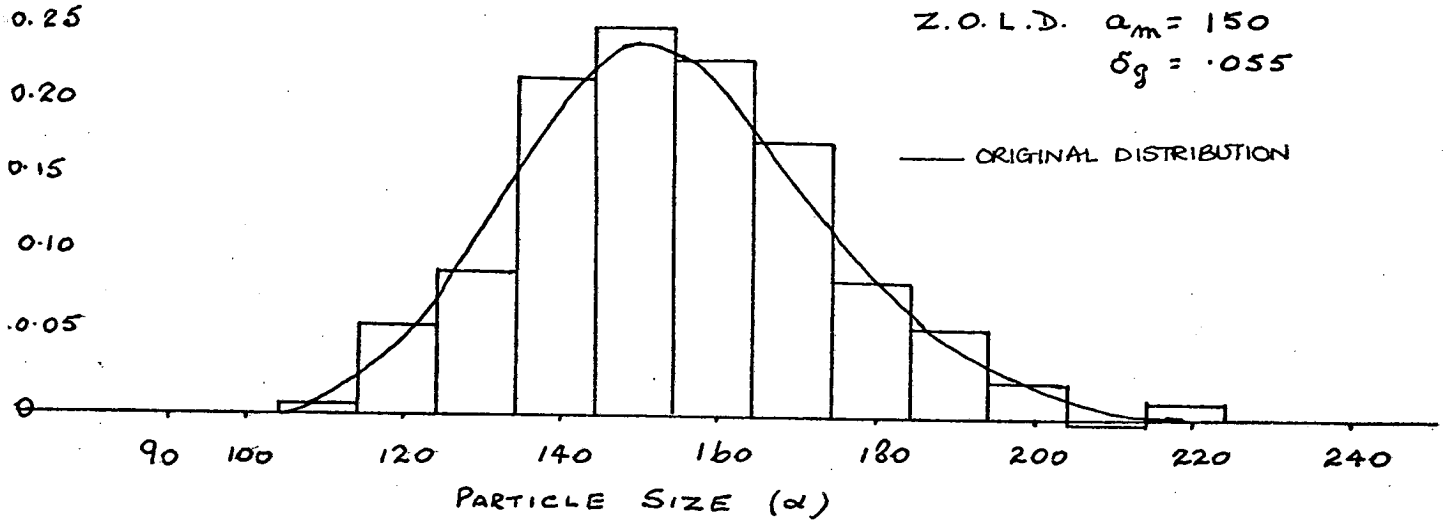

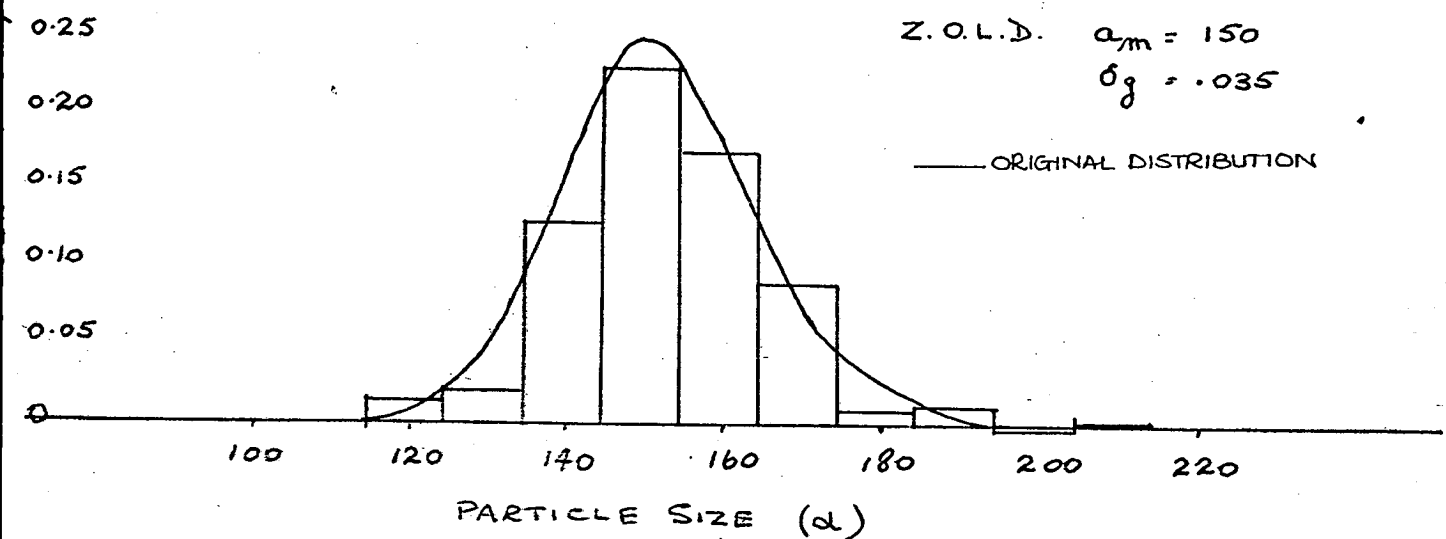

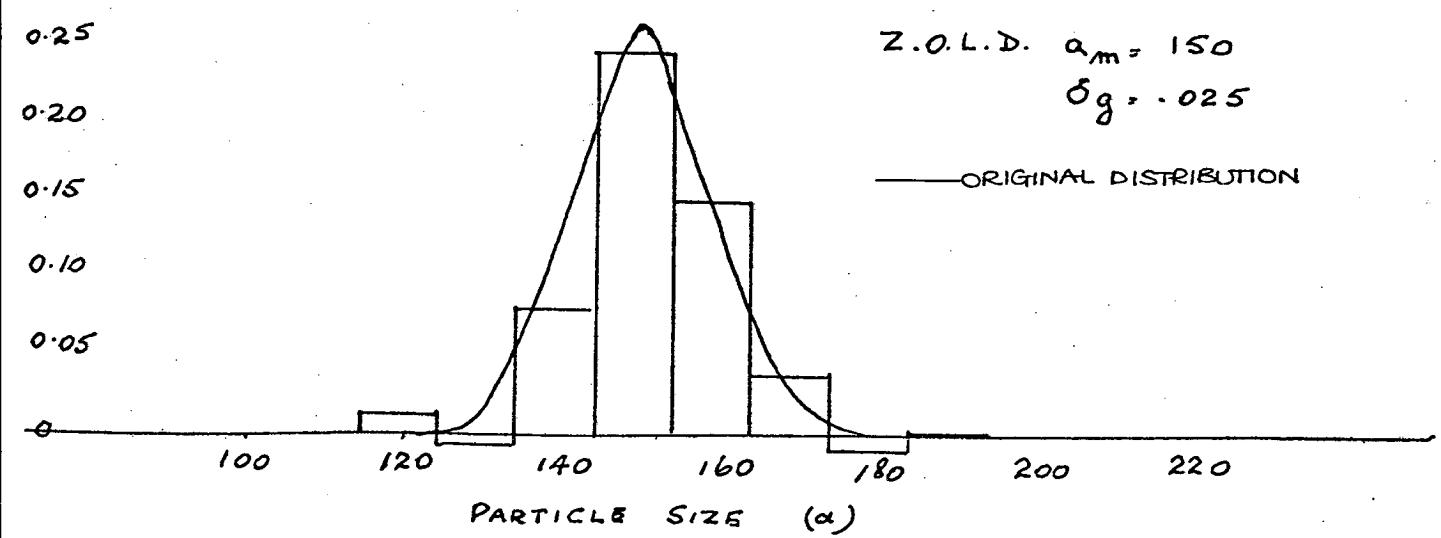

FIG. 17A

THE EFFECT OF DATA TRUNCATION ON THE LEAST SQUARES RECONSTRUCTION OF A LOG DISTRIBUTION.

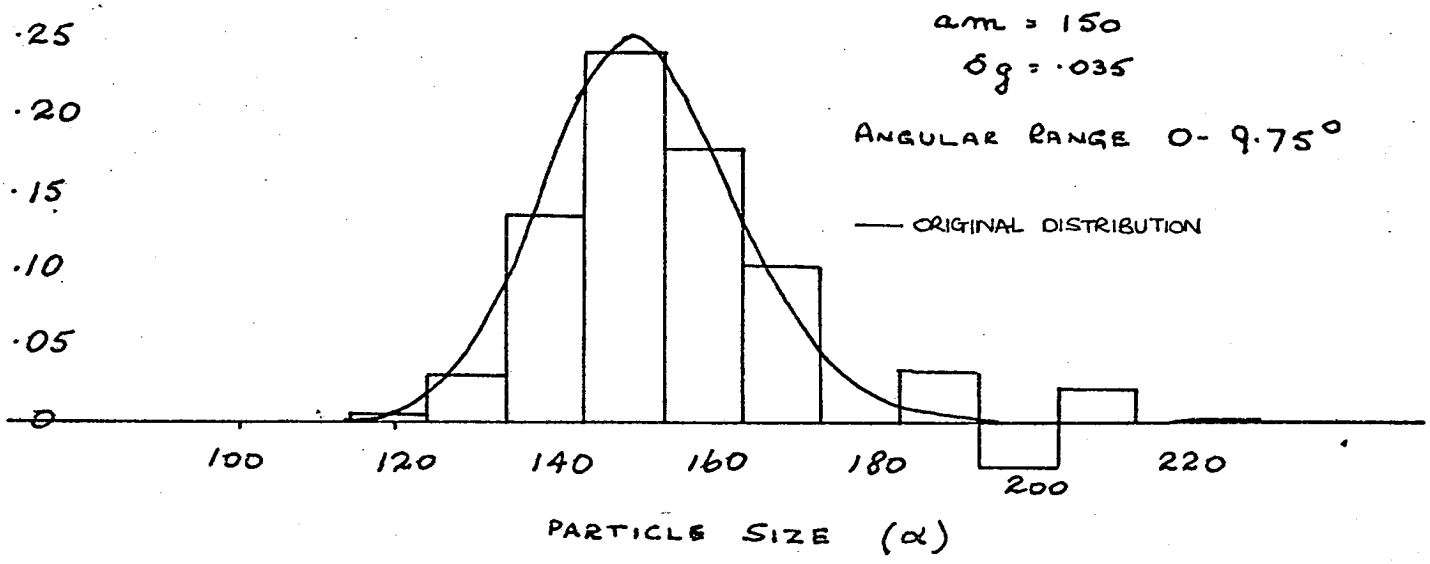

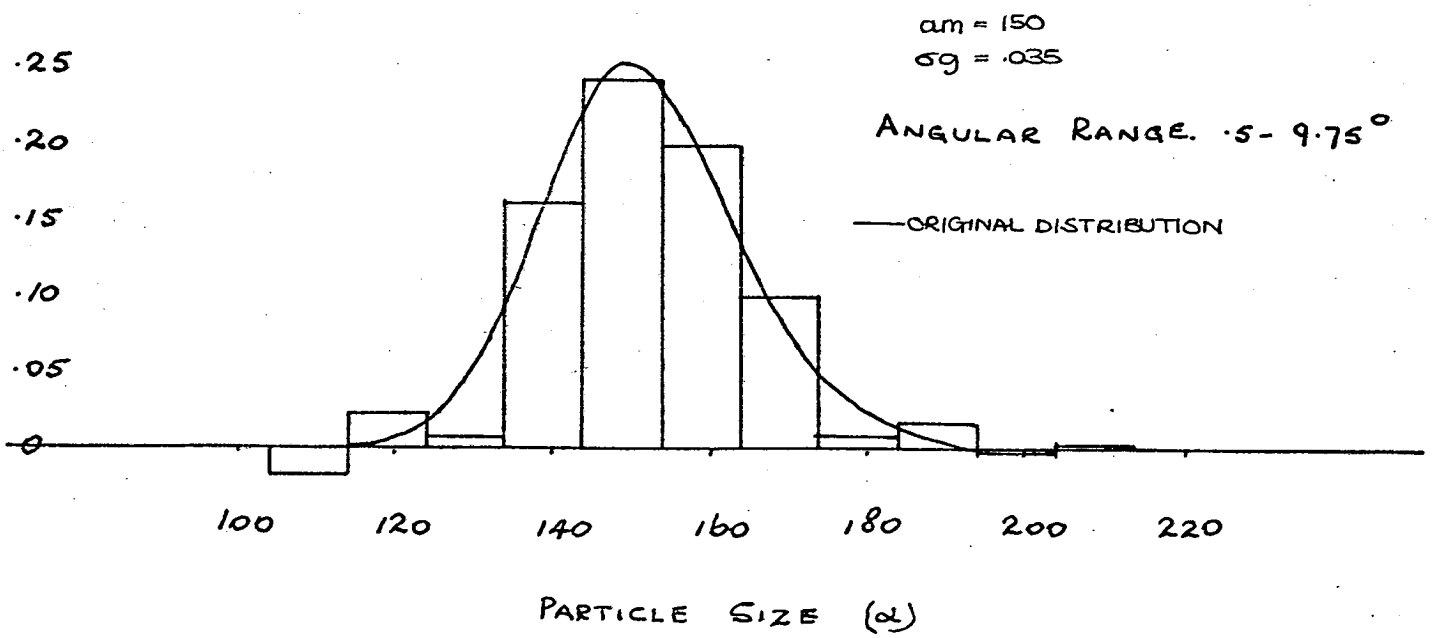

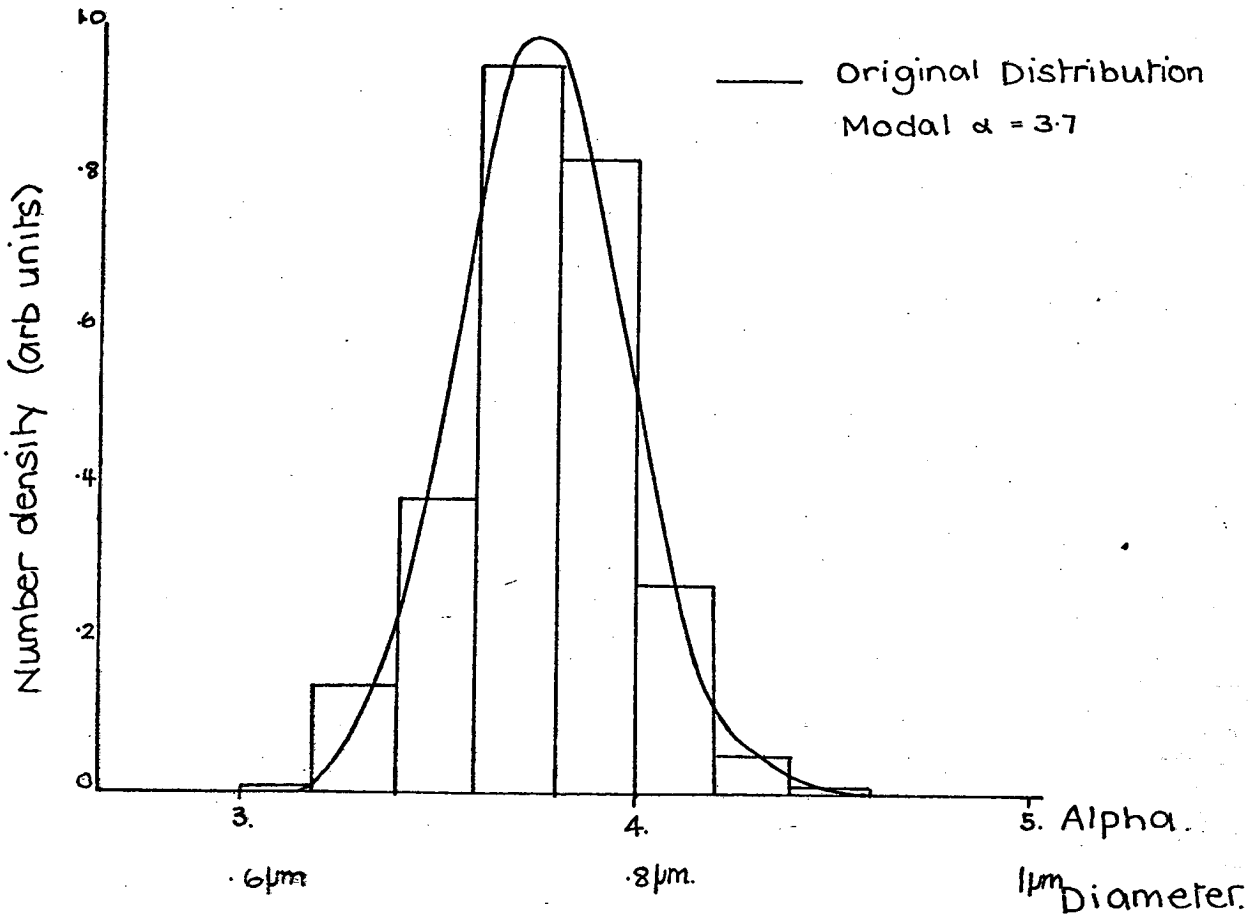

FIG. 17B.

ORTHONORMALISED LEAST SQUARES RECONSTRUCTION OF A SUBMICRON LOG DISTRIBUTION.

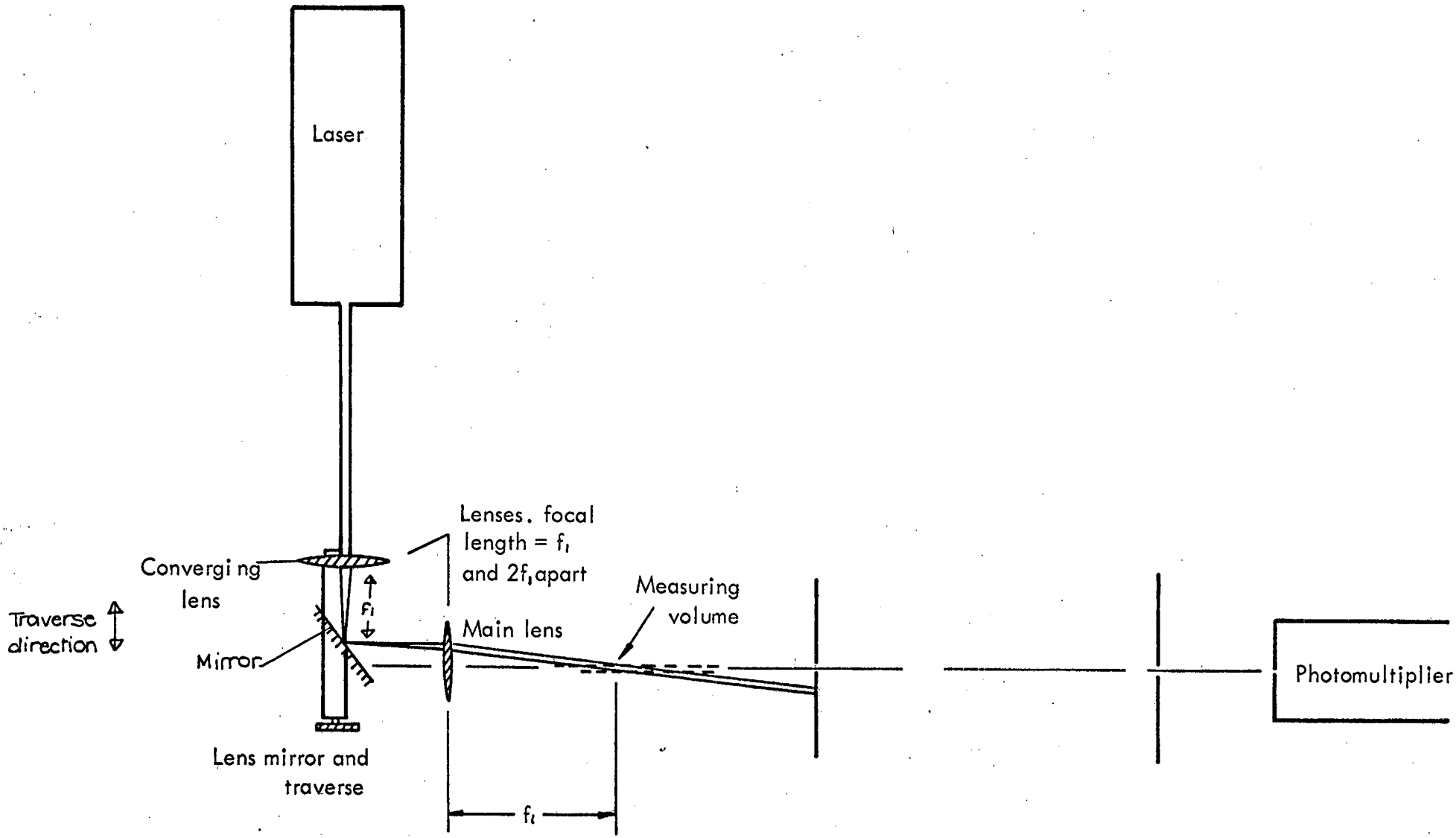

EXPERIMENTAL APPARATUS FOR MEASURING SCATTERED LIGHT FROM A SUSPENSION.

FIG.18a

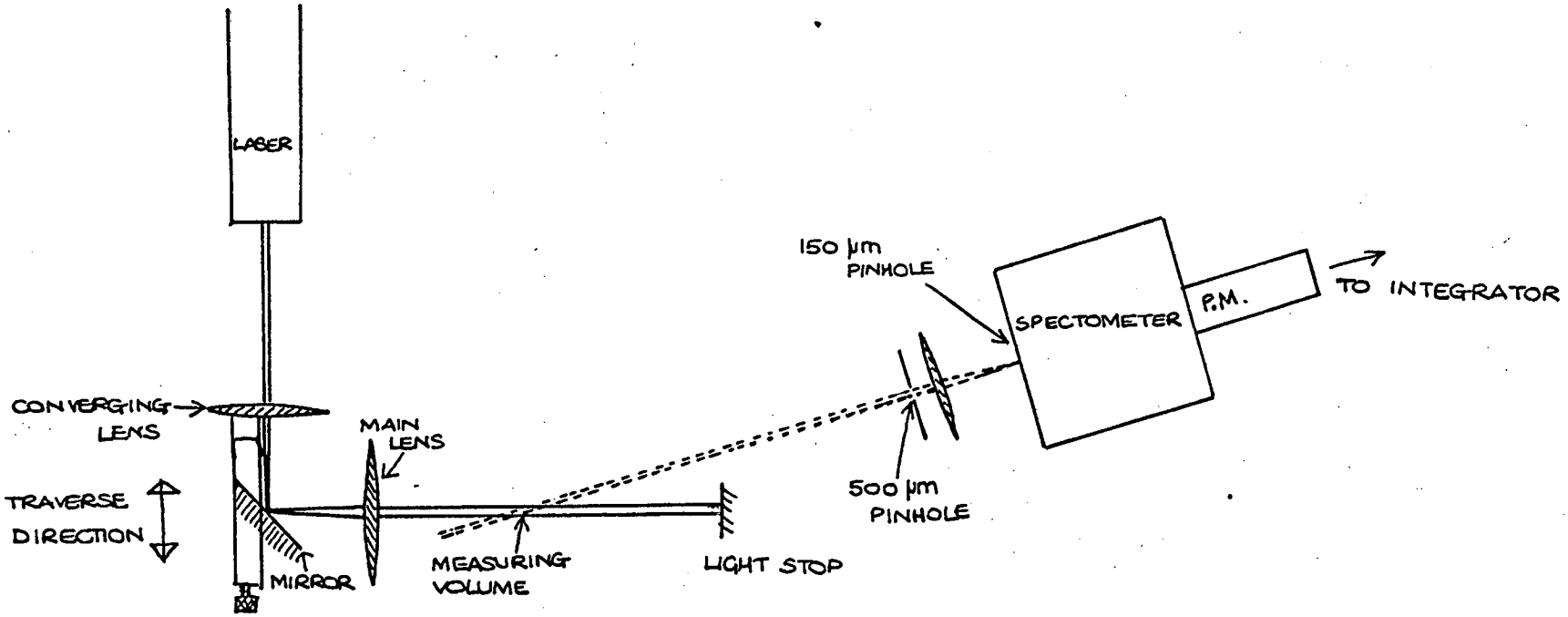

FIG 18b

SCATTERED. LIGHT APPARATUS USING A SPECTROMETER

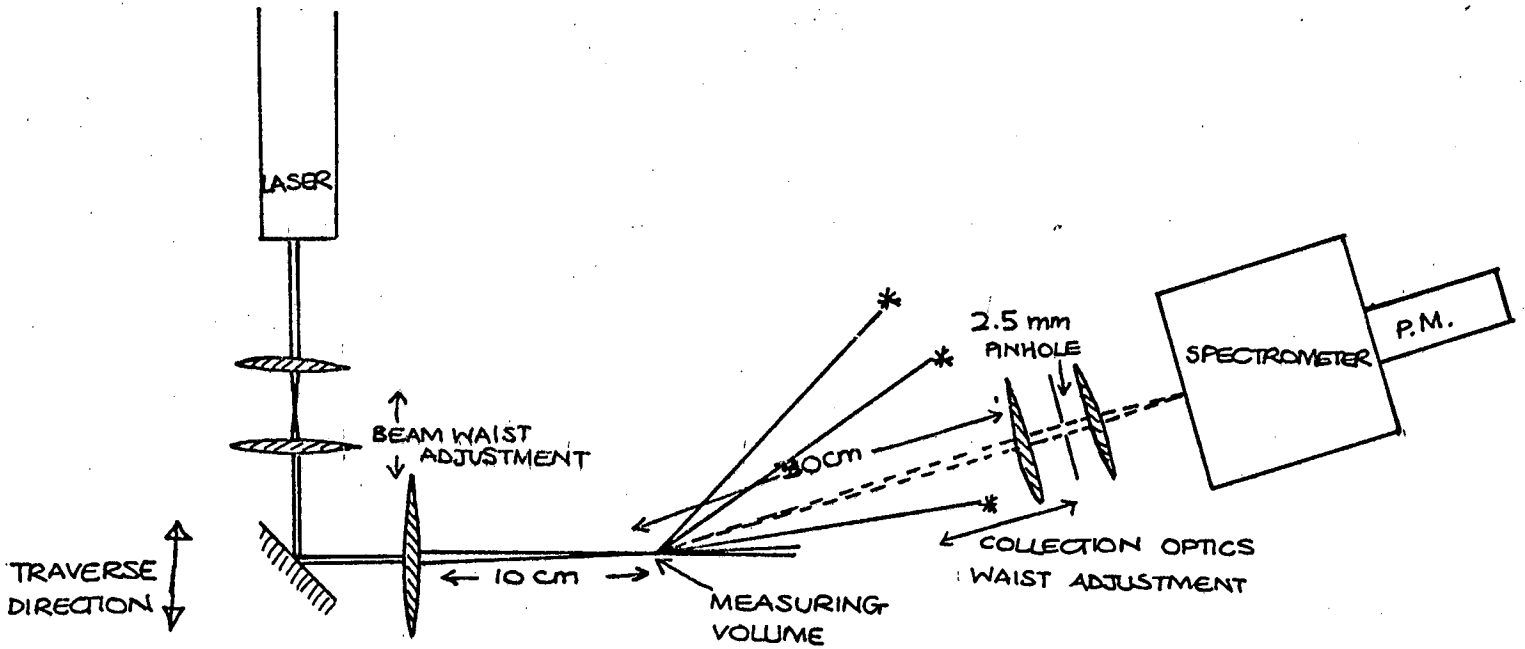

FIG 18C

SCHEMATIC OF PROPOSED LIGHT SCATTERING APPARATUS

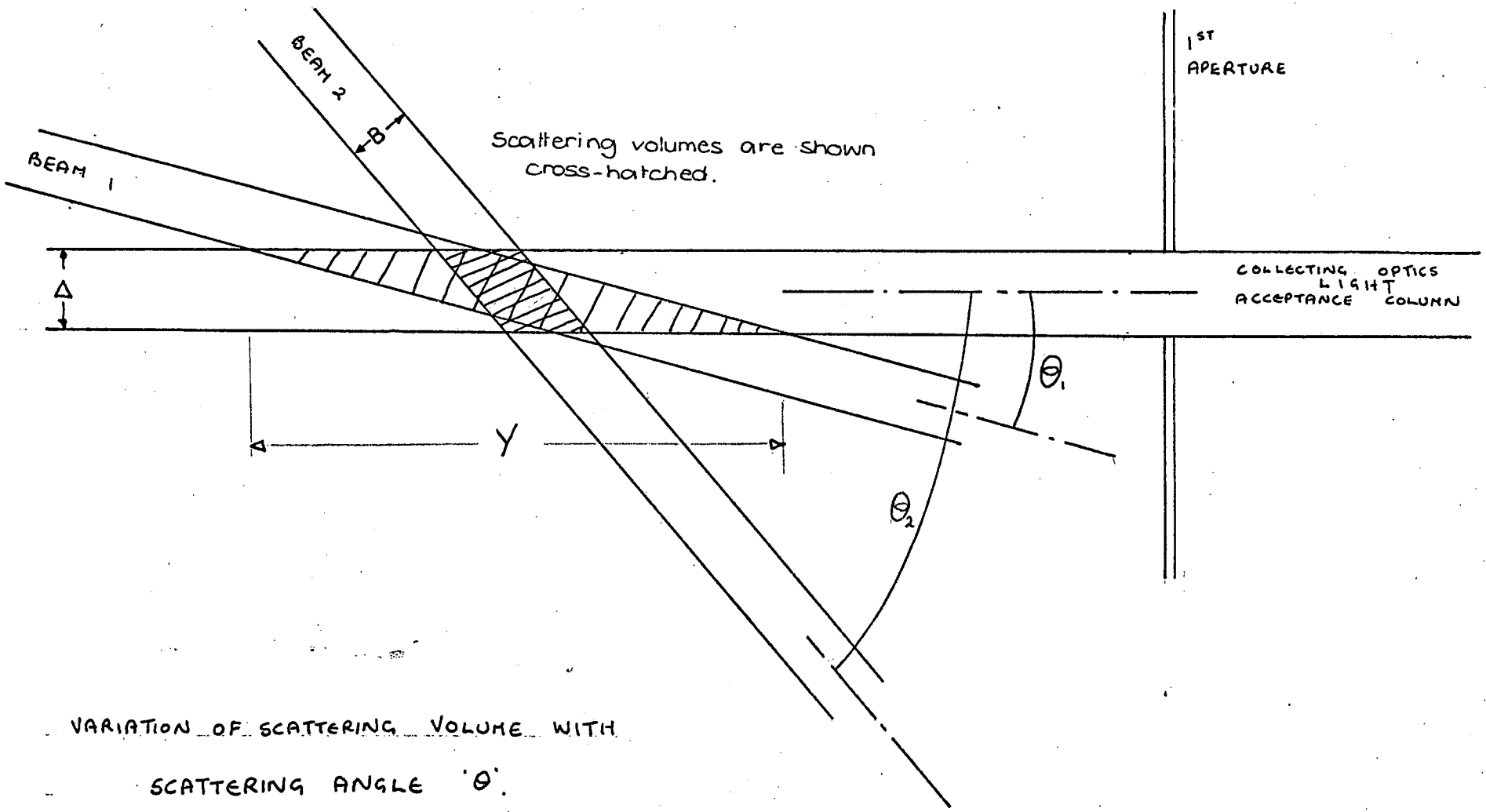

VARIATION OF SCATTERING VOLUME WITH SCATTERING ANGLE 'θ'.

FIG.19a

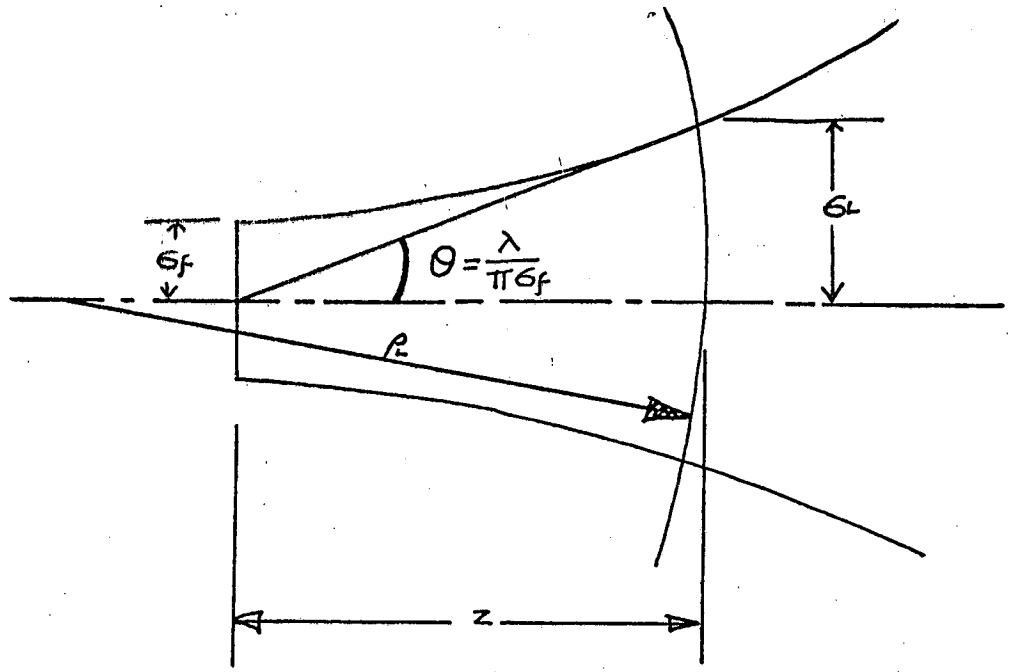

FIG 19b

CONTOUR OF A GUASSIAN BEAM

FIG.20

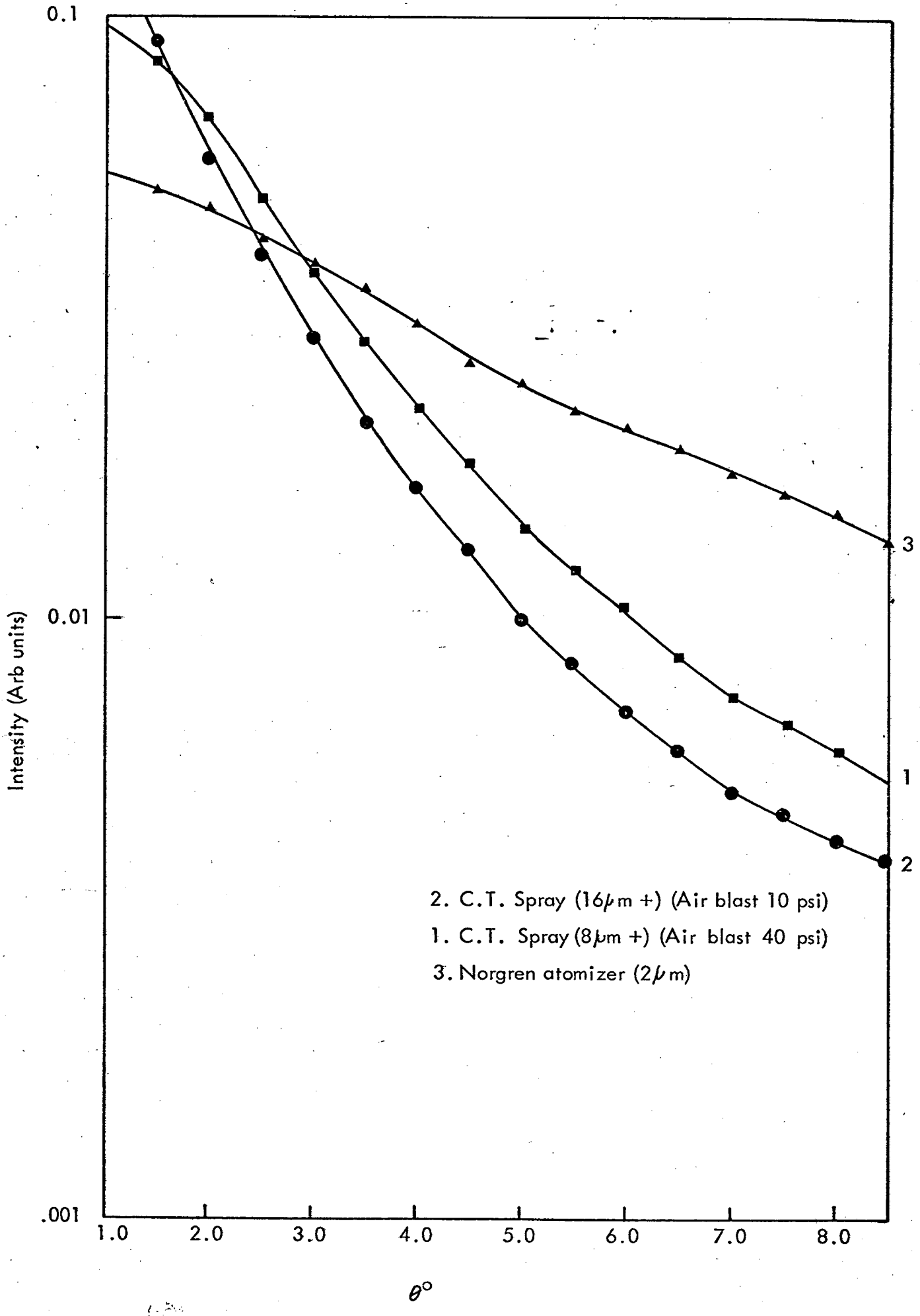

FIG.3 CHANGING INTENSITY SIGNATURE WITH ALTERATION OF PARTICLE SIZE.

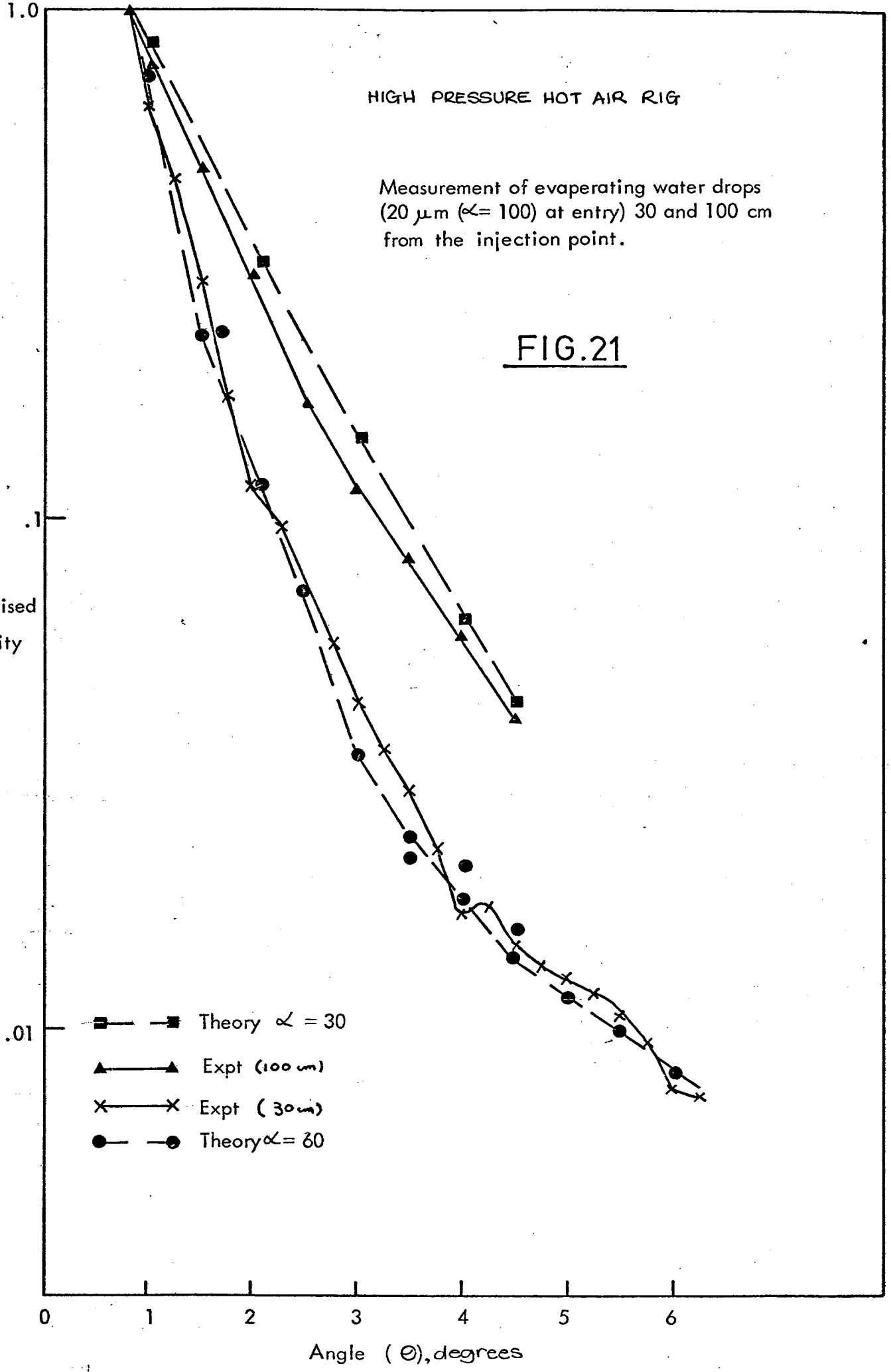

COMPARISON OF EXPERIMENTAL DATA WITH MIE THEORY.

FIG. 22,
INVERSION OF EXPERIMENTAL DATA.
USING GRAM-SCHMIDT ORTHONORMALISED
LEAST SQUARES METHOD

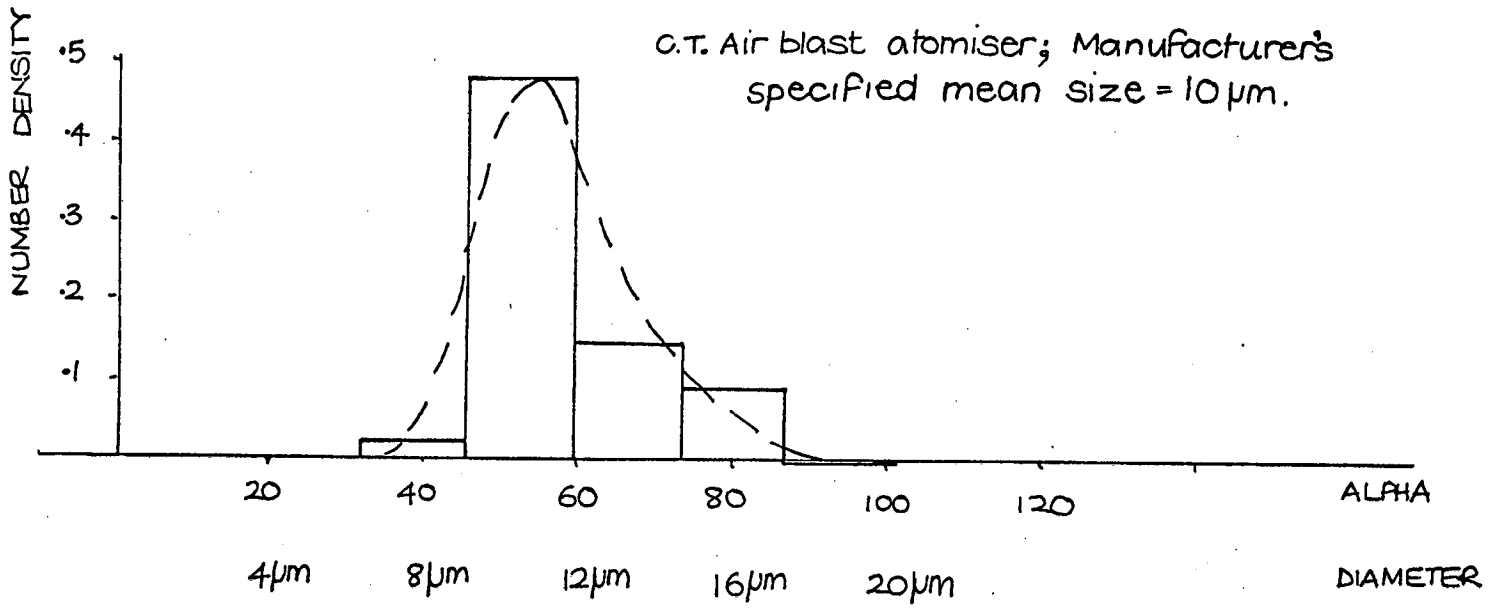

FIG 23

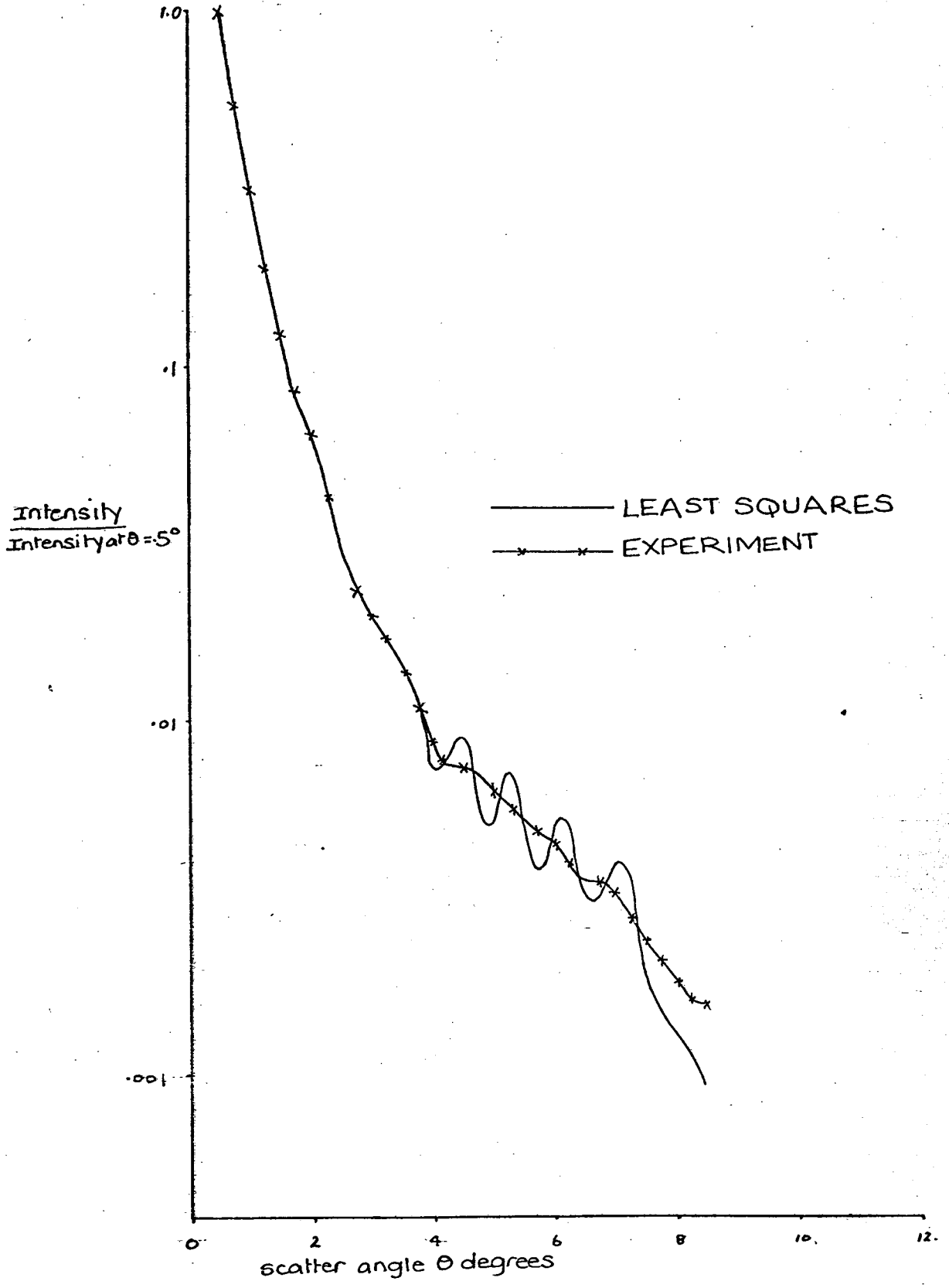

COMPARISON OF THE LEAST SQUARES APPROXIMATION OF THE ATOMIZER ANGULAR INTENSITY VARIATION WITH EXPERIMENTAL DATA.

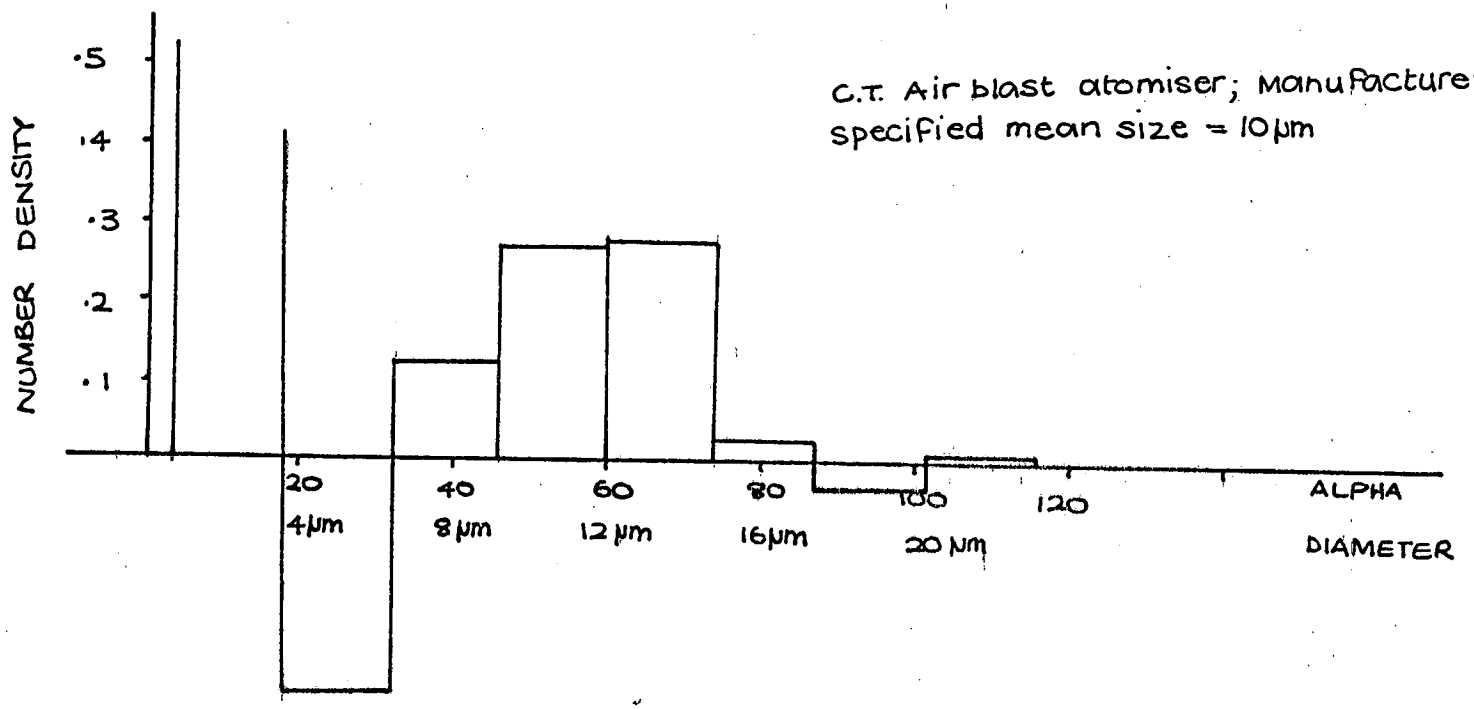

FIG 24

LEAST SQUARES RECONSTRUCTION WITH AN INTERVAL BETWEEN ADJACENT SUB-SIZE CLASSES OF $\Delta\alpha = 2$

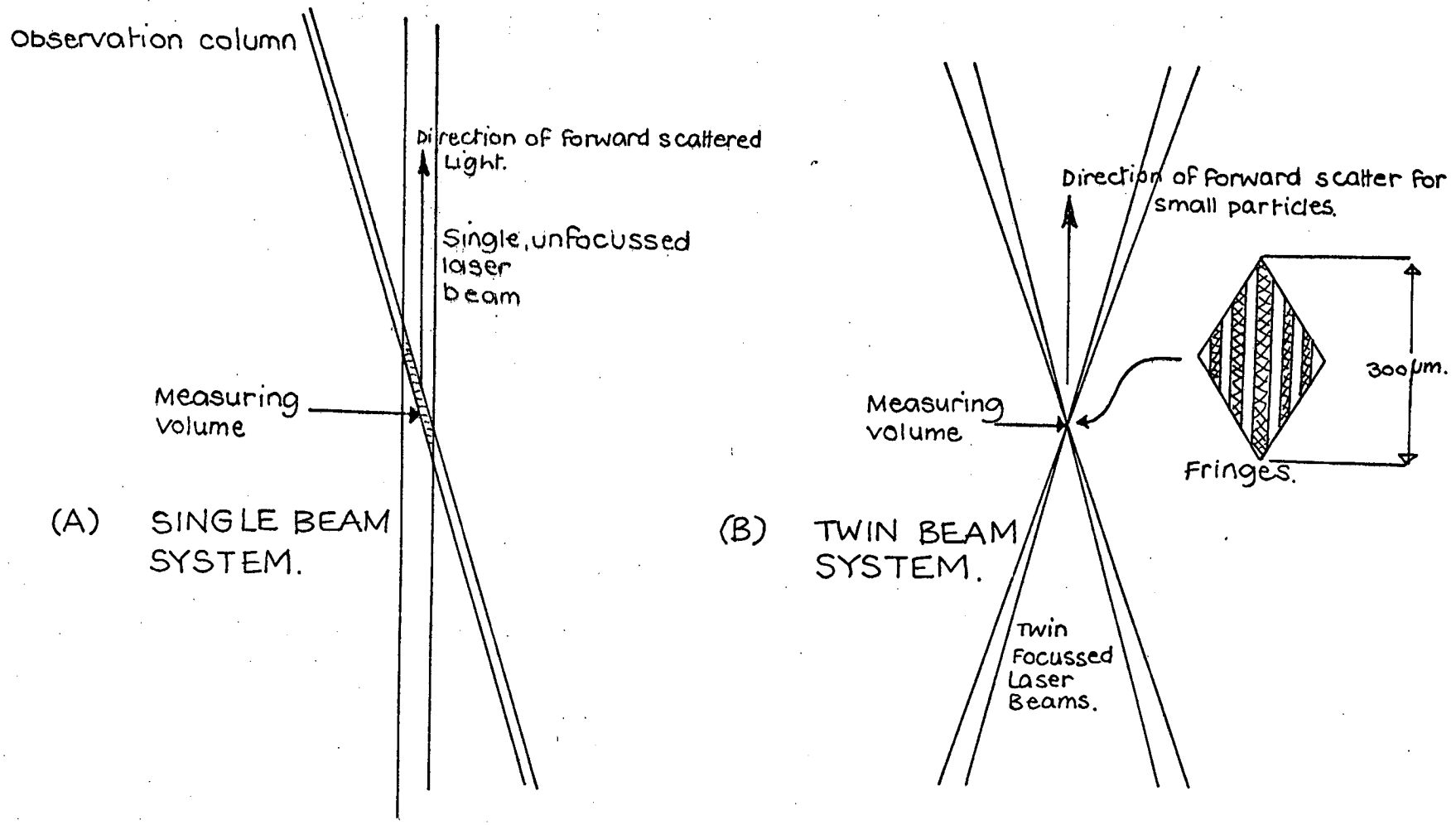

FIG. 25. COMPARISON OF MEASURING VOLUMES OF SINGLE AND TWIN BEAM SYSTEMS OF ILLUMINATION.

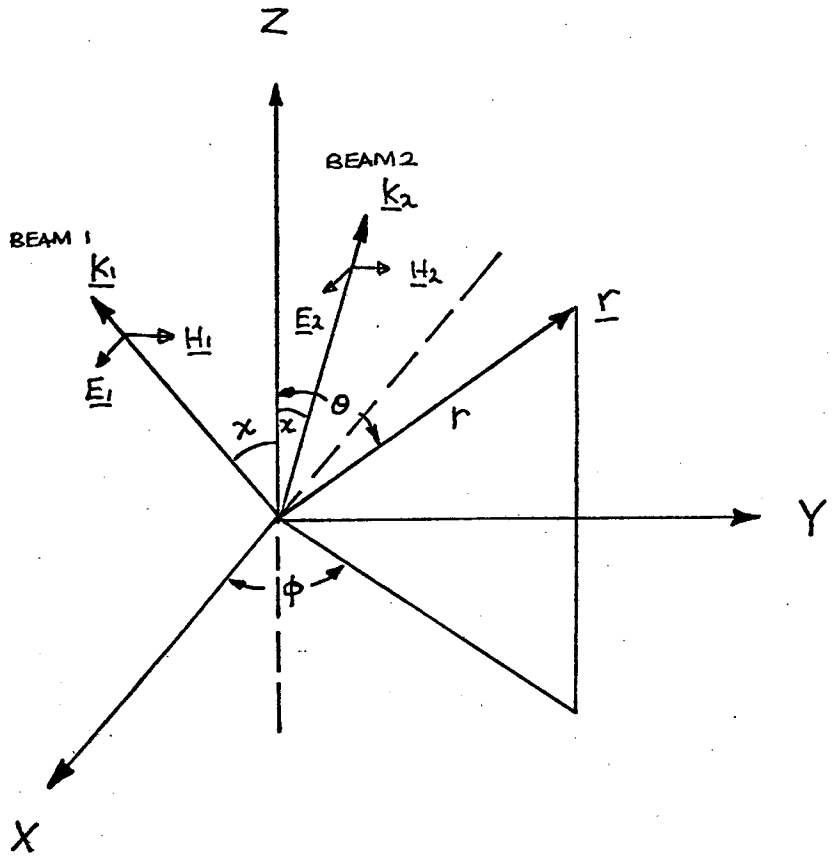

FIG. 26

FIELD CO-ORDINATES AND NOTATION

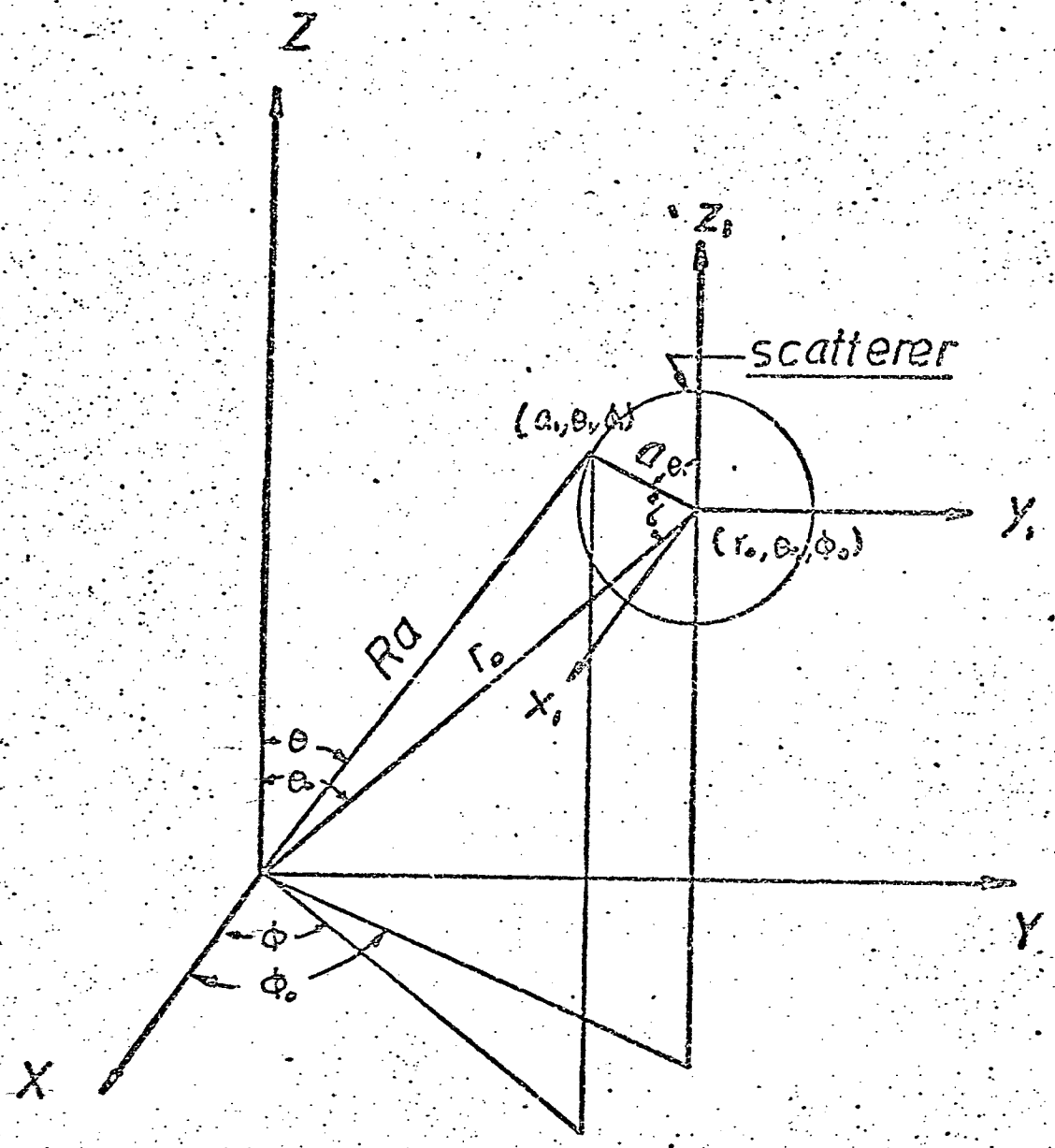

Particle Coordinates and notation

FIG.27

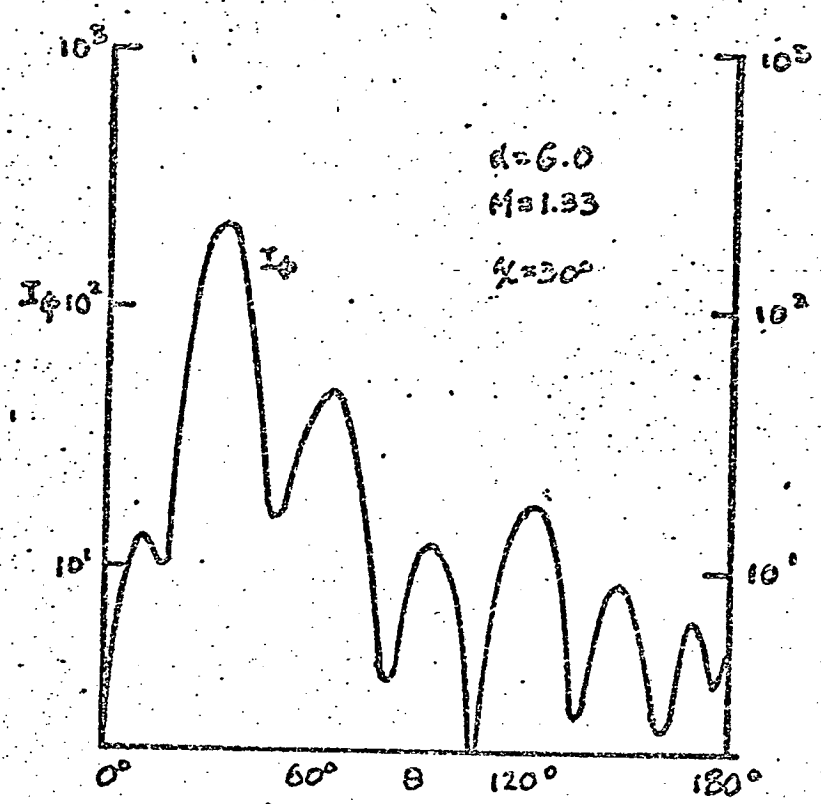

Fig.29 Calculated Scattering intensity - Asymmetric case

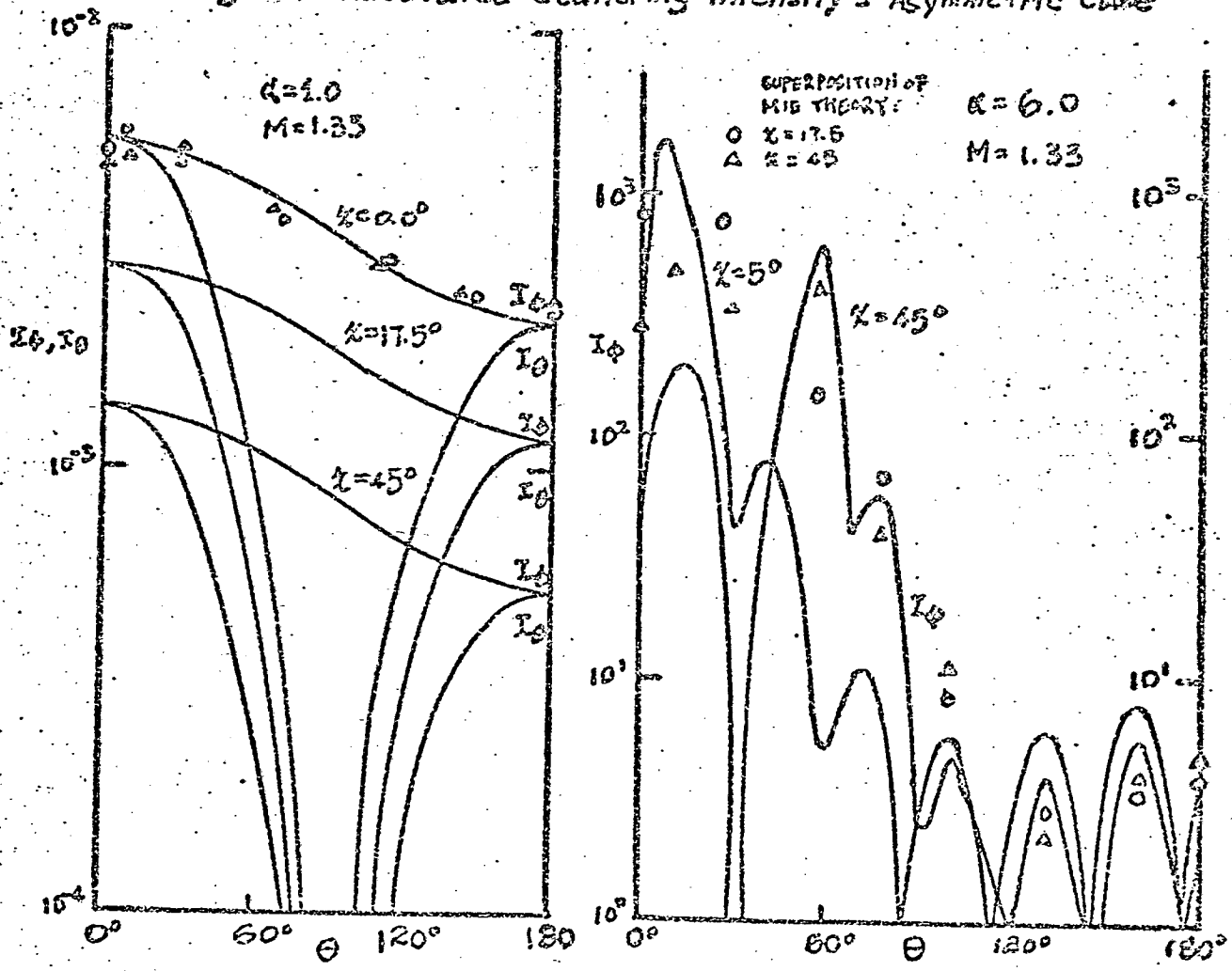

Calculated Scattering intensity - Symmetric Case

Fig.28

VARIATION OF FORWARD TO BACK SCATTERING RATIO WITH NON-DIMENSIONAL SIZE.

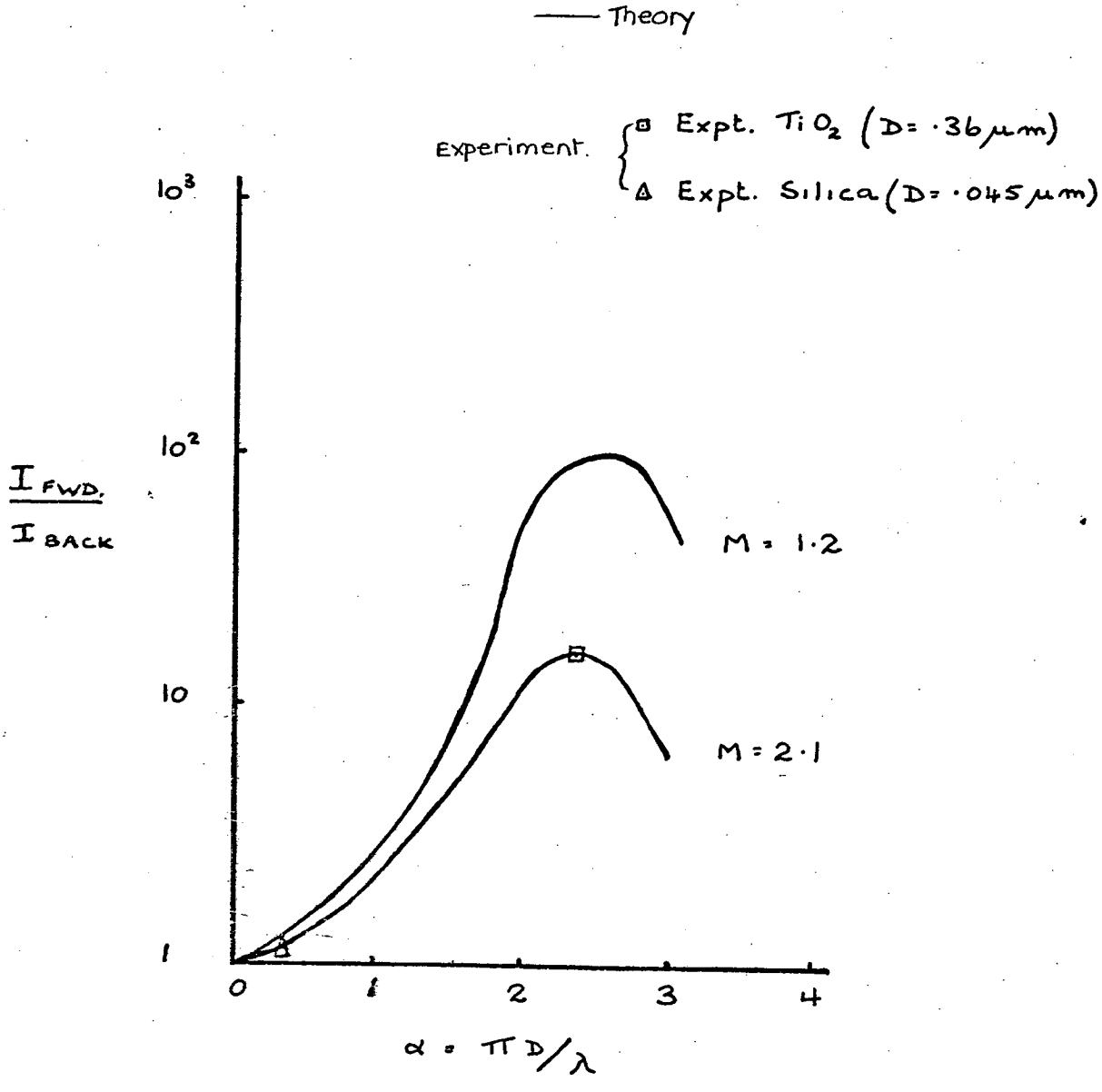

FIG 30

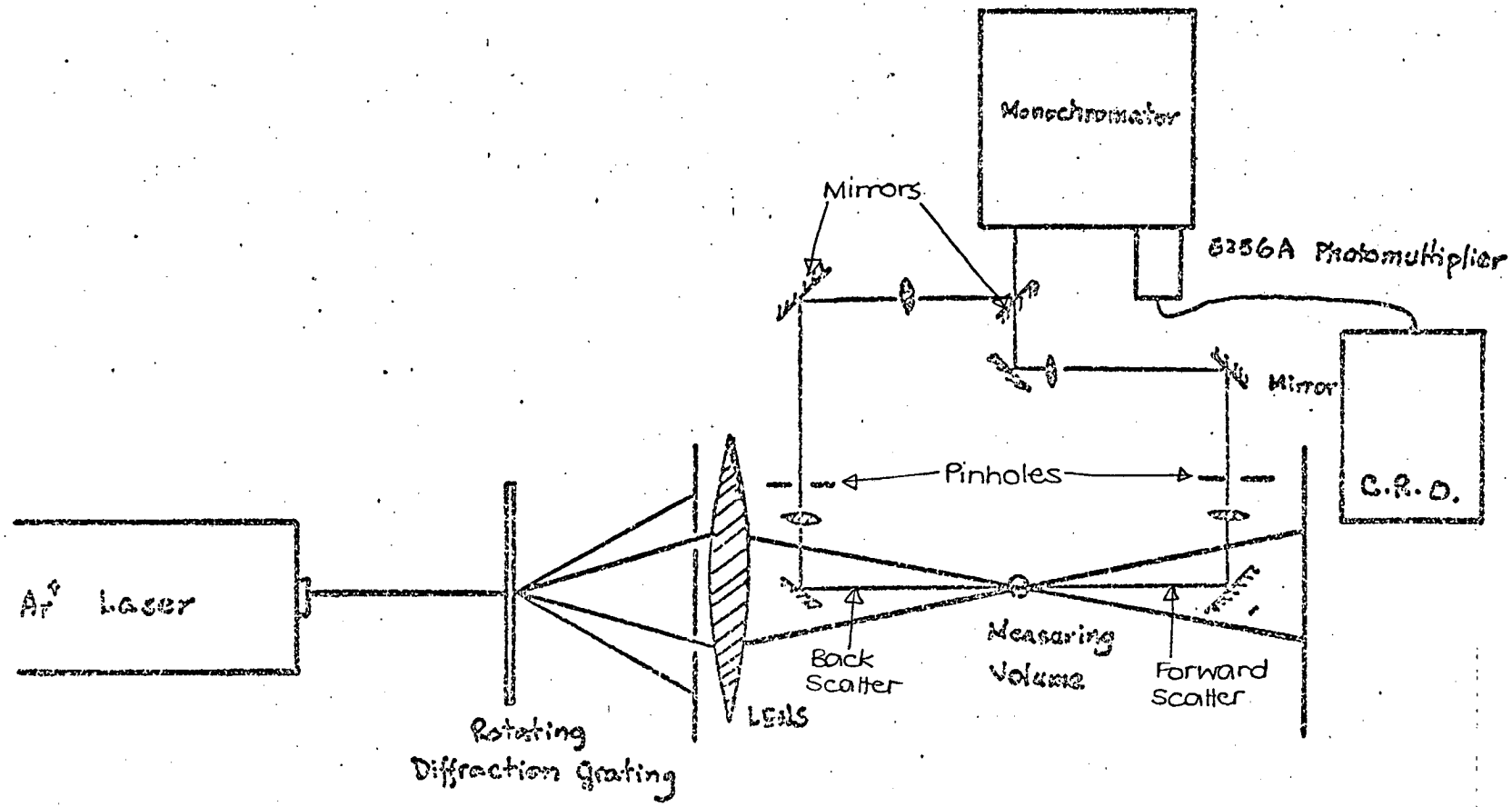

Crossed Beam Optical System for Particle Sizing

Fig. 31

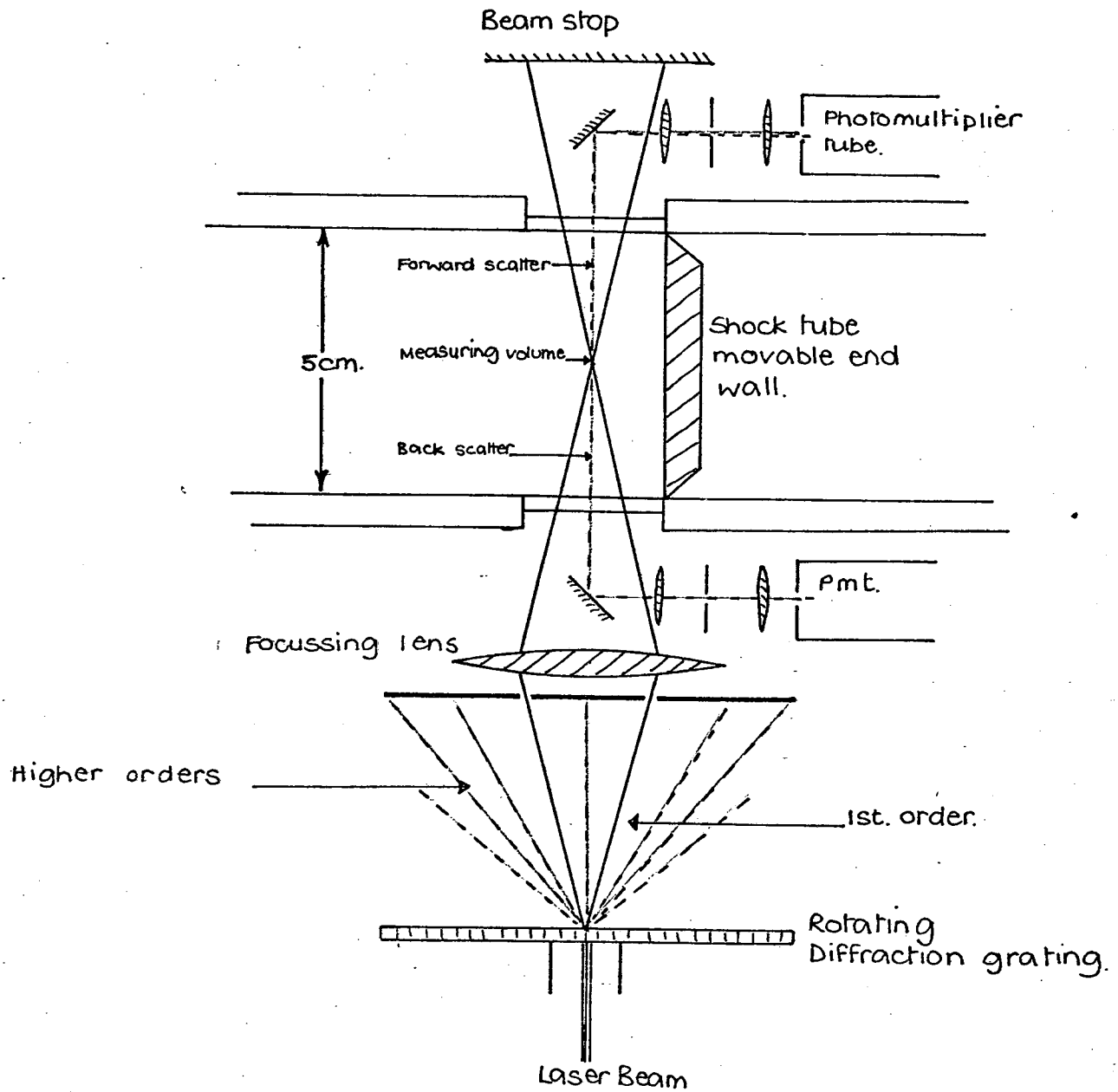

FIG. 32

SHOCK TUBE EXPERIMENTAL APPARATUS